

2015-04-20

# Development of a Satellite-Based Forest Fire Danger Forecasting System and its Implementation Over the Forest Dominant Regions in Alberta, Canada

Chowdhury, Ehsan Hafiz

---

Chowdhury, E. H. (2015). Development of a Satellite-Based Forest Fire Danger Forecasting System and its Implementation Over the Forest Dominant Regions in Alberta, Canada (Doctoral thesis, University of Calgary, Calgary, Canada). Retrieved from <https://prism.ucalgary.ca>. doi:10.11575/PRISM/25674  
<http://hdl.handle.net/11023/2143>

*Downloaded from PRISM Repository, University of Calgary*

UNIVERSITY OF CALGARY

Development of a Satellite-Based Forest Fire Danger Forecasting System and its Implementation  
Over the Forest Dominant Regions in Alberta, Canada

by

Ehsan Hafiz Chowdhury

A THESIS

SUBMITTED TO THE FACULTY OF GRADUATE STUDIES  
IN PARTIAL FULFILMENT OF THE REQUIREMENTS FOR THE  
DEGREE OF DOCTOR OF PHILOSOPHY

GRADUATE PROGRAM IN GEOMATICS ENGINEERING

CALGARY, ALBERTA

APRIL, 2015

© Ehsan Hafiz Chowdhury 2015

## Abstract

Forest fire is a natural phenomenon in many ecosystems across the world. One of the most important components of forest fire management is forecasting of fire danger conditions. My aim was to develop a daily-scale forest fire danger forecasting system (FFDFS) using remote sensing inputs over the northern part of Canadian province of Alberta during 2009-2011 fire seasons. In this research, I critically analyzed the current operational fire danger forecasting systems and other remote sensing-based methods in order to determine the knowledge gaps. In general, the operational systems use point-based measurements of meteorological variables and generate danger maps upon employing interpolation techniques. It is possible to overcome the uncertainty associated with the interpolation techniques by using remote sensing data. It was observed that most of the fire danger monitoring systems focused on determining the danger during and/or after the period of image acquisition, thus unable to forecast the fire danger accurately. A limited number of studies were conducted to forecast fire danger conditions, which could be adaptable. In this thesis, I developed FFDFS's useful for mid-term (i.e., 8-day) and daily-scale forecasting. The newly developed 8-day scale FFDFS uses Moderate Resolution Imaging Spectroradiometer (MODIS)-derived 8-day composite of surface temperature ( $T_s$ ), normalized multiband drought index (NMDI), and normalized difference vegetation index (NDVI). In order to eliminate the data gaps in the input variables, I propose a gap-filling technique that considered both of the spatial and temporal dimensions. The input variables were calculated during the  $i$  period and then integrated to forecast the danger conditions into four categories during the  $i + 1$  period. I observed that 90.94% of the fire fell under 'very high' to 'moderate' danger classes when compared with Alberta Environment and Sustainable Resource Development (ESRD) fire spots. As regards to operational perspective, I opted to develop daily-scale FFDFS comprised of MODIS-derived 8-day composite

of Ts, NDVI, and NMDI; and daily precipitable water (PW). The Ts, NMDI, and NDVI variables were calculated during  $i$  period and PW during  $j$  day; and then integrated to forecast fire danger conditions into five categories during  $j+1$  day. Results were significant with 95.51% of fires in the 'extremely high' to 'moderate' danger classes. Therefore, I infer that the refined FFDFS approach developed using remote sensing variables has operational value and can be routinely incorporated into meteorological based fire forecasting systems. Therefore, I apprehend that FFDFS could be used as an operational one; and has the potential to supplement information to the operational meteorological-based forecasting systems.

## Preface

The outcomes of this research have been published and/or presented as listed below:

### Journal publications

1. Chowdhury, E.H.; Hassan, Q.K., 2013. Use of remote sensing-derived variables in developing a forest fire danger forecasting system. *Natural Hazards* 67, 321-334.
2. Chowdhury, E.H.; Hassan, Q.K., 2014. Operational perspective of remote sensing-based forest fire danger forecasting systems. *ISPRS Journal of Photogrammetry and Remote Sensing*. doi:10.1016/j.isprsjprs.2014.03.011.
3. Chowdhury, E.H.; Hassan, Q.K., 2015. Development of a new daily-scale forest fire danger forecasting system using remote sensing data. *Remote Sensing* 7(3), 2431-2448.

### Abstract presentations

4. Chowdhury E. H.; Hassan Q. K., 2012. Development of advanced cloud infilling algorithm for remote sensing-based surface temperature, *CWRA / CGU National Conference 2012* (June 5-8), Banff, Alberta.
5. Chowdhury E. H.; Hassan Q. K., 2012. A Remote Sensing-based framework for forecasting forest fire danger conditions, *Wildland Fire Canada Conference 2012* (October 1-4), Kananaskis, Alberta.

### Poster presentations

6. Chowdhury E. H.; Hassan Q. K., 2013. Can remote sensing be effective for forecasting fire danger conditions? *MultiTemp 2013 Workshop* (June 25-27), Banff, Alberta.
7. Chowdhury E. H.; Hassan Q. K., 2014. A review on the applicability of remote sensing-based techniques in forecasting forest fire danger conditions, *Wildland Fire Canada Conference 2014* (October 7-9), Halifax, Nova Scotia.

## Acknowledgements

I am sincerely grateful to Dr. Quazi K. Hassan for his supervision, sincere support and encouragement during my PhD program. I am grateful to him for providing technical guidance and help on scientific publications. I would like to thank to my supervisory committee members Dr. Naser El-Sheimy and Dr. Ruisheng Wang, for their support in my research work. I also highly acknowledges the inputs and suggestions provided by the examiners, Dr. Krishna Vadrevu and Dr. Markus Dann.

I would like to acknowledge the funding from several sources: (i) Dr. Quazi K. Hassan's NSERC Discovery Grant; (ii) Queen Elizabeth II scholarships, University of Calgary; (iii) Faculty of Graduate Studies Scholarship Award, University of Calgary; (iv) Schulich School of Engineering in the form of travel grants; and (v) funds for publishing open access journal articles from The University of Calgary.

I also acknowledge the following agencies for providing the data and information: (i) NASA for MODIS data at free of cost; (ii) Alberta Environment and Sustainable Resource Development for fire related data; and (iii) GeoGratis, Natural Resources Canada for geospatial data.

My appreciation goes to my wife Lutfunnessa Lily, my children Julkarnain Chowdhury and Sadia Arefin for their love, support, encouragement, and patience. I personally thank my brothers, sisters, and friend Mr. Ekramuzzaman Sheikh for their intensive encouragement. I wish to thank all of my 'Earth Observation for Environment Laboratory' group members especially Mr. Mostafa Mosleh for their support and encouragement. I would also like to thank the staff of Geomatics Dept. for their support.

## **Dedication**

*In the memory of my father Late Hafez Ahmed Chowdhury*

*and*

*mother Mrs. Akhter Banu.*

## Table of Contents

Abstract .....	ii
Preface .....	iv
Acknowledgements .....	v
Dedication .....	vi
Table of Contents .....	vii
List of Tables .....	x
List of Figures .....	xi
List of Plates .....	xiii
List of Symbols, Abbreviations and Nomenclature .....	xiv
CHAPTER 1 : INTRODUCTION .....	1
1.1 Background .....	1
1.2 Problem statement .....	4
1.3 Research objectives .....	7
1.4 Thesis structure .....	8
CHAPTER 2 : LITERATURE REVIEW .....	10
2.1 Current operational forest fire danger rating system .....	10
2.1.1 Fire Weather Index (FWI) System in Canada .....	11
2.1.2 McArthur’s Forest Fire Danger Rating System (FFDRS) .....	12
2.1.3 Russian Nesterov Index .....	14
2.1.4 National Fire Danger Rating System (NFDRS) in USA .....	15
2.1.5 Limitations of the operational systems .....	17
2.2 Remote sensing-based fire danger monitoring .....	18
2.2.1 Vegetation greenness .....	19
2.2.2 Meteorological variables .....	24
2.2.3 Surface wetness conditions .....	26
2.2.4 Vegetation wetness condition .....	28
2.2.5 Fire danger monitoring using SAR images .....	32
2.2.6 Limitations of remote sensing-based monitoring systems .....	33
2.3 Remote sensing-based fire danger forecasting systems .....	35
2.4 Synergy between operational forecasting systems and remote sensing-based methods ..	40
2.5 MODIS characteristics .....	42
CHAPTER 3 : STUDY AREA & DATA PRE-PROCESSING .....	45
3.1 Description of study area .....	45
3.2 Dataset used .....	47
3.3 Data pre-processing .....	48
3.3.1 MODIS data pre-processing .....	48

3.3.2 Processing of fire spot data.....	55
3.3.3 Processing of GIS shape files .....	55
3.4 Computation of remote sensing-based indices .....	55
3.4.1 Normalized difference vegetation index (NDVI) .....	55
3.4.2 Normalized multiband drought index (NMDI).....	57
3.5 Constraints in relation to the employed input variables .....	58
<b>CHAPTER 4 : METHODS .....</b>	<b>60</b>
4.1 Development of a gap-filling algorithm for the input variables of FFDFS system .....	60
4.1.1 Development of data gap-filling algorithm .....	60
4.1.2 Validation of data gap-filling method .....	63
4.2 Enhancement of 8-day scale FFDFS system for mid-term forecasting.....	65
4.2.1 Calculation of individual variable-specific fire danger conditions .....	65
4.2.2 Generation of combined fire danger maps.....	65
4.2.3 Validation with actual fire spots data .....	67
4.2.3.1 Evaluation of variable-specific fire danger conditions .....	67
4.2.3.2 Evaluation of the potential of combined fire danger conditions.....	68
4.3 Development of a remote sensing-based daily-scale FFDFS system.....	68
4.3.1 Development of a daily-scale FFDFS .....	68
4.3.2 Generation of fire danger maps at daily-scale .....	70
4.3.3 Validation of daily-scale FFDFS system with ground-based fire spot data.....	70
4.3.3.1 Evaluation of daily PW-based fire danger conditions.....	70
4.3.3.2 Evaluation of the combined fire danger conditions .....	71
<b>CHAPTER 5 : RESULTS &amp; DISCUSSION.....</b>	<b>72</b>
5.1 Evaluation of gap-filling algorithm.....	72
5.1.1 Calculation of data gaps .....	72
5.1.2 Evaluation of the gap-filling algorithm .....	72
5.2 Temporal dynamics of the input variables of FFDFS system .....	78
5.2.1 Study-area specific average values of 8-day composite $T_s$ , NMDI, and NDVI.....	78
5.2.2 Study area-specific average values of daily PW .....	80
5.3 Evaluation of FFDFS system at mid-term forecasting .....	82
5.3.1 Assessment of variable-specific $T_s$ , NMDI, and NDVI on fire danger conditions .	82
5.3.2 Evaluation of combined fire danger condntions and its impacts .....	85
5.3.3 Fire danger maps for each period of interest .....	86
5.4 Evaluation of FFDFS system at daily-scale forecasting.....	90
5.4.1 Assessment of the impact of daily PW on fire danger conditions .....	90
5.4.2 Evaluation of daily-scale FFDFS system .....	92
5.4.3 Generation of fire danger forecasting map at daily-scale.....	93
5.5 Enhancement of forecasting capability of daily-scale over the 8-day scale FFDFS.....	95

CHAPTER 6 : CONCLUSIONS & RECOMMENDATIONS .....	99
6.1 Summary .....	99
6.2 Contribution to science .....	103
6.3 Recommendations for future work.....	104
REFERENCES .....	105
APPENDIX .....	131
Appendix A1: Copyright related information.....	132
A.1 Copyright permissions .....	133
A.1.1 Certificate for published journal articles .....	134
A.1.2 Certificate of a book chapter .....	137
A.1.3 Certificate from publications .....	138
Appendix A2: Data Tables .....	143
Appendix A3: Model development for the FFDFS systems .....	162

## List of Tables

Table 2.1: List of common vegetation indices used for fire danger monitoring and their mathematical formulas.....	20
Table 2.2: Example of remote sensing-based vegetation greenness indices used in fire danger monitoring studies. ....	21
Table 2.3: List of common vegetation wetness indices used for fire danger monitoring and their mathematical formulas.....	29
Table 2.4: Example of remote sensing-based vegetation wetness indices used in fire danger monitoring.....	30
Table 2.5: Brief description of some remote sensing-based fire danger forecasting systems.....	36
Table 2.6: MODIS specifications (NASA, 2011).....	43
Table 2.7: Characteristics of MODIS spectral bands (reflected: 1–19, 26; emitted: 20–25, 27–36) (NASA, 2011). ....	44
Table 3.1: List of MODIS data used during the period of 2009-2011.....	49
Table 3.2: Science data sets (SDS) of MODIS Terra T <sub>s</sub> , surface reflectance, and PW.....	54
Table 5.1: Average co-efficient of determination (r <sup>2</sup> ) and root mean square error (RMSE) between observed and predicted T <sub>s</sub> variable using different window size during 2009-2011. ....	78
Table 5.2: Quadratic fits ( $y = ax^2 + bx + c$ ) of the variables T <sub>s</sub> , NMDI, and NDVI variables as a function of DOY for the fire seasons of 2009–2011 (i.e., between DOY 89 and 265).....	80
Table 5.3: Percentage of fire spots fell under variable-specific fire danger conditions (i.e., either high or low, extracted one period earlier than the fire occurrence) during the period of 2009-2011. ....	83
Table 5.4: Percentage of data fell under each fire danger category using the combined variable of T <sub>s</sub> , NMDI, and NDVI in comparison with the fire spot. ....	86
Table 5.5: Percentage of data fell under each fire danger category using the combined variable of T <sub>s</sub> , NMDI, NDVI, and PW in comparison with the fire spot.....	92

## List of Figures

Figure 1.1: The extent of boreal forested regions in Canada with the provincial boundaries and forest burned areas over 200 ha during 1980-2013. ....	3
Figure 1.2: Major factors responsible for forest fire occurrences. ....	5
Figure 1.3: Schematic diagram of the chapters of the thesis. ....	9
Figure 2.1: Simplified schematic diagram of Forest Fire Weather Index System (adapted from van Wagner, 1987). ....	12
Figure 2.2: Schematic diagram of McArthur’s Forest Fire Danger Rating System (adapted from McArthur, 1967). ....	13
Figure 2.3: Schematic diagram of the Russian Nesterov Index. ....	14
Figure 2.4: Structure of the US National Fire Danger Rating System (adapted from Burgan, 1988). ....	16
Figure 2.5: (a) Triangular and (b) trapezoidal forms based on a relationship between $T_s$ and VIs (adapted from Sandholt et al., 2002 and McVicar and Jupp, 1998). ....	27
Figure 2.6: Fire danger map for the period May 9–16, 2011 generated by combining $T_s$ , NMDI, and TVWI (after Akther and Hassan, 2011a) variables acquired during the prior 8-day period (i.e., May 1–8, 2011). ....	39
Figure 2.7: The operational system to produce the fire potential map using remote sensing-derived variable and National Fire Danger Rating System (see Figure 2.4) (adapted from Burgan et al., 1998). ....	41
Figure 3.1: (a) Location map of Alberta Province in Canada; (b) extent of study area within a MODIS-based land cover map of 2008 and ESRD fire spots during 2009-2011. ....	46
Figure 3.2: The spectral reflectance curves of green, dry vegetation and soil (after Clark et al., 1999). ....	56
Figure 3.3: Model simulated canopy spectra at different leaf water content (after Wang and Qu, 2007). ....	58
Figure 4.1: The schematic diagram of the proposed gap-filling method at 8-day scale for $T_s$ , NMDI, and NDVI variables. ....	61
Figure 4.2: The conceptual diagram of: (a) 8-day scale FFDFS using $T_s$ , NMDI, and NDVI variables (i.e., between DOY 89 and 265); (b) fire danger conditions of daily PW; and (c) the criterion of describing fire danger conditions for the input variables of $T_s$ , NMDI, NDVI, and PW. ....	66

Figure 4.3: The conceptual diagram of daily-scale FFDFS using $T_s$ , NMDI, NDVI, and PW variables. ....	69
Figure 5.1: Percentage of gap pixels in $T_s$ images upon gap-filling using various window sizes during 2009–2011. ....	73
Figure 5.2: Comparison between observed and predicted $T_s$ upon using $3 \times 3$ window size for gap-filling: (a) 97 DOY, $F = 286507$ , $p$ value $<0.0001$ (b) 137 DOY, $F = 368260$ , $p < 0.0001$ (c) 177 DOY, $F = 320805$ , $p < 0.0001$ , (d) 217 DOY, $F = 382576$ , $p < 0.0001$ , (e) 249 DOY, $F = 607077$ , $p < 0.0001$ .....	74
Figure 5.3: Comparison of observed and predicted NMDI upon using $3 \times 3$ window size for gap-filling: (a) 113 DOY, $F = 18880$ , $p < 0.0001$ , (b) 153 DOY, $F = 241571$ , $p < 0.0001$ , (c) 193 DOY, $F = 263602$ , $p < 0.0001$ , (d) 233 DOY, $F = 111437$ , $p < 0.0001$ , (e) 265 DOY, $F = 510446$ , $p < 0.0001$ .....	75
Figure 5.4: Comparison of observed and predicted NDVI upon using $3 \times 3$ window size for gap-filling: (a) 105 DOY, $F = 18880$ , $p < 0.0001$ , (b) 145 DOY, $F = 241571$ , $p < 0.0001$ , (c) 185 DOY, $F = 263602$ , $p < 0.0001$ , (d) 225 DOY, $F = 111437$ , $p < 0.0001$ , (e) 257 DOY, $F = 510446$ , $p < 0.0001$ .....	76
Figure 5.5: Study-area specific average values for $T_s$ , NMDI, and NDVI variables for 2009–2011 fire seasons (i.e., between DOY 89 and 265). ....	79
Figure 5.6: Study area-specific average values of PW (i.e., 8–day average) with DOY for the fire seasons of 2009–2011 (i.e., between DOY 89 and 272). ....	81
Figure 5.7: Frequency distribution of the fires with respect to $T_s$ , NMDI, and NDVI variables and its corresponding study area average values during the $i$ period when actual fires were taken place in the following $i+1$ period on the basis of the ‘study area-specific average $\pm 3$ standard deviation’ values and percentage of fire spots during 2009-2011.....	84
Figure 5.8: (a) Fire danger map for the period June 10-17, 2009 forecasted by combining the $T_s$ , NMDI, and NDVI variables exploited during the immediate preceding period i.e., June 2-9, 2009; and actual fire spots during the June 13, 2009 (i.e., 164 DOY); (b) fire danger classes with actual fire spots.....	87
Figure 5.9: (a) Fire danger map for the period June 18-25, 2010 forecasted by combining the $T_s$ , NMDI, and NDVI variables exploited during the immediate preceding period i.e., June 10-17, 2010; and actual fire spots during the June 20, 2010 (i.e., 171 DOY); (b) fire danger classes with actual fire spots.....	88
Figure 5.10: (a) Fire danger map for the period May 9-16, 2011 forecasted by combining the $T_s$ , NMDI, and NDVI variables exploited during the immediate preceding period i.e., May 1-8, 2011; and actual fire spots during the May 14, 2011 (i.e., 134 DOY); (b) fire danger classes with actual fire spots.....	89

Figure 5.11: Frequency distribution of the fires with respect to PW and its corresponding study area average values during the  $j$  day when actual fires were taken place in the following  $j+1$  day on the basis of the ‘study area-specific average  $\pm$  3 standard deviation’ values and percentage of fire spots during (a) 2009, (b) 2010, (c) 2011, and (d) 2009-2011.....91

Figure 5.12: Fire danger maps for mid-May, 2011 forecasted by combining the  $T_s$ , NMDI, NDVI, and PW variables exploited during the immediate preceding day at: (a) Slave lake (May 13, 2011), and (b) Fort McMurray (May 9, 2011) regions. ....94

Figure 5.13: (a) Fire danger map for June 13, 2009 forecasted by combining the  $T_s$ , NMDI, NDVI, and PW variables exploited during the immediate preceding day i.e., June 12, 2009; and actual fire spots during the June 13, 2009 (i.e., 164 DOY); (b) fire danger classes with actual fire spots. ....96

Figure 5.14: (a) Fire danger map for June 20, 2010 forecasted by combining the  $T_s$ , NMDI, NDVI, and PW variables exploited during the immediate preceding day i.e., June 19, 2010; and actual fire spots during the June 20, 2010 (i.e., 171 DOY); (b) fire danger classes with actual fire spots. ....97

Figure 5.15: (a) Fire danger map for May 14, 2011 forecasted by combining the  $T_s$ , NMDI, NDVI, and PW variables exploited during the immediate preceding day i.e., May 13, 2011; and actual fire spots during the May 14, 2011 (i.e., 134 DOY); (b) fire danger classes with actual fire spots. ....98

### List of Plates

Plate 3.1: Conversion of MODIS HDF file into Geo-tiff format using MODIS MRT tool.....51

Plate 3.2: Conversion of MODIS HDF file into Geo-tiff format using MODIS MRT Swath tool.....52

## List of Symbols, Abbreviations and Nomenclature

### *List of Symbols*

<u>Symbol</u>	<u>Definition</u>
$T_s$	Surface temperature
$T_a$	Air temperature
$\rho$	Surface reflectance
$D$	Dew point temperature
$W$	Number of days since last precipitation
$N$	Nesterov index
$e_a$	Water vapor pressure
$e_0$	Saturation vapor pressure
$g$	Acceleration of gravity
$\lambda$	Exponent of power law that describe the atmospheric profile
$\delta$	Ratio of specific gas constants of water vapor to dry air
$W_w$	Wet weight of the sample
$W_d$	Oven dry weight of the sample
$A$	Area in square meter
$C_w$	Water content
$C_{ab}$	Chlorophyll content
$C_m$	Leaf dry matter content
$N$	Leaf internal structure
$\theta$	Soil moisture
$r^2$	Co-efficient of determination
$n$	Number of observations

## *List of Abbreviations*

<u>Abbreviations</u>	<u>Definition</u>
AVHRR	Advanced Very High Resolution Radiometer
AVIRIS	Airborne Visible Infrared Imaging Spectrometer
BI	Burning index
BUI	Buildup index
CFFDRS	Canadian forest fire danger rating system
CWC	Canopy water content
DC	Drought code
DI	Disturbance index
DMC	Duff moisture code
EMC	Equivalent moisture content
EOSDIS	Earth Observing System data Information System
ERC	Energy release component
ERS	European remote sensing
ESRD	Environment and Sustainable Resource Development
EVI	Enhanced vegetation index
EWT	Equivalent water thickness
FAO	Food and Agriculture Organization of the United States
FFDFS	Forest fire danger forecasting system
FFDRS	Forest fire danger rating system of Australia
FFMC	Fine fuel moisture code
FM	Fuel moisture
FMC	Fuel moisture content
FPI	Fire potential index
FWI	Fire weather index
GEMI	Global environmental monitoring index
GIS	Geographic information system
GOES	Geostationary Operational Environmental Satellite
GVMi	Global vegetation moisture index
HDF	Hierarchical data format
IC	Ignition component
ISI	Initial spread index
KBDI	Keetch-Byram drought index
Landsat TM	Landsat Thematic Mapper
MRT	MODIS Reprojection Tool
MRT Swath	MODIS Reprojection Tool Swath

<u>Abbreviations</u>	<u>Definition</u>
MSG-SEVIRI	Meteosat Second Generation Spinning Enhanced Visible and Infrared Imager
MSI	Moisture stress index
NDII	Normalized difference infrared index
NDVI	Normalized difference vegetation index
NDWI	Normalized difference water index
NFDRS	National fire danger rating system
NIR	Near Infrared
NMDI	Normalized multiband drought index
NOAA	National Oceanic and Atmospheric Administration
PW	Precipitable water
QA	Quality assurance
QC	Quality control
RADARSAT	Radar Satellite
RG	Relative greenness
RH	Relative humidity
RS	Rate of spread
SAR	Synthetic Aperture Radar
SAVI	Soil adjusted vegetation index
SC	Spread component
SFFM	Surface fine fuel moisture
SRWI	Simple relation water index
SWIR	Shortwave infrared
TVWI	Temperature vegetation wetness index
USA	United States of America
UTM	Universal transverse mercator
VARI	Visible atmospherically resistant index
VI	Vegetation index
WDI	Water deficit index
WI	Water index

## **CHAPTER 1 : INTRODUCTION**

### **1.1 Background**

Forest fire is a natural phenomenon in many ecosystems across the world. Forest biomass burning occurs in almost all climatic conditions and geographical latitudes (Chuvieco et al., 2008). It is considered as an ecological disturbance which is responsible for burning about 350 million hectares (ha) of forested land per annum on an average-basis (FAO, 2007). At regional scale, the largest forest fire burned areas were found in Africa sub-Saharan (i.e., 200.82 million ha), Australasia (i.e., 52.98 million ha), Central and Southeast Asia (i.e., 19.85 million ha), and North and South America (i.e., 10.85 million ha), among others during 2000 (GBA, 2000). Several countries invest billions on an annual basis in suppression, prevention, and prescribe burning. For example, the United States Department of Agriculture Forest Service has spent more than US\$ 14.63 billion; Canada spent US\$ 5.91 billion; and Chile expends US\$ 0.12 billion, respectively during 2000-2010 (González-Cabán, 2013).

Damages from forest fires have direct impact on human lives and livelihoods and also critical to the economy. Forest fires have both negative and positive consequences on the ecosystem and impacts us in many ways (Bleken et al., 1997; Martell, 2011). In general, they are perceived as a threat (Amiro et al., 2009; Huesca et al., 2009; Sifakis et al., 2011; Montealegre et al., 2014), because the burning of forest causes: economic losses [e.g., average US\$ 2.4 billion per annum between 2002 and 2011 period as a result of biomass burning (Chatenoux and Peduzzi, 2012)]; release of CO<sub>2</sub> into the atmosphere [e.g., the 1997 Indonesian wildfires have released about 13–40% of average annual global carbon emissions produced by the use of fossil fuels (Page et al.,

2002)]; and health hazard due to smoke [e.g., inhalation of toxic gases from smoke worsen the heart and lung diseases, cough and breath, sore eyes, tears, etc. (Stefanidou et al., 2008)]. In addition, large fires can potentially kill the firefighters [e.g., in the United States 1144 firefighters killed during the 1994–2004 period (Kales et al., 2007)] and destroy human settlements [e.g., the 2011 Slave Lake fire in Alberta, Canada has destroyed 40% of the town that includes 454 dwellings, public library, town hall and office buildings costing CAD\$ 700 million (CBS News, 2011; FTCWRC, 2012)]. However, forest fires have also many benefits such as regulating fuel accumulation, regeneration of vegetation by removing fungi and microorganisms, disease and insect control, receive more energy through exposure to solar radiation, mineral soil exposure and nutrient release (Bond et al., 2005; Ruokolainen and Salo, 2009; Pausas and Paula, 2012; Chu and Gao, 2014). In addition, fires also influence the regional biogeochemical processes (e.g., carbon cycling), climate change, etc. (Govind et al. 2011). These concerns are attracting a high level of interest among researchers in quantifying its impact on forest fire regimes (Flannigan et al., 2009; Loehman et al., 2011).

In Canada, forest fire is considered as one of the critical natural disturbances [that represents approximately 10% of the global forest (NRCAN, 2014)]. In fact, Canadian forest has experienced approximately 8300 fires that burned 2.3 million ha every year on an average during the last 25 years (NRCAN, 2014). Mostly large fires dominate the burned areas, i.e., each year fire greater than 200 ha representing 97% of the burned area. The boreal forested region of Canada occupies 77% of its forested land and experience recurrent fire disturbances. Figure 1.1 shows the extent of boreal forest along with the provincial boundaries and the forest fire occurrences over 200 ha in Canada during the period 1980-2013. In order to suppress the fires, Canada has spent in the range

CAD \$500 million to \$1 billion every year on an average during the last decade in order to suppress the fires (NRCAN, 2014).

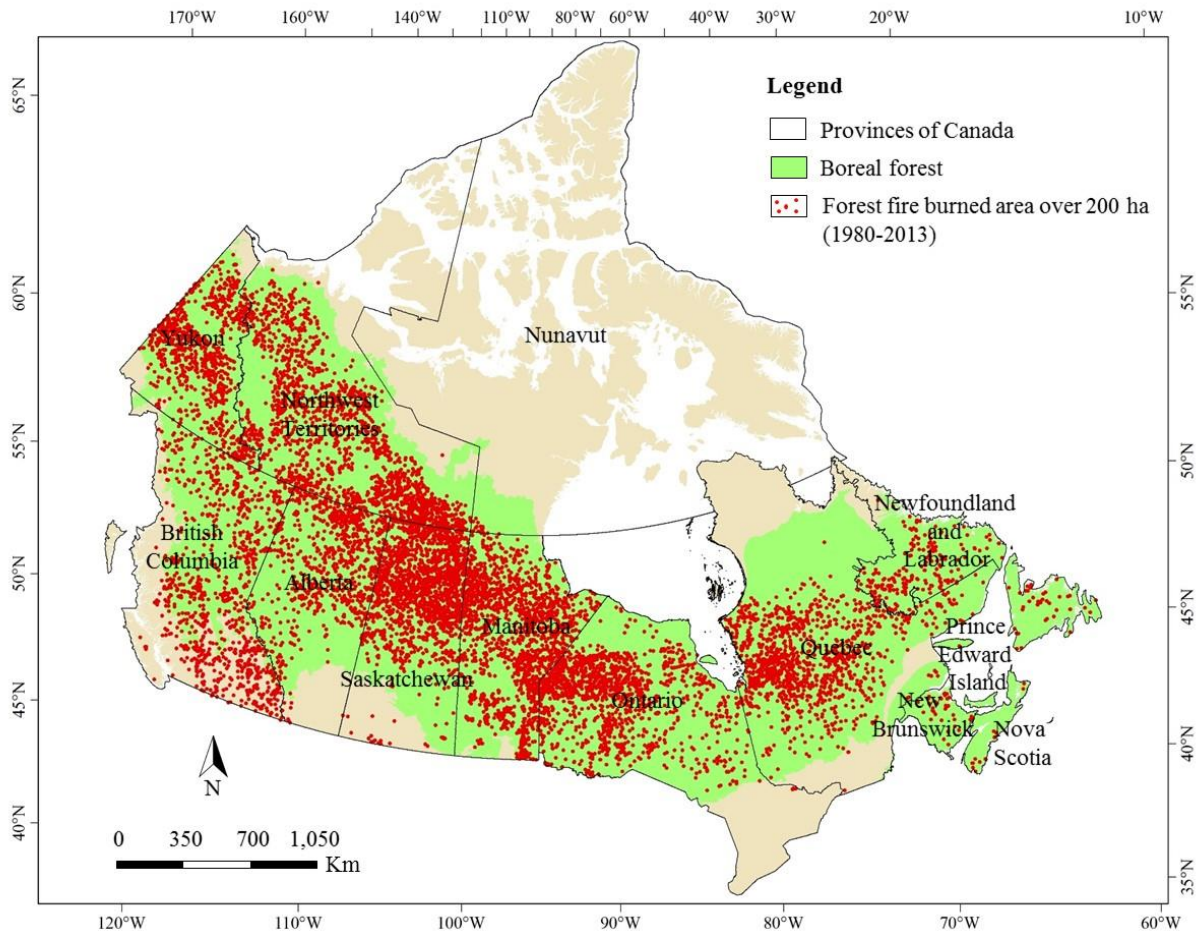


**Figure 1.1: The extent of boreal forested regions in Canada with the provincial boundaries and forest burned areas over 200 ha during 1980-2013.**

One of the most important components of integrated forest fire management is the forecasting of fire danger conditions (i.e., probability of fire occurrences). In general, the fire danger conditions are dynamic in both space and time (Vasilakos et al., 2009; Chuvieco et al., 2010; Saglam et al., 2008), and highly dependable on a set of factors. Those include: meteorological variables [e.g., temperature, wind speed and direction, relative humidity (RH), precipitation, etc.]; fuel conditions (e.g., live and dead fuel load, and fuel moisture content); topography (e.g., elevation, aspect, and slope); and sources of ignition such as human interferences (e.g., arson) or natural causes (e.g., lightning) (Jain et al., 1996; Chuvieco et al., 2004a; Adab et al., 2013). Among these factors, the topography is usually static in the temporal dimension, and influences the fire behavior (i.e., intensity and spreading after the ignition) to a large extent (Carlson and Burgan, 2003). As such, the fire danger conditions can be depicted as a function of meteorological variables and forest fuel conditions (also both of them are highly interrelated); while fire occurrences rely on the source of ignition (Wotton, 2009; Running and Coughlan, 1988; Malone et al., 2011). In fact, fire occurrence is defined as the number of fires started in a given area over a particular time period, as a function of meteorological, fuel conditions and source of ignition (BLM, 2012). Figure 1.2 shows the fire triangle that includes the meteorological variables, fuel conditions, and source of ignition as a prerequisite of forest fire occurrence.

## **1.2 Problem statement**

Most of the operational forest fire danger forecasting systems across the world are primarily based on meteorological variables (Allgöwer et al., 2003; Abbott et al., 2007). Among the existing operational systems, the most prominent ones are the Canadian Fire Weather Index (FWI) System,

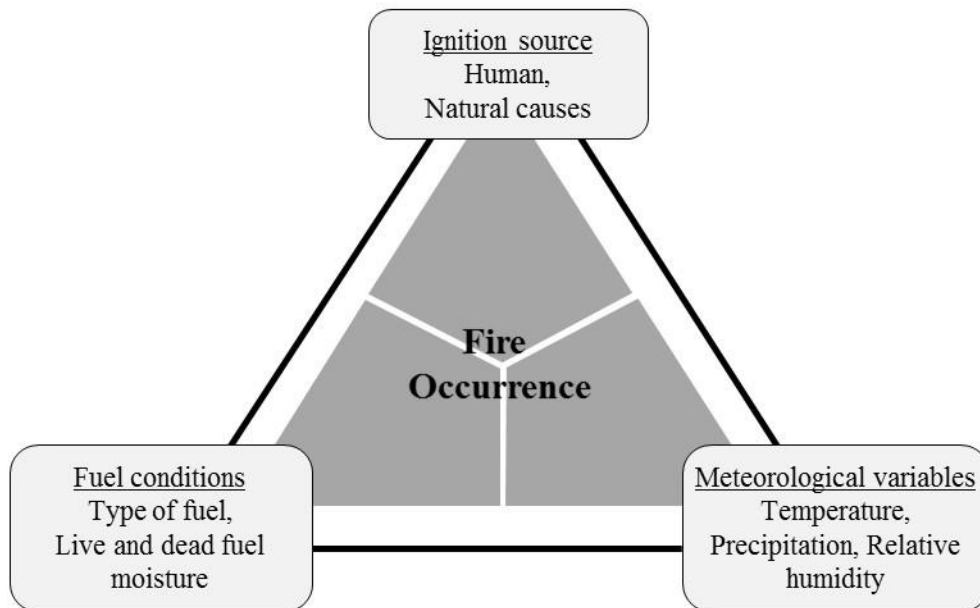


**Figure 1.2: Major factors responsible for forest fire occurrences.**

US National Fire Danger Rating System (NFDRS), Australian McArthur Forest Fire Danger Rating System (FFDRS), and Russian Nesterov Index. These systems consist of following three aspects: (i) acquisition of meteorological variables at point locations over an area of interest; (ii) generate the surface maps for the variable of interest using geographic information system (GIS)-based interpolation techniques (e.g., inverse distance weighting, spline, kriging, etc.); and (iii) forecast the spatial dynamics of the fire danger conditions at landscape level. Note that various GIS-based interpolation techniques could potentially generate different map outputs using the same input variables (Chilès and Delfiner, 2012). In order to eliminate such uncertainties, remote sensing-based data have greater advantage over the point-based data as it accounts for the spatial variability and can represent information over remote areas (Wang et al., 2013). As such, remote sensing platforms are quite often useful for acquiring spatial data in a timely manner, which have already been proven as an effective way for monitoring and forecasting fire danger conditions

(Ceccato et al., 2001). Thus, several studies incorporated remote sensing derived variables in forest fire danger management (Aguado et al., 2003; Bajocco et al., 2010; Chuvieco et al., 2004b; Rahimzadeh-Bajgiran et al., 2012). Such attempts could be broadly categorized into two distinct groups: fire danger monitoring, and fire danger forecasting.

During the last several decades, remote sensing-based methods have been developed for monitoring the fire danger conditions. Most of these methods employed the remote sensing-derived environmental variables to assess the fire danger conditions during and/or after the fire events. As such, these methods would be unable to forecast fire danger conditions; however, they might be useful in exploiting relationships between environmental variables and fire occurrences. In case of forecasting the fire danger conditions, some remote sensing-derived environmental variables had also been used, such as surface temperature ( $T_s$ ) and normalized difference vegetation index (NDVI: an indicator of vegetation greenness) (Oldford et al., 2003);  $T_s$ , NDVI and water deficit index (WDI: soil and vegetation canopy water stress) (Vidal and Devaux-Ros, 1995);  $T_s$  condition prior to fire occurrence (Guangmeng and Mei, 2004); and  $T_s$ , normalized multi-band drought index (NMDI: a measure of water content measurement in the vegetation canopy), and temperature–vegetation wetness index (TVWI: an indirect way of estimating soil water content) (Akther and Hassan, 2011a). Though these developments demonstrated their capabilities of forecasting fire danger conditions, further research is needed to enhance both spatial temporal resolutions, predicting the values in the event of cloud-contamination, and incorporating other remote sensing-derived meteorological variables (e.g., relative humidity, precipitation, etc.). In addition, these systems must be calibrated and validated prior to implementing over a new ecosystem of interest. Furthermore, drivers of fires such as deforestation, land use change and

extreme climate events have been increasing in both frequency and severity across the globe (Souza et al., 2013; Flannigan et al., 2009). Thus, it would be worthwhile to study the fire danger conditions in order to develop appropriate fire management strategies to reduce the losses and enhance the benefits from wildfires (Stocks et al., 1989; de Groot et al., 2003; Leblon et al., 2012; Vadrevu et al., 2012).

### **1.3 Research objectives**

The overall objective of the research was to develop a forest fire danger forecasting systems (FFDFS) and its implementation over the northern boreal forested regions of the Canadian province of Alberta. The specific objectives were the:

- (i) comprehensive understanding of the currently operational fire danger forecasting systems and other remote sensing-based methods/system in order to determine the knowledge gaps;
- (ii) development of a gap-filling algorithm for the input variables of the FFDFS system to enhance the quality of the images;
- (iii) enhancement of a remote sensing-based forest fire danger forecasting system (i.e., FFDFS at 8-day scale) developed in an earlier study (Akther and Hassan, 2011a); and
- (iv) development of a remote sensing-based daily-scale FFDFS and implementation over the forest dominant regions of Alberta.

## **1.4 Thesis structure**

This thesis has been organized in six chapters (Figure 1.3). Chapter 1 provides background information about consequences of forest fires and their impacts; environmental variables those are responsible for forest fire; and problem statements of the current systems. This chapter also provides the study objectives and structure of this thesis. Chapter 2 presents the literature review of the current operational forest fire danger forecasting systems and their limitations; development of remote sensing-based danger monitoring and forecasting systems and their functional implications as an operational perspective. Chapter 3 explains the major characteristics of the study area, input variables and their pre-processing, computation of remote sensing-based indices including input variable constraints. Chapter 4 illustrates the development of remote sensing-based methods for fire danger forecasting system. It mainly comprises of three sub-sections: (i) development of a gap-filling algorithm for the input variables of the FFDFS system; (ii) enhancement of FFDFS system at mid-term forecasting (i.e., 8-day); and (iii) development of the FFDFS system at daily-scale forecasting. Chapter 5 presents the overall findings of this research work. It covers the results for each analyzed component, i.e., (i) status of the input variables after implementation of the gap-filling algorithm; (ii) the temporal dynamics of the input variables of the FFDFS system; and (iii) evaluation of the FFDFS system both for mid-term (i.e., 8-day) and daily-scale forecasting including generation of fire danger maps. Finally, Chapter 6 summarizes the research outcomes, and recommendations for further enhancement. This work has led to publications in peer-reviewed journals and different chapters highlight the work in much detail.

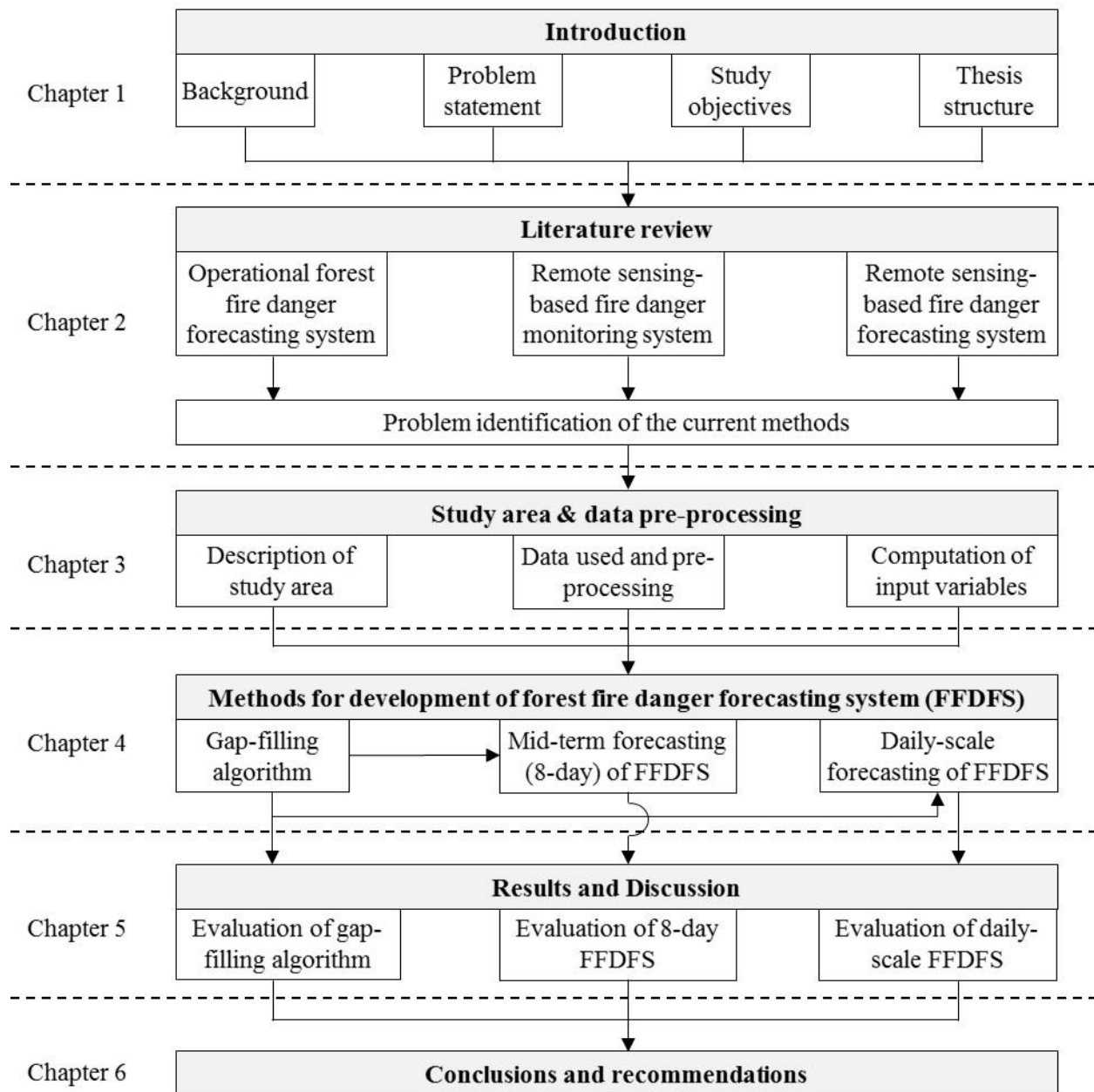


Figure 1.3: Schematic diagram of the chapters of the thesis.

## **CHAPTER 2 : LITERATURE REVIEW**

The goals of the literature review were to critically analyse the following four issues, such as (i) current operational forest fire danger forecasting systems and their limitations; (ii) remote sensing-based fire danger monitoring systems and effectiveness as an operational one; (iii) remote sensing-based fire danger forecasting systems and their functional implications; and (iv) synergy between operational forecasting systems and remote sensing-based methods. Thus, the detailed understanding about these developments would be worthwhile to progress research in the area of fire danger in the context of making them operational.

### **2.1 Current operational forest fire danger rating system**

Fire danger rating systems have been in operation in many countries around the world, especially in Canada, Australia, Russia and the United States (Stocks et al., 1989; Luke and McArthur, 1978; Deeming et al., 1978). The danger rating is a systematic process to estimate and integrate the variables of interest of the fire environment to quantify the potential of fire start, spread and impact in the form of fire danger (Merrill and Alexander, 1987; Sebastián-López et al., 2008; Albin, 1976; Rothermel et al., 1986; Deeming et al., 1972). These numerical ratings of fire potential are used in fire management both in wildfires and prescribed fires. The following sections describe the most prominent operational fire danger rating systems and their limitations.

### *2.1.1 Fire Weather Index (FWI) System in Canada*

In Canada, the forest fire danger conditions are calculated on daily basis using a component of Canadian Forest Fire Danger Rating System (CFFDRS), that is, known as Fire Weather Index (FWI) (van Wagner, 1987). The FWI system has been widely used in Canada for fire danger forecasting since the 1980s, which is designed based on the characteristics of the Canadian forested ecosystems (CFS, 1984; van Wagner, 1987). It is the most established system, which are being implemented in many parts of the world, e.g., New Zealand (Alexander and Fogarty, 2002), Alaska (Alexander and Cole, 2001), Mexico (Lee et al., 2002), Argentina (Taylor, 2001), European countries (i.e., Sweden, Portugal, Spain) (Granstrom and Schimmel, 1998; San-Miguel-Ayanz et al., 2003a; Viegas et al., 1999), and eastern Asia (i.e., Indonesia, Malaysia) (de Groot et al., 2007). These wider adaptations have been possible as the FWI system solely uses four meteorological variables as input ones (i.e., temperature, wind speed, relative humidity at noon time; and accumulated precipitation during earlier 24-h). The FWI system produces six indices on the basis of a reference fuel type (e.g., mature pine stands for Canadian ecosystems) (van Wagner, 1987) (see Figure 2.1 for details). These indices include: fine fuel moisture code (FFMC) calculated as a function of temperature, wind speed, relative humidity, and precipitation; duff moisture code (DMC) as a function of temperature, relative humidity, and precipitation; drought code (DC) as a function of temperature, and precipitation; initial spread index (ISI) as a function of FFMC and wind speed; buildup index (BUI) as a function of the DMC and DC; and fire weather index (FWI) as a function of ISI and BUI.

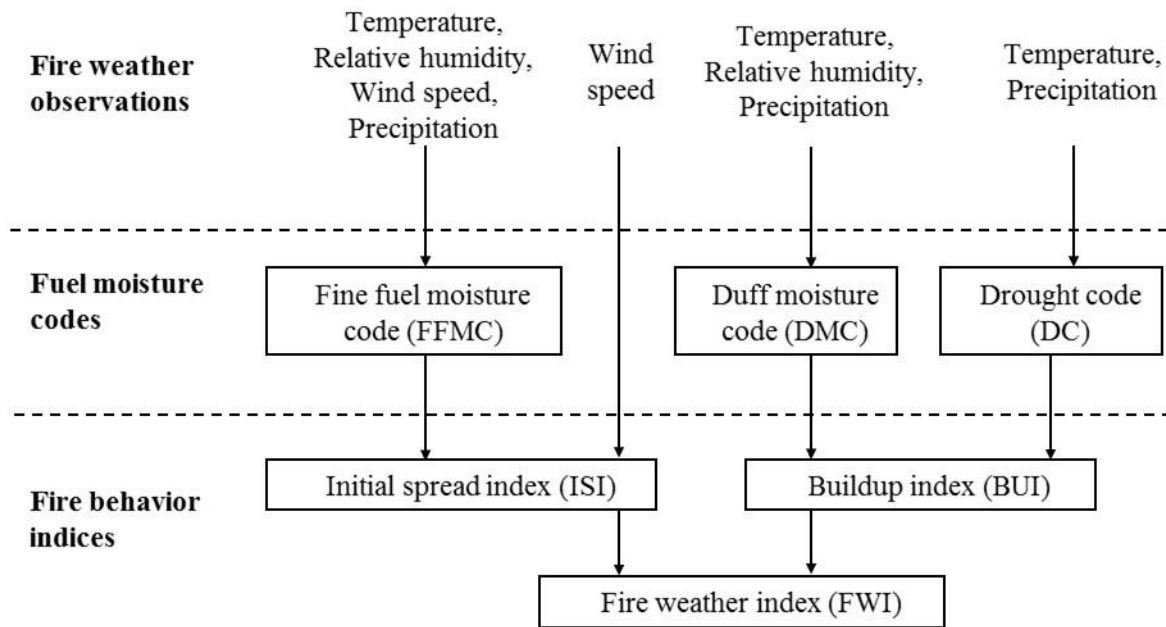


**Figure 2.1: Simplified schematic diagram of Forest Fire Weather Index System (adapted from van Wagner, 1987).**

### 2.1.2 McArthur's Forest Fire Danger Rating System (FFDRS)

In Australia, a comprehensive Forest Fire Danger Rating System was formulated by McArthur (1958) using meteorological conditions to predict the fire spread rate on the basis of the amount of dead fuel burning and difficulty of suppressing them. The input variables of the FFDRS are: (i) Keetch–Byram Drought Index (KBDI: calculated as a function of average annual precipitation, 24-h precipitation, and maximum temperature)-based long-term seasonal soil dryness (Keetch and Byram, 1968); (ii) daily average temperature, 24-h accumulated precipitation, relative humidity and wind speed at 1500 h local time (McArthur, 1967). The FFDRS system consists of four sub-models (see Figure 2.2): fine fuel availability or drought reason (calculated as a function of KBDI, precipitation, and days since precipitation); surface fine fuel moisture (SFFM: derived as a

function of relative humidity, and temperature); rate of spread (RS: as a function of wind speed, fuel moisture, and fuel availability); and the difficulty of suppression (calculated as a function of RS, SFFM and wind speed). Note that several experimental fires were conducted using three distinct fuel models (e.g., grassland, eucalypt forest and pine tree) in the development of this system.

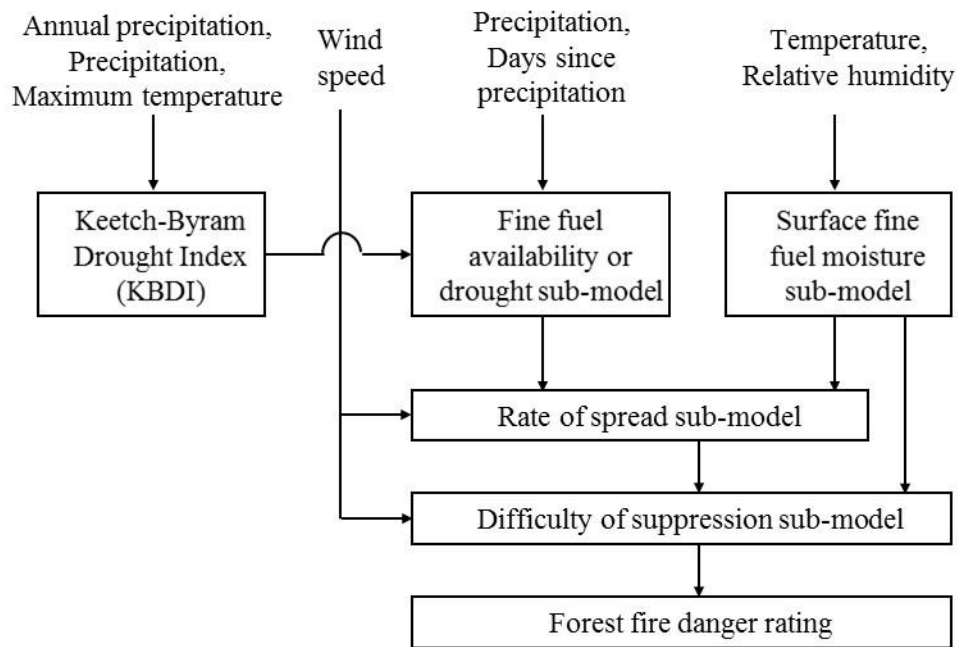


**Figure 2.2: Schematic diagram of McArthur's Forest Fire Danger Rating System (adapted from McArthur, 1967).**

### 2.1.3 Russian Nesterov Index

The Nesterov Index is a simple Fire Danger Rating System developed by Nesterov in 1949 and widely used in the boreal forested regions of Russia. This index is computed based on daily observations of meteorological variables, such as dew point temperature, air temperature ( $T_a$ ) at 1500 h local time; and the number of dry days since the last precipitation (Figure 2.3). The Nesterov's index considers the sum of all the preceding values in each day having precipitation less than 3 mm and the previous day's index. If the precipitation in a particular day is 3 mm or more, then the index is 'zeroed' and a new index is computed based on the current day meteorological variables (Khan, 2012). Further changes of the Nesterov's index have been carried out by considering the forest fire drought indices or moisture indices PV-1 (i.e., related to moisture content of moss/top layer) and PV-2 (i.e., related to moisture content of duff layer) (Vonsky and Zhdanko, 1976).

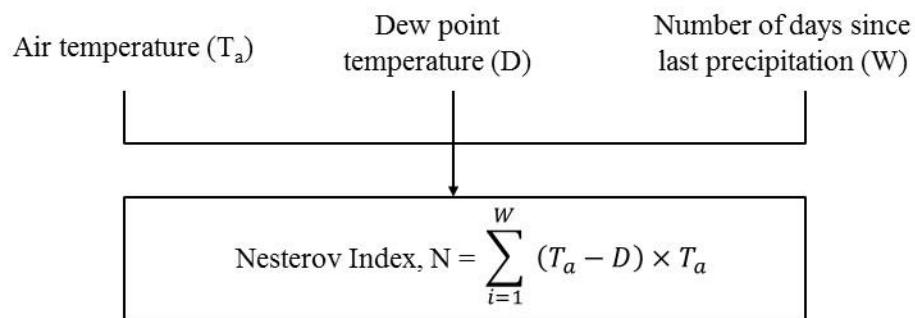


**Figure 2.3: Schematic diagram of the Russian Nesterov Index.**

#### *2.1.4 National Fire Danger Rating System (NFDRS) in USA*

The NFDRS operational system was first released for public use in 1972 in the United States. This system is a complex operational system that uses a set of user defined constants, several meteorological variables, fuel types, both live and dead fuel moisture, and generates output at different tiers of operation and illustrated in Figure 2.4 (Burgan, 1988; Deeming et al., 1972; Bradshaw et al., 1983). It requires two sets of inputs, such as site description that includes fuel model, slope class, live fuel types, climate class, latitude, and average annual precipitation; and daily meteorological observations acquired at 1300 h local time that includes dry bulb temperature, relative humidity, dew point, wind speed, wind direction, state of weather (illustrating information on stage of cloud, precipitation, fog, and thunderstorms/lightning), and solar radiation. In addition another index namely KBDI (Burgan, 1988; Andrews et al., 2005) are also used as an external response to the system. This system generates two tiers of outputs. Firstly, the intermediate outputs (that serve as pre-processor for the next day's processing) are the estimation of: (i) live fuel moisture for woody and herbaceous (i.e., expressed as percentage of the oven dry weight of the sample); and (ii) dead fuel moisture (i.e., moisture content of the dead organic fuels on the forest floor which consisted of 1-h, 10-h, 100-h and 1000-h time lag fuels derived as function of temperature, precipitation, cloudiness and relative humidity). Finally, the NFDRS provides four major fire behavior components and indices [calculated by using the Rothermel (1972) mathematical fire spread model], i.e., spread component (SC) is the predicted rate of spread (calculated as a function of wind speed, slope, fine fuel moisture, live woody fuel moisture); ignition component (IC) is the likelihood of a reportable fire from firebrand that needs suppression (calculated as function of fine fuel moisture and SC); energy release component (ERC) is the total energy released during flaming of a fire (calculated considering the dead and live fuel moisture);

and burning index (BI) as function of SC and ERC, which is used as a fire danger indicator by most of the fire managers.

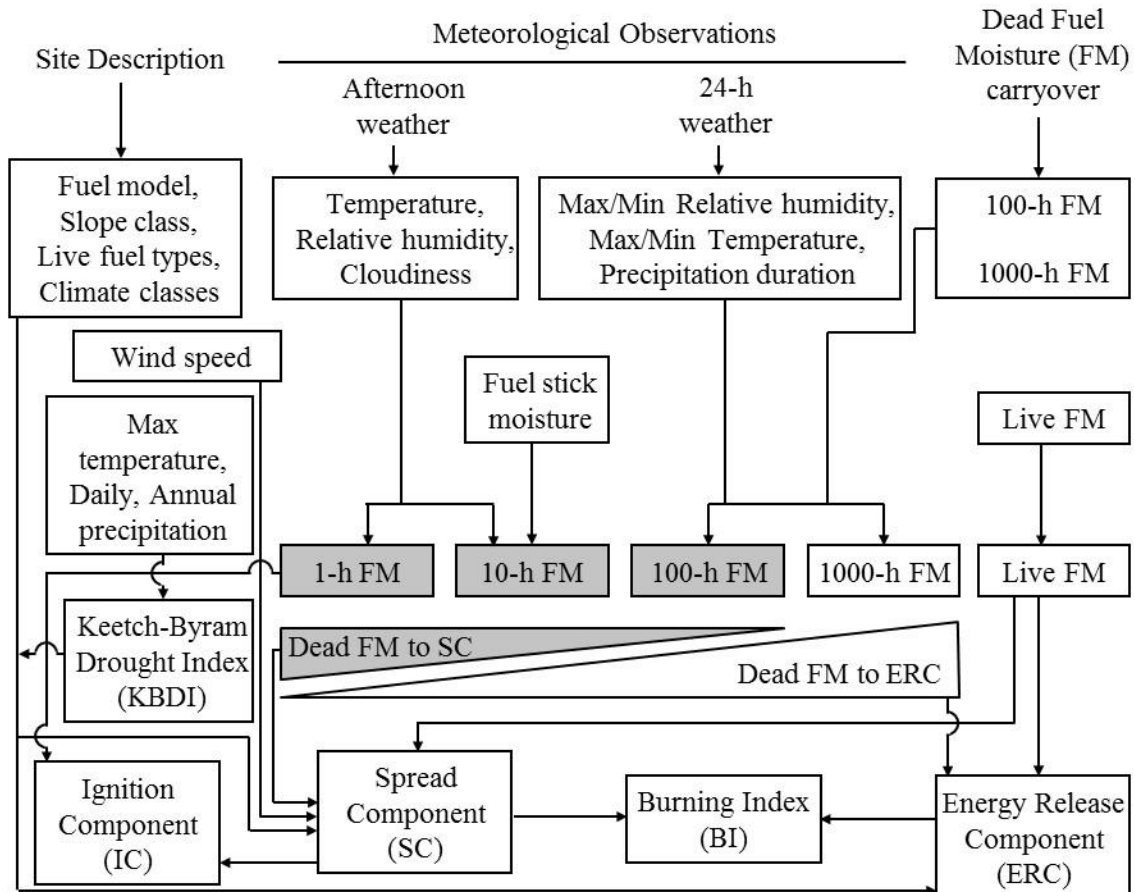


**Figure 2.4: Structure of the US National Fire Danger Rating System (adapted from Burgan, 1988).**

### *2.1.5 Limitations of the operational systems*

All of the major operational systems described in the earlier sub-sections, in general, suffer from the following drawbacks, such as:

- (i) All the operational systems are based on point-source meteorological data, located sparsely in a vast geographic extent. In general, the forecasting of danger conditions at or near meteorological stations resembles more accurate information compared to other parts of the landscape. In order to address this, it required installation of more meteorological stations (Hijmans et al., 2005; King and Furman, 1976), which would be quite expensive in terms of installation and maintenance, data collection and its processing.
- (ii) To delineate the spatial dynamics of the fire danger conditions the point-source observations of meteorological variables are used in the scope of all of the operational systems. In general, GIS based interpolation techniques are adopted to generate the surface maps of the variable of interest. It is worthwhile to emphasize that employment of different interpolation methods can produce different map outputs using the same input variables (Oldford et al., 2006; Leblon, 2005; Longley et al., 2010), thus forecasting of danger conditions over a large forested area limits the usability of the operational systems (Leblon et al., 2012).
- (iii) All the operational systems except the Russian Nesterov Index consider the dead fuel moisture as the danger indicator; however, the fire danger conditions may also depend on live fuel moisture conditions (Bajocco et al., 2010; De Angelis et al., 2012; Yebra et al., 2013). In fact, the live fuel moisture condition is a critical variable in defining fire danger conditions as it is closely related to the flammability of the live fuels and also propagation characteristics of fire.

- (iv) Apart from the Russian Nesterov Index system, a limited number of fuel types have been considered in the scope of all of the operational systems. These fuel-specific parameters (e.g., ignition temperature of woody material, rates of combustion, and extinction of moisture from vegetation, etc.) are determined by laboratory-based experiments (Wilson, 1985, 1990; Byram, 1963; Nelson, 1984). Thus, the characteristics of additional fuel types are required to be determined in the event of implementing these systems over other ecosystems.
- (v) In the framework of both Australian FFDRS and US NFDRS systems, KBDI has been used as a proxy of soil water content. The calculation of KBDI can be improved by incorporating the duration and intensity of precipitation (San-Miguel-Ayanz et al., 2003b).
- (vi) In general, the fire danger rating systems are fairly complex from an operational point of view and need complex data inputs in most of the instances (Lawler, 2004).

## **2.2 Remote sensing-based fire danger monitoring**

Remote sensing-based fire danger monitoring is the act of delineating danger conditions at the current time. It consists of the following four stages: acquisition of the remote sensing data of interest; calculation of remote sensing-derived variables/indices relevant to danger conditions; establishment of the relation between remote sensing-derived variables and danger-related indicators; and generation of the danger map. In terms of remote sensing-derived variables, these can be broadly grouped into several categories, e.g., vegetation greenness; meteorological variables; surface wetness conditions calculated by exploiting the relations between  $T_s$  and vegetation indices; and vegetation wetness condition, which are described in the following subsections.

### *2.2.1 Vegetation greenness*

Among the various vegetation greenness-related indices, the commonly used ones are: NDVI (i.e., calculated as function of surface reflectance of red [0.60–0.70  $\mu\text{m}$ ] and near infrared (NIR) [0.70–0.90  $\mu\text{m}$ ] spectral bands) (Rouse et al., 1973); soil adjusted vegetation index (SAVI: calculated as a function of red and NIR spectral bands) (Huete, 1988); global environmental monitoring index (GEMI: function of red and NIR spectral bands) (Pinty and Verstraete, 1992); relative greenness [RG: function of seasonal dynamics of NDVI or visible atmospherically resistant index (VARI: function of blue, green [0.50–0.60  $\mu\text{m}$ ] and red spectral bands)] (Burgan and Hartford, 1993; Kogan, 1990; Gitelson et al., 2002); and enhanced vegetation index (EVI: function of blue [0.40–0.50  $\mu\text{m}$ ], red and NIR spectral bands) (Huete et al., 2002) (see Table 2.1). Table 2.2 summarizes some of the example cases of these vegetation greenness indices in the literature.

**Table 2.1: List of common vegetation indices used for fire danger monitoring and their mathematical formulas.**

Index	Abbreviation	Formula	Reference
Normalized Difference Vegetation Index	NDVI	$\frac{\rho_{NIR} - \rho_R}{\rho_{NIR} + \rho_R}$	Rouse et al., 1973
Soil-Adjusted Vegetation Index	SAVI	$\frac{\rho_{NIR} - \rho_R}{\rho_{NIR} + \rho_R + L} (1 + L)$	Huete, 1988
Global Environmental Monitoring Index	GEMI	$eta(1 - 0.25eta) - \frac{\rho_R - 0.125}{1 - \rho_R}$ $eta = \frac{2(\rho_{NIR}^2 - \rho_R^2) + 1.5\rho_{NIR} + 0.5\rho_R}{\rho_{NIR} + \rho_R + 0.5}$	Pinty and Verstraete, 1992
Visible Atmospherically Resistant Index	VARI	$\frac{\rho_G - \rho_R}{\rho_G + \rho_R - \rho_B}$	Gitelson et al., 2002
Relative Greenness	RG <sub>NDVI</sub>	$\frac{NDVI_{cur} - NDVI_{min}}{NDVI_{max} - NDVI_{min}} \times 100$	Burgan and Hartford, 1993
Relative Greenness	RG <sub>VARI</sub>	$\frac{VARI_{cur} - VARI_{min}}{VARI_{max} - VARI_{min}} \times 100$	Kogan, 1990
Enhanced Vegetation Index	EVI	$2.5 \frac{\rho_{NIR} - \rho_R}{\rho_{NIR} + 6\rho_R + 7.5\rho_B + 1}$	Huete et al., 2002

Note:  $\rho$  is the surface reflectance values for blue (B), red (R), green (G), and near infrared (NIR);  $L=0.5$ .

$NDVI_{cur}$  is the current NDVI value of a pixel; and  $NDVI_{min}$  and  $NDVI_{max}$  are the historical minimum and maximum values of that particular pixel.

$VARI_{cur}$  is the current VARI value of a pixel; and  $VARI_{min}$  and  $VARI_{max}$  are the historical minimum and maximum values of that particular pixel.

**Table 2.2: Example of remote sensing-based vegetation greenness indices used in fire danger monitoring studies.**

Indices	Sensor	Method	Locations	Reference
		Estimated the dead fuel moisture indices (DMC, DC and BUI) of the Canadian FWI system over Canadian boreal forested ecosystems. In these cases, AVHRR-derived 10-day composite of NDVI were used. In all these studies, the correlations were reasonable (i.e., $r^2$ values in the range of 0.03-0.65).	Northwest Territories, Canada	Leblon et al., 2001
	Advanced Very High Resolution Radiometer (AVHRR)		Northern Alberta and southern Northwest Territories, Canada	Leblon et al., 2007
			Saskatchewan and Manitoba, Canada	Dominguez et al., 1994
NDVI	AVHRR	Developed a dynamic fire risk index as a function of NDVI and a set of static variables (that include proximity to road, slope, altitude, and type of vegetation cover). In general, the decrements in NDVI-values in the temporal dimension had an influence on the increment of the fire risk.	Mediterranean forests of Tenerife Island, Spain	Hernandez-Leal et al., 2006
	MODIS	Calculated monthly-composite of NDVI and correlated with the fire frequencies determined by MODIS-based hotspot data; and found a reasonable accuracy (i.e., $r^2$ value of 0.34).	Mazandaran forest, northern Iran.	Ardakani et al., 2011

Indices	Sensor	Method	Locations	Reference
	MODIS	Commissioned 16-day composite of NDVI data during 2001-2006 fire seasons. The differences of indices for every 16 days were fitted to the fire frequencies; and found no relationship.	Forested regions of Galicia and Asturias, Spain	Bisquert et al., 2014
RG	MODIS	Calculated as a function of 16-day composite of MODIS-derived NDVI and VARI. They observed that VARI-based RG had a strong relationship with the observed live fuel moisture (i.e., average $r^2$ value of 0.73) over evergreen shrubs. They also evaluated VARI-based RG values in calculating fire potential index (FPI) and then compared with the MODIS-based active fire products. These comparisons revealed reasonable correlation (i.e., $r^2$ value of 0.27).	Southern California, USA	Schneider et al., 2008
	AVHRR	Calculated from 10-day composite of NDVI and determined dead fuel moisture codes (i.e., DMC and DC) of the Canadian FWI system; and revealed good relationships (i.e., $r^2$ value in the range of 0.43-0.50).	Boreal forests of Saskatchewan and Manitoba, Canada  Northern boreal forests of Alberta and southern Northwest	Dominguez et al., 1994  Oldford et al., 2006

<b>Indices</b>	<b>Sensor</b>	<b>Method</b>	<b>Locations</b>	<b>Reference</b>
			Territories, Canada	
		Used 16-day composite of EVI with day of year to quantify fire activity. These models were able to differentiate the various fire danger levels having about 5% estimation errors.	Mediterranean forests, north-west Spain	Bisquert et al., 2011
EVI	MODIS	Employed the difference between two consecutive 16-day composite of EVI; and compared with the fire frequency during 2001-2006 fire seasons. It revealed that these differences were having good correlations (i.e., $r^2$ values in between 0.62 and 0.84).	Forested regions of Galicia and Asturias, Spain	Bisquert et al., 2014
SAVI, VARI GEMI	MODIS	Used 8-day composite of surface reflectance to calculate the vegetation indices and compared with fire frequencies during 2001-2006; and found good correlations for SAVI and GEMI (i.e., $r^2$ values in between 0.60 and 0.81).	Forested regions of Galicia and Asturias, Spain	Bisquert et al., 2014

### 2.2.2 Meteorological variables

Remote sensing-based meteorological variables (e.g.,  $T_s$ ,  $T_a$ , and RH) were used in monitoring fire danger conditions. For example:

- (i) AVHRR 10-day composite of  $T_s$  images were used in the boreal forests of northern Alberta and southern Northwest Territories, Canada (Leblon et al., 2007). The individual compositing period and cumulative  $T_s$  were correlated with the DC values of the Canadian FWI system. It was found that the cumulative  $T_s$  performed better than the individual  $T_s$  (i.e.,  $r^2$  value in the range of 0.32–0.76);
- (ii) Dead fuel moisture content was estimated using Meteosat Second Generation Spinning Enhanced Visible and Infrared Imager (MSG-SEVIRI) remote sensing data in the Iberian Peninsula of Spain (Nieto et al., 2010). In this study, two meteorological variables, such as the  $T_a$  (calculated by exploiting  $T_s$  and NDVI scatterplot) and RH (as a function of vapor pressure and precipitable water content, see equations 2.1–2.3) were derived. These were combined to calculate the equivalent moisture content (EMC) of vegetation and observed promising results (i.e., mean errors ranging from 1.9 to 2.7%);

$$e_a = g \frac{W(\lambda + 1)}{\delta} \quad (2.1)$$

where,

$W$  = precipitable water;

$g$  = acceleration of gravity;

$\lambda$  = exponent of power law that describe the atmospheric profile;

$\delta = 0.622$  is the ratio of specific gas constants of water vapor to dry air; and

$e_a$  = water vapor pressure.

$$e_0(T) = 0.6108 \exp \left[ \frac{17.027T}{T+273.3} \right] \quad (2.2)$$

where,

$e_0(T)$  = saturation vapor pressure at temperature T.

$$\text{Relative humidity, } RH = 100 \frac{e_a}{e_0} \quad (2.3)$$

- (iii) The dead fuel moisture codes of the FWI system (i.e., DC and DMC) were modeled using 10-day composite of AVHRR  $T_s$  images over the boreal forests in northern Alberta and the southern Northwest Territories of Canada (Oldford et al., 2006). The  $T_s$  was revealed good correlation with the DMC during the spring season (i.e.,  $r^2$  value of 0.34); and
- (iv) AVHRR-derived monthly composite of  $T_s$  were used to determine the fire risk indicator over the temperate forest in Central Mexico. During the period of November–February, the maximum and minimum values of  $T_s$  were computed and then generated the difference between them. These differences were evaluated against the actual fire occurrences and found that ~60% of the fires took place when they were between 8 and 15 °C (Manzo-Delgado et al., 2004).

Usually, both precipitation and humidity related variables derived from meteorological observations are an integral part in the frame of the operational forest fire danger forecasting systems throughout the world, such as CFFDRS system (van Wagner, 1987), US National Fire Danger Rating System (Burgan, 1988), Australian McArthur Forest Fire Danger Rating System (McArthur, 1967), and Russian Nesterov Index (Nesterov, 1949). It would be interesting to

mention that remote sensing-derived precipitable water (PW)-related variables were also used in various fire related studies. Those included: (i) Han et al., 2003 used the AVHRR and GOES-derived daily PW in conjunction with NDVI and  $T_s$  to calculate the FWI codes of the CFFDRS over the forested land in western Quebec, Canada during 1997; (ii) Sitnov and Mokhov, 2013 observed that the MODIS-derived PW values were less than the long term monthly average values over the fire spots in forested land of European Russia during July-August 2010; and (iii) Nieto et al., 2010 used the MSG SEVIRI-derived PW images to calculate relative humidity over Iberian Peninsula, Spain during 2005; which was one of the input variable in determining the dead fuel specific EMC and compared against the meteorological-based EMCs.

### *2.2.3 Surface wetness conditions*

For the last two decades, the relationship between vegetation index (VI) and  $T_s$  variables were exploited for estimating the surface wetness conditions. The  $T_s$ -VIs relationship are generally presented in scatter plots that generate either triangular or trapezoidal forms (Hassan et al., 2007) (see Figure 2.5). In the literature, several studies had demonstrated the effectiveness of  $T_s$ -VI in monitoring fire danger conditions, e.g.,

- (i) 10-day composite of AVHRR-derived NDVI and  $T_s$  images were used to calculate the slope between them that acted as a fire danger indicator (i.e., decrease in slope was related to increases in water stress) over the Mediterranean forest in east Spain (Illera et al., 1996). The derived slopes were found to detect approximately 68% of the fire events while the slopes were having a decreasing trend;

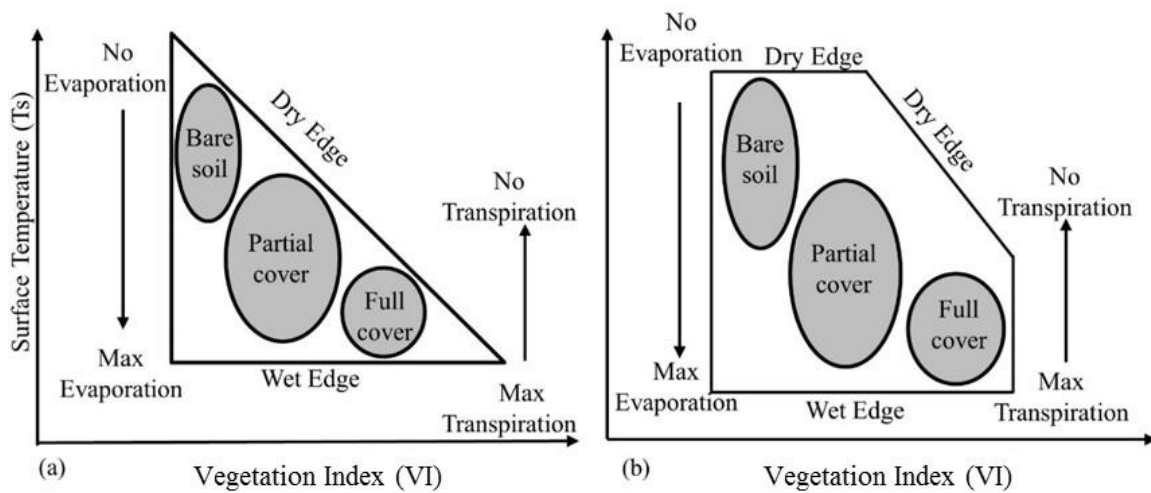


**Figure 2.5: (a) Triangular and (b) trapezoidal forms based on a relationship between  $T_s$  and VIs (adapted from Sandholt et al., 2002 and McVicar and Jupp, 1998).**

- (ii) 10-day composite of AVHRR-derived NDVI/ $T_s$  ratio, RG and accumulated sunshine hours (meteorological data) were integrated and found good agreement with the DC values of the Canadian FWI system (i.e.,  $r^2$  value of 0.79) over the Mediterranean forest in south Spain (Aguado et al., 2003);
- (iii) 8-day composite of AVHRR-derived NDVI and  $T_s$  in conjunction with the day of year were employed for estimating the fuel moisture content as part of fire danger rating over the Mediterranean grasslands and shrubs in Spain (Chuvieco et al., 2004c). The model showed good agreements with the ground-based estimates of fuel moisture content (FMC) (i.e.,  $r^2$  values greater than 0.8 for both grass and shrubs); and

- (iv) MODIS-derived 8-day composite of  $T_s$  and 16-day composite of EVI data were used to develop a disturbance index (DI) over a broad range of bioclimatic regions in the western United States (Mildrexler et al., 2007). The DI values were generated using the annual maximum  $T_s$ /EVI ratios to multi-year mean values. Under normal conditions (i.e., absence of disturbance) the DI value would be  $\sim 1.0$  and in case of wildfire, it would be  $>1.0$  (i.e.,  $T_s$  would increase and EVI would decrease for the current year compared to multi-year mean value). Comparison of the DI values ( $>1.64$ ) against MODIS active fire data and other fire perimeter maps found close correspondence.

#### *2.2.4 Vegetation wetness condition*

Several indices representing vegetation wetness conditions [i.e., calculated as a function of NIR and shortwave infrared (SWIR) spectral bands] were implemented to determine the fuel moisture content as an indicator of fire danger (see Table 2.3). The commonly used indices include: NMDI, normalized difference water index (NDWI), simple relation water index (SRWI), normalized difference infrared index (NDII), global vegetation moisture index (GVMI), canopy water content (CWC), water index (WI), and moisture stress index (MSI). Some of the example cases by use of these indices are summarized in Table 2.4.

**Table 2.3: List of common vegetation wetness indices used for fire danger monitoring and their mathematical formulas.**

Index	Abbreviation	Formula	Reference
Normalized Difference Vegetation Index	NMDI	$\frac{\rho_{NIR} - (\rho_{SWIR_2} - \rho_{SWIR_3})}{\rho_{NIR} + (\rho_{SWIR_2} + \rho_{SWIR_3})}$	Wang and Qu, 2007
Normalized Difference Water Index	NDWI*	$\frac{\rho_{NIR} - \rho_{SWIR_1}}{\rho_{NIR} + \rho_{SWIR_1}}$	Gao et al., 1996
Simple Relation Water Index	SRWI	$\frac{\rho_{NIR}}{\rho_{SWIR_1}}$	Zarco-Tejada et al., 2003
Normalized Difference Infrared Index	NDII	$\frac{\rho_{NIR} - \rho_{SWIR_2}}{\rho_{NIR} + \rho_{SWIR_2}}$	Hardisky et al., 1983
Global Vegetation Moisture Index	GVMI	$\frac{(\rho_{NIR} + 0.1) - (\rho_{SWIR_2} + 0.02)}{(\rho_{NIR} + 0.1) + (\rho_{SWIR_2} + 0.02)}$	Ceccato et al., 2002a,b
Water Index	WI	$\frac{\rho_{NIR}}{\rho_{SWIR_1}}$	Peñuelas et al., 1993
Moisture Stress Index	MSI	$\frac{\rho_{SWIR_2}}{\rho_{NIR}}$	Hunt and Rock, 1989

*Note:  $\rho$  is the surface reflectance value of near infrared (NIR), and shortwave infrared (SWIR<sub>1</sub>, SWIR<sub>2</sub>, and SWIR<sub>3</sub> centered at ~1.24, ~1.64, and ~2.14  $\mu$ m) bands.*

*\*In the formulation of NDWI, several wavelengths such as ~1.24, ~1.64, and ~2.14  $\mu$ m can be employed.*

**Table 2.4: Example of remote sensing-based vegetation wetness indices used in fire danger monitoring.**

Indices	Sensor	Method	Locations	Reference
NDWI	MODIS	Established relations between FMC and: (i) 8-day composite of NDWI (Stow et al., 2005); and (ii) 10-day composite of NDWI (Dennison et al., 2005). The agreements were reasonable in both of the cases, such as $r^2$ value of: (i) 0.50 in case of Stow et al., 2005; and (ii) between 0.39 to 0.80 for Dennison et al., 2005.	Chaparral shrublands in California, USA	Stow et al., 2005; Dennison et al., 2005
NDWI, NDII, GVMI, MSI, SRWI	MODIS	Used 8-day composite for the index of interest and compared with the FMC and equivalent water thickness (EWT); and found good agreements in most of the cases (i.e., $r^2$ values in the range of 0 to 0.81).	Savanna forests in Senegal, West Africa	Sow et al., 2013
NMDI, NDWI	MODIS	Employed daily NMDI and NDWI-values in detecting forest fires. The performance was evaluated against the MODIS-based active fire spots during the fire occurrences and observed that NMDI performed better (i.e., matched with over 75% of the fire instances).	Southern Georgia, USA and mixed forests in southern Greece.	Wang et al., 2008
GVMI, NDVI	MODIS	Employed 8-day composite to calculate the vegetation water content (VWC) using the empirical relationship of GVMI and	Inner Mongolia plateau and	Jiang et al., 2012

Indices	Sensor	Method	Locations	Reference
		EWT. In addition, monthly composite of NDVI were also compared with the VWC. Both of the indices indicated that their lowest values were coincided with the fire occurrences during the period of spring fires (March to May).	Song Liao plain.	
NDWI, CWC	MODIS	Compared 8-day composite of these indices with the FMC; and found to have reasonable relations (i.e., $r^2$ values in the range of 0.26 to 0.44).	Northern Utah, USA	Qi et al., 2012
NDII, NDWI	MODIS	Used 16-day composite and compared with the FMC. Multiple regressions was performed during the period of 2000-2006 and found good relationships (i.e., $r^2$ values in the range of 0.64 to 0.70).	Chaparral shrublands in California, USA	Peterson et al., 2008
NDII, WI, NDWI, EWT	Airborne Visible Infrared Imaging Spectrometer (AVIRIS), MODIS	Employed both AVIRIS and MODIS-derived indices during the period 1994-2004 with the FMC; and found that the AVIRIS-derived indices were better correlated (i.e., $r^2$ values in between 0.72 to 0.85) than the MODIS-derived ones (i.e., $r^2$ values in between 0.55 to 0.61)	Shrublands in California, USA	Roberts et al., 2006

### *2.2.5 Fire danger monitoring using SAR images*

In addition to optical and thermal remote sensing data for monitoring forest fire danger conditions, a number of studies had been carried out to assess the possibilities of using Synthetic Aperture Radar (SAR). The SAR was used due to its ability to capture images independently from daylight, cloud coverage and weather conditions. In particular to forest coverage, the backscatter energy received by the sensors depends on the moisture conditions of the forest floor, canopy and precipitation events which could be utilized for describing the fire danger conditions. Some such studies using SAR images are as follows: (i) ERS-1 SAR data were used to assess the dead fuel moisture conditions over the northern boreal forest in Northwest Territories, Canada (Leblon et al., 2002); and good relationships were found between the radar backscatter and FWI codes (i.e.,  $r^2$  values in between 0.30 and 0.40 for DMC, DC and BUI); (ii) ERS-1 and ERS-2 SAR-derived backscatter values were used to calculate the DC values of the FWI system over boreal forests of Alaska, USA (Bourgeau-Chavez et al., 2007); and found to have reasonable agreements (i.e.,  $r^2$  values  $\sim$ 0.64); and (iii) Radarsat-1 images were used to extract the backscatter values over the northern boreal forest in south-central of Northwest Territories, Canada (Abbott et al., 2007); and the comparison of radar backscatter values were found to have a strong relationship with the FWI codes (i.e.,  $r^2$  values in between 0.68 and 0.83, 0.77 and 0.82, 0.72 and 0.86, and 0.62 and 0.85 for DMC, DC, BUI, and FWI respectively).

### *2.2.6 Limitations of remote sensing-based monitoring systems*

The review of the remote sensing-based monitoring systems revealed that the accuracies of the environmental variables as a fire danger indicator have shown a wide range of  $r^2$  values. As fire occurrences depend on both meteorological and biophysical variables, thus, the use of single variable might not be able to show the fire danger conditions appropriately due to the following reasons:

- (i) Vegetation greenness-related variables are slow responding ones, which reflects long-term conditions (i.e., does not change over short period even though drought persists in vegetation) (Leblon et al., 2001; Vicente-Serrano et al., 2012) and relates to several other variables, such as sunlight; temperature; soil moisture; and inter and intra species competition.
- (ii) The precisions observed using the meteorological variable  $T_S$  found to be varied considerably due to several reasons, e.g., the sensor signals might be saturated due to high temperature difference between fires and earth's surface (Realmuto et al., 2011); low spatial resolution of  $T_S$  might lessen the circumstantial information (Leblon et al., 2007); fires manifest a diurnal cycle (Zhang et al., 2011; Beck et al., 2001) which might be biased due to observation in fixed time by the sensors; and heterogeneous properties of the emissivity of the land surface.
- (iii) Combination of  $T_S$ -VI would not be suitable over topographically variable terrains (Carlson, 2007). It is the case as  $T_S$  is often lower in high elevation areas compared to low-lying areas within the same geographical region. As such, employment of non-elevation corrected  $T_S$  images could incorrectly delineate that surface wetness conditions in upland areas are wetter than in low-lying areas (Hassan et al., 2007; Akther and Hassan, 2011b).

- (iv) Application of vegetation wetness condition using NIR and SWIR spectral bands have several limitations, such as vegetation moisture estimation is an approximation method (both field and remote sensing); difficult to measure EWT at field level (Chuvienco et al., 2003); relationship between FMC/EWT and vegetation moisture are species-specific (thus understanding of biophysical properties of species mixtures would be useful); and SWIR generally affected by other factors (e.g., vegetation canopy, illumination and viewing positions, and soil characteristics), etc. Also issues like quantification the error-levels of the remote sensing-derived FMC values and their implementation in the scope of operational fire danger forecasting systems pose enormous challenges (Yebra et al., 2013).
- (v) SAR usually provides higher resolution images, but has an inherent problem of speckles which look as a grainy texture due to random constructive and destructive interference from the multiple scattering. Other problems that are noticeable includes, e.g., right angle surfaces causes double bounce reflection; volume scattering may occur when the radar beam penetrates the top most surface; and the brightness of the image increase due to high moisture content of the target surface (Moreira et al., 2013). Moreover, the radar operates under commercial mode and the revisits time period is quite long (i.e., ERS-1/2 repeat cycle is around 35 days compared to Radarsat-1/2 almost 24 days coverage) (Joyce et al., 2009; Leblon et al., 2012) which limits capturing the temporal dynamics of the moisture conditions. On the contrary, some of the optical and thermal remote sensing images (e.g., AVHRR, MODIS, Landsat, etc.) are completely free for public uses and also the temporal resolution of these images are relatively higher, e.g., AVHRR and MODIS at daily and Landsat at 16-days.

In addition to the above mentioned limitations of the remote sensing-based fire danger monitoring methods, in principle, have suffered much from the operational perspective. Because fire danger condition cannot be monitored as it portrays futuristic events (i.e., the occurrences of the fire events have not been materialized). However, the fire occurrences could be monitored using the current time variables and helpful in assessing the forest fire related disaster. Moreover, MODIS-based fire detection data are available at a daily temporal scale which is well accepted, fully operational and used by the fire managers for monitoring purposes. So, the remote sensing-based methods developed during the past several decades mostly suffer from the forecasting capabilities, and not considered as operational ones.

### **2.3 Remote sensing-based fire danger forecasting systems**

In addition to the above remote sensing-based monitoring techniques described in section 2.2, it would be worthwhile to note that a limited number of studies had found in the literature on the use of remote sensing in forecasting forest fire danger conditions. In these cases, the remote sensing-based indicators were calculated prior to the fire occurrences and then compared with the actual fire occurrences for validation purposes. Some of such example studies are briefly described in Table 2.5.

**Table 2.5: Brief description of some remote sensing-based fire danger forecasting systems.**

<b>Reference</b>	<b>Method</b>	<b>Limitations</b>
Vidal and Devaux-Ros, 1995	Calculated water stress in vegetation as a fire risk indicator over the Les Maures Mediterranean forest in southern France. In this study, Landsat TM-derived NDVI and $T_S$ images were used during dry periods of 1990 and 1992 as well as the $T_a$ maps generated from point-source measurements available at weather stations. The scatter-plots between NDVI and $T_S$ - $T_a$ interpreted to calculate the WDI. These plots were having trapezoid shapes and defined by dry (i.e., line of highest temperature to NDVI that represents an insufficient amount of water for evapotranspiration) and wet edges (i.e., representing the lowest temperature line to NDVI and have enough amount water for evapotranspiration) (Akther and Hassan, 2011a; Hassan and Bourque, 2009). The comparison between the real fire occurrences data and pre-fire WDI found that location where $WDI \geq 0.6$ coincided with 100% of the fires.	The major issue was the limited use of satellite data (i.e., only three images). Thus, the authors intended to extend the scope of validation, which was not materialized (Vidal, personal communication)
Guangmeng and Mei, 2004	Used MODIS-derived $T_S$ images to evaluate the forest fire risk over the evergreen and deciduous forested region in northeast China during the period of April-May of 2003. The $T_S$ was evaluated over $20 \times 20$ pixels around the fire site and found an increasing trend at least 3-days before fire occurrence.	The study did not quantify the rate of increment of the $T_S$ values.
Oldford et al., 2003	Employed AVHRR-derived $T_S$ and NDVI images for mapping the pre-fire forest conditions during 11-day period preceding to fire occurrences over the northern	The $T_S$ alone might not be sufficient enough

Reference	Method	Limitations
	boreal forests in Northwest Territories, Canada. The temporal trends of both of the variables revealed that the $T_s$ -values were increasing at least 3-days earlier than the fire occurrences, while NDVI didn't show clear indications. In addition, $T_s$ values compared against the FWI code derived from meteorological variables; and revealed a good relationship for burned (i.e., $r^2$ value of 0.55) and unburned (i.e., $r^2$ value of 0.65) forested areas.	for forecasting danger conditions as such danger depends on so many other biophysical variables.
Bisquert et al., 2011	Used MODIS-based 16-day composite EVI difference images and period of year for calculating fire occurrence over Galicia, Spain during 2001-2006 and found overall accuracy of 58.2% when compared with observed fires. In this study, input variable (i.e., EVI of $250 \times 250$ m resolution) was resampled into low spatial resolution ( $10 \times 10$ km).	Prediction for 16-day period was inappropriate for day-to-day forecasting purposes.
Akther and Hassan, 2011a	Commissioned MODIS-derived variables (i.e., $T_s$ , NMDI and TVWI at 8-day temporal scale) to forecast the forest fire danger conditions over the boreal forested region of Alberta during 2006-2008. The fire danger forecasting system was formulated by integrating all the three variables. For example: during $i+1$ period the fire danger conditions would be determined upon comparing the instantaneous values of the variable of interest and their study area-specific average values during $i$ period. The danger would be high if: (i) $T_s$ values would be higher or equal (i.e., high temperature might favor fire ignition); or (ii) NMDI or TVWI values less or equal (i.e., low	Despite having reasonable agreements, two specific shortcomings could be noted, such as (i) data gaps due to cloud contamination in the input variables were excluded; and (ii)

Reference	Method	Limitations
	vegetation moisture and/or surface wetness might sustain fire); in comparison to the study area-specific average values. As such, four fire danger classes were possible, such as (i) very high - all variables designated as high danger; (ii) high – at least two variables designated as high; (iii) moderate – at least one variable label as high; and (iv) low – all variables indicated low danger category. The comparison of the above mentioned fire danger categories with the real wildfire data (available from Alberta Government) revealed that ~91.6% of the fires fell under the ‘very high’ to ‘moderate’ categories.	computation of TVWI was relatively complex and highly dependent on the skills of the professionals involved.

In order to evaluate the performance of the systems described in the scope of Akther and Hassan (2011a), I applied them to forecast the danger conditions during the catastrophic fires in 2011 taken place during mid-May, in particular to Slave Lake [that incurred an estimated economic loss of \$700 million (FTCWRC, 2012)] and Fort McMurray regional fires [responsible for burning of 595,000 ha of muskeg and bush (Treenotic, 2011)] in Alberta. In the danger map, the input variables (i.e.,  $T_s$ , NMDI and TVWI in Figure 2.6) was acquired during May 1–8, 2011. The method demonstrated its excellent abilities to forecast these fires (i.e., 100% and 88.7% of the fire spots fell under ‘very high’ to ‘high’ danger categories for Slake Lake and Fort McMurray regional fires).

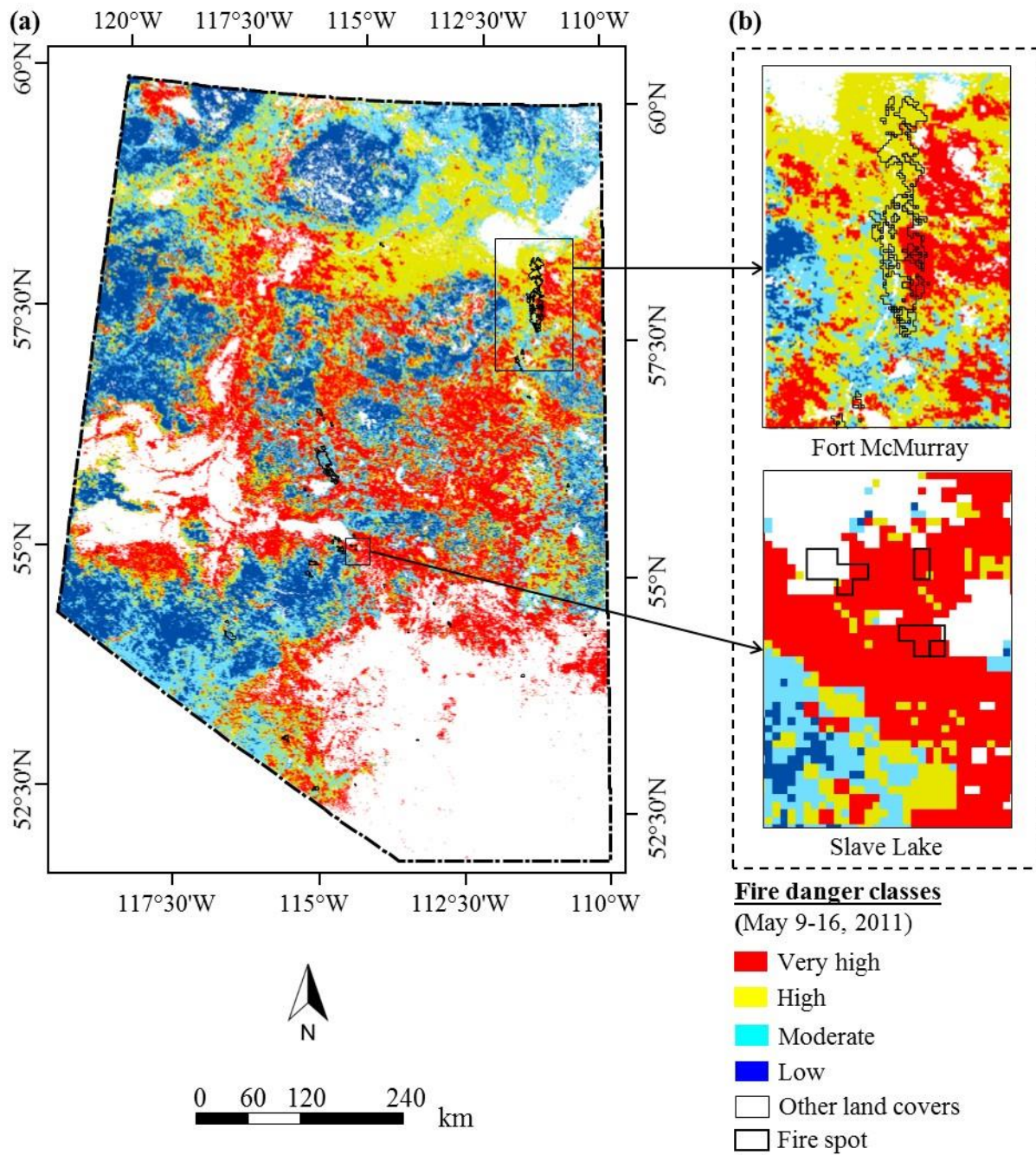


**Figure 2.6: Fire danger map for the period May 9–16, 2011 generated by combining  $T_s$ , NMDI, and TVWI (after Akther and Hassan, 2011a) variables acquired during the prior 8-day period (i.e., May 1–8, 2011).**

It would be worthwhile to note that remote sensing-based forecasting systems would be more robust upon incorporating other critical variables, such as incident solar radiation, precipitation, relative humidity, and wind speed; human induce fire ignition sources and lightning frequency; spatially dynamic but temporally static variables, these are elevation, aspect, slope, proximity to roads, and vicinity to settlements; impact of long weekend that relates with movement of people in particular to forested areas and its relation; phenological stages of the vegetation (i.e., impact of climate on vegetation development phases); enhancement of both spatial and temporal resolutions; and evaluation of the systems in other ecosystems.

#### **2.4 Synergy between operational forecasting systems and remote sensing-based methods**

The synergy between the operational fire danger forecasting systems and remote sensing-based methods are rarely found in the literature due to the variation in temporal (i.e., daily to hourly observations of meteorological parameters and remote sensing-derived variables acquired depending on the revisit time of the satellites) and spatial (i.e., discrete objects in case of meteorological observations and continuous field of observations for remotely sensed data) dimensions of the both systems. However, the Wildland Fire Assessment System of US Forest Service integrates multitemporal and multi-spatial observations to forecasts a series of environmental conditions that delineate fire prone areas (Burgan et al., 1997). It combines fuel models, meteorological observations, and remote sensing-derived variable (i.e., NDVI). The system has been generating FPI (i.e., synergy between NFDRS described in section 2.1.4 and remotely sensed NDVI) on a daily basis since 1990s (Burgan et al., 1996, 1998; Preisler et al., 2009).

In the process of FPI development, there are three input variables (see Figure 2.7). Those include: (i) 10-h dead fuel moisture conditions produced as a function of meteorological variables in the framework of NFDRS (see Figure 2.4); (ii) RG-derived from AVHRR-based 7-day composite of NDVI at 1 km spatial resolution; and (iii) dead fuel moisture of extinction calculated as a function of 8-month composites of NDVI (Goward et al., 1990), land cover maps (Loveland et al., 1991), and ground-based information about fuel characteristics. Comparison between the FPI and standard NFDRS maps have revealed that FPI maps are showing better spatial variability (Burgan et al., 1998). In general, this synergy requires several input variables and also complex in nature. Thus, adopting this system in another ecosystem would require significant amount of effort.

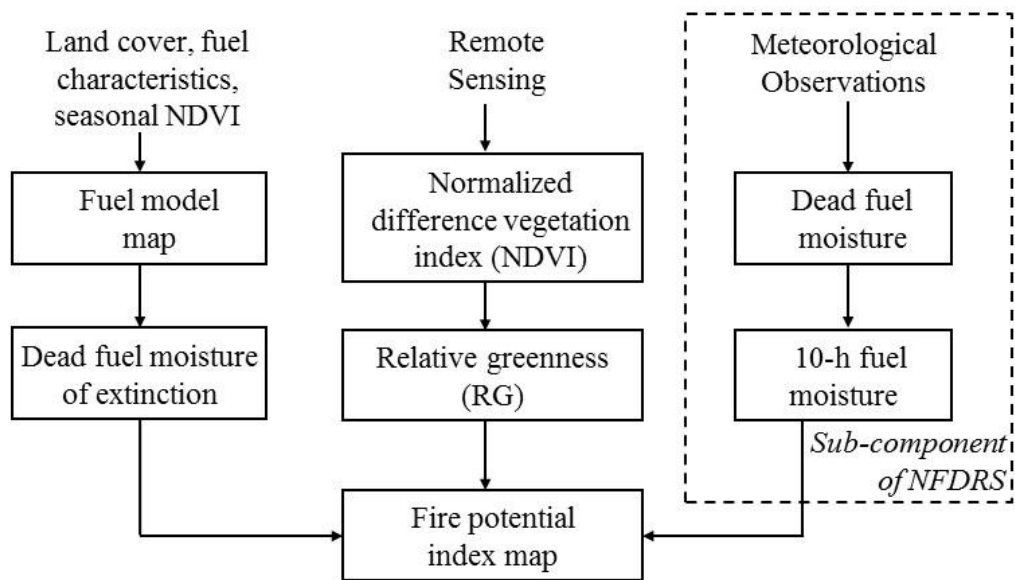


**Figure 2.7: The operational system to produce the fire potential map using remote sensing-derived variable and National Fire Danger Rating System (see Figure 2.4) (adapted from Burgan et al., 1998).**

## 2.5 MODIS characteristics

MODIS is considered as one of the most widely used remote sensor in determining various environmental hazards around the world including the forest fire. MODIS instrument is aboard with Terra and Aqua satellites. Terra satellite orbits the earth in descending mode (i.e., north to south) and acquires data about 10:30 am local time; and Aqua acquires data around 1:30 pm local time in an ascending mode (i.e., south to north). MODIS platforms are near polar, sun synchronous, and traverse in circular orbit of 705 km above the earth surface with a swath of 2330 km (cross track) by 10 km (along track). The MODIS satellite enables us to understand the global dynamics and processes occurring on the earth surface (i.e., land and ocean), and lower atmosphere (NASA, 2011). The characteristics of MODIS sensors and spectral bands are presented in Tables 2.6 and 2.7.

Among the other multispectral remote sensors (e.g., NOAA-AVHRR, LANDSAT, etc.), MODIS is used extensively due to its various advantages over other remotely sensed platforms/sensors.

The MODIS standard products are preferable by the scientists due to the following reasons:

- (i) MODIS data products are available at high temporal resolution (i.e., daily-scale in most parts of the world);
- (ii) MODIS instrument provides high radiometric sensitivity (12 bit) in 36 spectral bands ranging a spectrum of 0.4  $\mu\text{m}$  to 14.4  $\mu\text{m}$ . Whereas, AVHRR (10 bit) has 6 spectral bands that covers visible (i.e., centered at 0.6  $\mu\text{m}$ ), NIR (i.e., centered at 0.86  $\mu\text{m}$ ), SWIR (i.e., centered at 3.74  $\mu\text{m}$ ), and long wave for surface temperature (i.e., 11–12  $\mu\text{m}$ ); and LANDSAT (8 bit) has 7 spectral bands in the range of 0.5  $\mu\text{m}$  to 12.5  $\mu\text{m}$  with coverage of visible, NIR, SWIR, and long wave for surface temperature;

- (iii) The MODIS data provides higher spatial resolution in various spectral bands that ranges from 250–1000 m. On the other hand, the AVHRR images have 1.1 km spatial resolution at nadir and 5 km off-nadir. However, LANDSAT data are most preferable as it has higher spatial resolution (i.e., 30 m). However, MODIS would more preferable in the event of monitoring the earth at higher temporal resolution (i.e., 1-2 days); and
- (iv) MODIS provides reflectance data which are geo-referenced, radiometrically calibrated, and atmospherically corrected. Similar remotely sensed data from other platforms require such pre-processing to be performed by the individual users.

Thus, in this research I opted to use various MODIS-based data products (i.e., see details in section 3.2) in the development of a forest fire danger forecasting system.

**Table 2.6: MODIS specifications (NASA, 2011)**

Parameters	Specifications
Orbit	705 km, 10:30 a.m. descending node (Terra) or 1:30 p.m. ascending node (Aqua), sun-synchronous, near-polar, circular
Scan rate	20.3 rpm, cross track
Swath dimensions	2330 km (cross track) by 10 km (along track at nadir)
Quantization	12 bit
Spatial resolution	250 m (bands 1-2) 500 m (bands 3-7) 1000 m (bands 8-36)
Repeat cycle	1-2 days
Design life	6 years

**Table 2.7: Characteristics of MODIS spectral bands (reflected: 1–19, 26; emitted: 20–25, 27–36) (NASA, 2011).**

<b>Band No.</b>	<b>Spectral resolution (µm)</b>	<b>Major use</b>
1	0.620–0.670	Absolute Land Cover Transformation, Vegetation Chlorophyll
2	0.841–0.876	Cloud Amount, Vegetation Land Cover Transformation
3	0.459–0.479	Soil/Vegetation Differences
4	0.545–0.565	Green Vegetation
5	1.230–1.250	Leaf/Canopy Differences
6	1.628–1.652	Snow/Cloud Differences
7	2.105–2.155	Cloud Properties, Land Properties
8	0.405–0.420	Chlorophyll
9	0.438–0.448	Chlorophyll
10	0.483–0.493	Chlorophyll
11	0.526–0.536	Chlorophyll
12	0.546–0.556	Sediments
13	0.662–0.672	Atmosphere, Sediments
14	0.673–0.683	Atmosphere, Sediments
15	0.743–0.753	Chlorophyll Fluorescence
16	0.862–0.877	Chlorophyll Fluorescence
17	0.890–0.920	Aerosol Properties
18	0.931–0.941	Aerosol Properties, Atmospheric Properties
19	0.915–0.965	Atmospheric Properties, Cloud Properties
20	3.660–3.840	Atmospheric Properties, Cloud Properties
21	3.929–3.989	Atmospheric Properties, Cloud Properties
22	3.929–3.989	Sea Surface Temperature
23	4.020–4.080	Forest Fires & Volcanoes
24	4.433–4.498	Cloud Temperature, Surface Temperature
25	4.482–4.549	Cloud Temperature, Surface Temperature
26	1.360–1.390	Cloud Fraction, Troposphere Temperature
27	6.535–6.895	Cloud Fraction, Troposphere Temperature
28	7.175–7.475	Cloud Fraction (Thin Cirrus), Troposphere Temperature
29	8.400–8.700	Mid Troposphere Humidity
30	9.580–9.880	Upper Troposphere Humidity
31	10.780–11.280	Surface Temperature
32	11.770–12.270	Total Ozone
33	13.185–13.485	Forest Fires & Volcanoes, Surface Temp.
34	13.485–13.785	Forest Fires & Volcanoes, Surface Temperature
35	13.785–14.085	Cloud Fraction, Cloud Height
36	14.085–14.385	Cloud Fraction, Cloud Height

## CHAPTER 3 : STUDY AREA & DATA PRE-PROCESSING

### 3.1 Description of study area

The Canadian province of Alberta is comprised of six natural regions (i.e., ecological units based on combined influence of climate, topography, vegetation, soils and geology). Among them, the boreal forest alone occupies approximately 58% of the province (Downing and Pettapiece, 2006), which often faces recurrent fire disturbances. Every year on an average approximately 1560 fires was taken place that was responsible for burning ~196 thousand ha during the period 2003-2012 (ESRD, 2014). In this research, the northern part of the province is considered as the study area, which lies between 52–60 °N latitude and 110–120 °W longitude. It is shown in Figure 3.1 using a MODIS-derived annual land cover composite map at 500 m spatial resolution (i.e., MCD12Q1 v.005) and fire spots from Alberta Environment and Sustainable Resource Development (ESRD). The study area is found to have eleven land coverage types (that include water, grasses/cereal crops, shrubs, broadleaf crops, savanna, evergreen broadleaf forest, deciduous broadleaf forest, evergreen needleleaf forest, deciduous needleleaf forest, non-vegetated, and urban). Among these, the four forest types (i.e., evergreen broadleaf forest, deciduous broadleaf forest, evergreen needleleaf forest, deciduous needleleaf forest) occupies approximately 75% of the study area, which is considered as the region of interest for forecasting the fire danger conditions. Topographically, the study area is variable in the range 162–3,596 m above the mean sea level and having a general increasing trend from north-east to south-west. The study area experiences cold winters and short warm summers; and moderate annual precipitation that increases with elevation. Climatically, the study area experiences mean annual temperature that varies in the range -3.6 to

1.1 °C; and mean annual precipitation varies in the range 377–535 mm (Downing and Pettapiece, 2006).

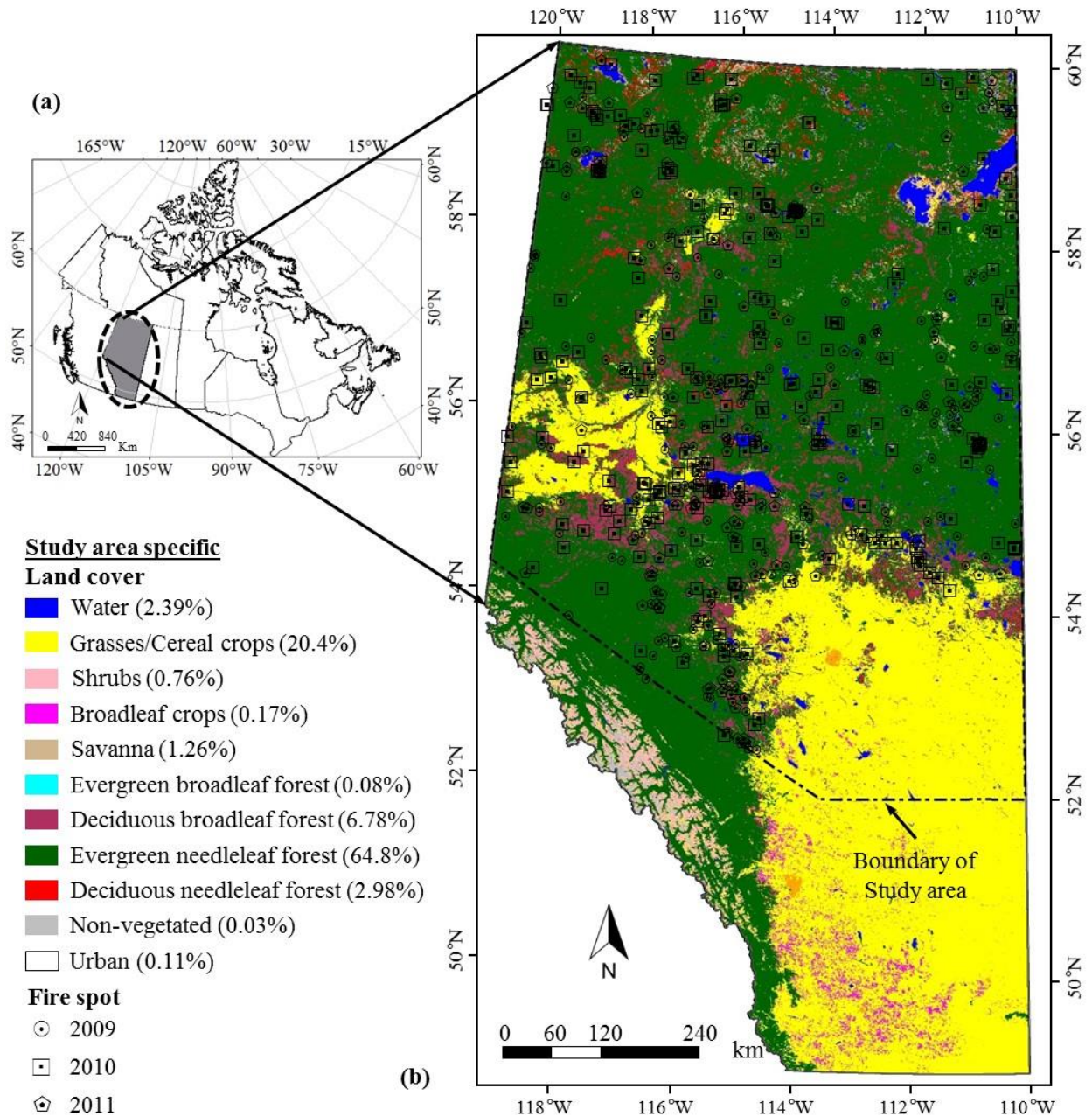


**Figure 3.1: (a) Location map of Alberta Province in Canada; (b) extent of study area within a MODIS-based land cover map of 2008 and ESRD fire spots during 2009-2011.**

### 3.2 Dataset used

Remote sensing data available from National Aeronautics and Space Administration (NASA) were used in the study. MODIS-derived environmental variables were employed for forecasting the forest fire danger conditions during 2009-2011 fire seasons [i.e., March–September in the range of 89–272 Julian day of year (DOY)]. Those included:

- (i) 8-day composite of  $T_s$  at 1 km spatial resolution (i.e., MOD11A2 v.005) and its associated quality control (QC) information at 1 km spatial resolution. The QC was used to quantify the amount of data gaps and/or good quality pixels;
- (ii) 8-day composite of surface reflectance at 500 m spatial resolution (i.e., MOD09A1 v.005); which provided surface reflectance at 7 (seven) spectral bands and its associated quality assurance (QA) information at 500 m spatial resolution. Among the seven spectral bands, the bands centered at 0.645  $\mu\text{m}$  (i.e., red), 0.86  $\mu\text{m}$  (i.e., near infrared [NIR]), 1.64  $\mu\text{m}$  (i.e., shortwave infrared [SWIR]), and 2.13  $\mu\text{m}$  (i.e., SWIR) were used. These surface reflectance images were used to calculate both NMDI and NDVI. Additionally, the QAs were used to quantify the amount of data gaps and/or good quality pixels in the NMDI and NDVI images;
- (iii) daily PW at 1 km spatial resolution (i.e., MOD05L2 v.051) and their corresponding geolocation images; and
- (iv) annual land cover map at 500 m spatial resolution (i.e., MCD12Q1 v.005) during 2008.

Apart from the satellite data, I also used historical wildfire information from Alberta ESRD during 2009-2011 fire seasons; and considered those fire spots that burned an area greater than or equal to 1 ha. It would be interesting to note that both  $T_s$  and surface reflectance data (i.e., used to

calculate NMDI, and NDVI) could be found at daily scale from MODIS satellite; however, I employed their 8-day composite. The prime rationale of considering 8-day composite of  $T_s$ , NMDI, and NDVI was related with the fact that the computation of all these variables would highly influence by the atmospheric conditions in particular to the presence of cloud (Wan, 1999; Vermote and Vermeulen, 1999).

### **3.3 Data pre-processing**

The pre-processing of all the input variables which mainly comprised of MODIS-based data products, fire spot data, and other relevant GIS data layers were executed in several steps and described in the following sub-sections.

#### *3.3.1 MODIS data pre-processing*

The pre-processing of MODIS data were done in four steps which comprised of data download, reprojection, mosaic of images, and retrieval of variables of interest.

##### Downloading of MODIS data

MODIS Terra  $T_s$ , and surface reflectance; and their corresponding quality data (i.e., QC and QA) were downloaded from the NASA's Earth Observing System Data and Information System (EOSDIS) website. MODIS Terra data was available in Hierarchical Data Format (HDF) with various spatial and temporal resolutions as a raster tile. Two raster tile images were selected to cover the entire study area; and downloaded the 8-day composite and daily data products. In total 276 images were downloaded for each year (i.e., 2009–2011) which comprised of 23 periodical data of  $T_s$  and corresponding QC images; 23 periodical data of surface reflectance and their

corresponding QA images; and 184 daily PW and their geolocations images. Table 3.1 shows the detail of the time periods of data downloaded and their respective DOY.

**Table 3.1: List of MODIS data used during the period of 2009-2011.**

<b>Period</b>	<b>DOY</b>	<b>Dates</b>	<b>Period</b>	<b>DOY</b>	<b>Dates</b>
<i>8-day composite of <math>T_s</math>, surface reflectance; and corresponding QC and QA images</i>					
1	89 – 96	30 Mar – 6 Apr	13	185 – 192	4 Jul – 11 Jul
2	97 – 104	7 Apr – 14 Apr	14	193 – 200	12 Jul – 19 Jul
3	105 – 112	15 Apr – 22 Apr	15	201 – 208	20 Jul – 27 Jul
4	113 – 120	23 Apr – 30 Apr	16	209 – 216	28 Jul – 4 Aug
5	121 – 128	1 May – 8 May	17	217 – 224	5 Aug – 12 Aug
6	129 – 136	9 May – 16 May	18	225 – 232	13 Aug – 20 Aug
7	137 – 144	17 May – 24 May	19	233 – 240	21 Aug – 28 Aug
8	145 – 152	25 May – 1 Jun	20	241 – 248	29 Aug – 5 Sep
9	153 – 160	2 Jun – 9 Jun	21	249 – 256	6 Sep – 13 Sep
10	161 – 168	10 Jun – 17 Jun	22	257 – 264	14 Sep – 21 Sep
11	169 – 176	18 Jun – 25 Jun	23	265 – 272	22 Sep – 29 Sep
12	177 – 184	26 Jun – 3 Jul			
<b>Day</b>	<b>DOY</b>	<b>Dates</b>	<b>Day</b>	<b>DOY</b>	<b>Dates</b>
<i>MODIS daily PW and geolocation images</i>					
1	89	30 Mar	...	...	...
2	97	7 Apr	...	...	...
...	...	...	183	271	28 Sep
...	...	...	184	272	29 Sep

### Reprojection of MODIS data

MODIS data were downloaded in sinusoidal projections system and further processed to convert into Universal Transverse Mercator (UTM). MODIS reprojection tool version 4.1 (MRT, 2011) and MODIS Swath reprojection tool version 2.2 (MRTSwath, 2010) were used to convert the  $T_s$ , surface reflectance, and their respective quality data; and daily PW images, respectively into Geo-tiff format. A batch process was run for each set of data, for example: the conversion of  $T_s$  and PW HDF file were converted to Geo-tiff format using the following conversion function (see Plate 3.1 and Plate 3.2).

### Mosaicking of Geo-tiff images

The geo-tiff data for each period/ day was consisted of two scenes to cover the whole study region. Each two scene was mosaicked together to obtain a continuous surface of the variable of interest. A subset of each mosaicked image was then created by clipping with the study area boundaries. ERDAS Imagine (ERDAS, 2011) software was used to process all of these activities.

**Plate 3.1: Conversion of MODIS HDF file into Geo-tiff format using MODIS MRT tool**

```
INPUT_FILENAME = C:\...\MOD11A2.A2009249.hdf

SPECTRAL_SUBSET = (1 1)
#ORIG_SPECTRAL_SUBSET = (1 1 0 0 0 0 0 0 0 0)

SPATIAL_SUBSET_TYPE = INPUT_LAT_LONG

SPATIAL_SUBSET_UL_CORNER = ( 60.0 -121.0 )
SPATIAL_SUBSET_LR_CORNER = ( 52.0 -109.0 )

OUTPUT_FILENAME = C:\...\MOD11A2.A2009249.tif

RESAMPLING_TYPE = NEAREST_NEIGHBOR

OUTPUT_PROJECTION_TYPE = UTM

OUTPUT_PROJECTION_PARAMETERS = (
0.0 0.0 0.0
0.0 0.0 0.0
0.0 0.0 0.0
0.0 0.0 0.0
0.0 0.0 0.0 )

DATUM = NAD83

UTM_ZONE = 12

OUTPUT_PIXEL_SIZE = 1000
```

**Plate 3.2: Conversion of MODIS HDF file into Geo-tiff format using MODIS MRT Swath tool**

```
INPUT_FILENAME = C:\...\MOD05_L2.A2009272.1715.051.2010343181719.hdf

GEOLOCATION_FILENAME = C:\...\MOD03.A2009272.1715.005.2010251232647.hdf

INPUT_SDS_NAME = Cloud_Mask_QA; Water_Vapor_Near_Infrared;
Water_Vapor_Correction_Factors

OUTPUT_SPATIAL_SUBSET_TYPE = LAT_LONG
OUTPUT_SPACE_UPPER_LEFT_CORNER (LONG LAT) = -121.0 60.0
OUTPUT_SPACE_LOWER_RIGHT_CORNER (LONG LAT) = -109.0 52.0

OUTPUT_FILENAME = C:\...\MOD05_L2A200927217150512010343181719_grid
OUTPUT_FILE_FORMAT = GEOTIFF_FMT

KERNEL_TYPE (CC/BI/NN) = NN

OUTPUT_PROJECTION_NUMBER = UTM

OUTPUT_PROJECTION_PARAMETER = 0.0 0.0 0.0 0.0 0.0 0.0 0.0 0.0 0.0 0.0 0.0 0.0 0.0 0.0 0.0 0.0

OUTPUT_PROJECTION_SPHERE = 8

OUTPUT_PROJECTION_ZONE = 12

OUTPUT_PIXEL_SIZE = 1000
```

### Retrieval of MODIS $T_s$ , surface reflectance, QA, QC, and PW values

MODIS Terra  $T_s$  (i.e., MOD11A2) and surface reflectance (i.e., MOD09A1) mosaicked images were further processed to generate the surface temperature and surface reflectance values by using the science data sets (SDS) of the data products (see Table 3.2). The scale factors were used to retrieve the real value of each pixel. Furthermore, the QC SDS of MOD11A2 (i.e., 8-day composite of  $T_s$ ) provided information on the algorithm results of each pixel. The QC information depicted the quality of each pixel i.e., algorithm results were nominal, abnormal, or if defined conditions were met. Such information would help in understanding the quality of retrieval for each pixel and could be extracted by observing the flags stored in an 8-bit unsigned integer (i.e., range in between 0 and 255). Table A2.1 demonstrates the QC SDS for the  $T_s$  variable explaining each bit combination and their quality flags. In addition, the QA SDS of MOD09A1 (i.e., 8-day composite of surface reflectance) provided information about the quality of the pixel retrieval at 500 m surface reflectance state flags i.e., 16 bit unsigned integer (i.e., range in between 0 and 65535, valid range is 0-57343) (see Table A2.2 for details). In this thesis, I evaluated the QC and QA images by extracting the decimal value for each pixel and converted it into binary number; and then used the SDS flags in identifying the quality of the  $T_s$  and surface reflectance images. For validation of the gap-filling algorithm, I retrieved only the good quality pixels (see section 4.1.2) for the variable of interest.

**Table 3.2: Science data sets (SDS) of MODIS Terra Ts, surface reflectance, and PW.**

Science data sets	Units	Bit Type	Fill value	Valid range	Scale factor
<b>Surface temperature (Ts), MOD11A2</b>					
8-day daytime 1 km grid Ts data	Kelvin	16-bit unsigned integer	0	7500–65535	0.02
QC: daytime Ts and emissivity	Bit Field	8-bit unsigned integer	See Table A2.1	0–255	N/A
<b>Surface reflectance, MOD09A1</b>					
500 m surface reflectance (centered at 0.64, 0.85, 1.64, and 2.13 μm were used)	Reflectance	16-bit signed integer	-28672	-100–16000	0.0001
QA: 500 m state flags	Bit field	16-bit signed integer	See Table A2.2	0–57343	N/A
<b>Precipitable water, MOD05L2</b>					
Daily daytime 1 km grid PW data	Centimeters	16-bit signed integer	-9999	0–20000	0.001

MODIS Terra daily PW variable (i.e., MOD05L2) was based on the total column of water vapor in the atmosphere; and derived using near-infrared algorithm during the day. The near-IR PW usually found to be very sensitive to boundary-layer water vapor, thus ratios of water vapor absorbing channels centered near 0.905, 0.936, and 0.94 μm with atmospheric window channels at 0.865 and 1.24 μm were used. The pixel values were stored in the SDS as short integer (except the geolocation file), and real value was calculated using the scale factor and off set value (see Table 3.2). So the following equation was employed to calculate the real value of the pixel for each image:

$$Real\ value = Scale\ factor \times (Pixel\ value - Offset\ value) \quad (3.1)$$

### *3.3.2 Processing of fire spot data*

Historical wild fire information was downloaded from Alberta ESRD website in MS Excel format for the period of 2009–2011. Each file was consisted of several fire related information, such as fire number; fire start date; fire location with latitude and longitude; fire burned area; etc. Individual data layer was then converted into ArcGIS shape file format using the geographical coordinates and transformed into UTM projection system. Relevant attribute information were aggregated with the point shape file for further analysis. ArcGIS software was used to convert this data into point shape files and all fire spot information were clipped within the study area.

### *3.3.3 Processing of GIS shape files*

The administrative-based geographic data were download in shape file format, which were freely available from Government of Canada website (<http://geogratis.gc.ca/api/en/nrcan-rncan/ess-sst/db83f9d4-40f7-5644-8949-e36616162c0e.html>) (NRCAN, 2014). All relevant shape files were converted to UTM projection system for further analysis in this research.

## **3.4 Computation of remote sensing-based indices**

### *3.4.1 Normalized difference vegetation index (NDVI)*

In general, the chlorophyll content affects the visible red band i.e., relatively low reflectance, but high reflectance observed in the NIR band. The normalized band ratio parameter of red and NIR bands were used to eliminate seasonal sun angle difference and minimize the effect of atmospheric attenuation. Figure 3.2 demonstrated the spectral characteristics of green, dry vegetation, and bare soil reflectance.

The NDVI is the most widely used index in the history of remote sensing. Its 8-day composite values at 500 m resolution were computed using the expression first described in (Rouse et al. 1973) as follows:

$$NDVI = \frac{\rho_{0.86} - \rho_{0.645}}{\rho_{0.86} + \rho_{0.645}} \quad (3.2)$$

where,

$\rho$  is the surface reflectance values of the NIR (centered at 0.86  $\mu\text{m}$ ) and red (centered at 0.645  $\mu\text{m}$ ) spectral bands.

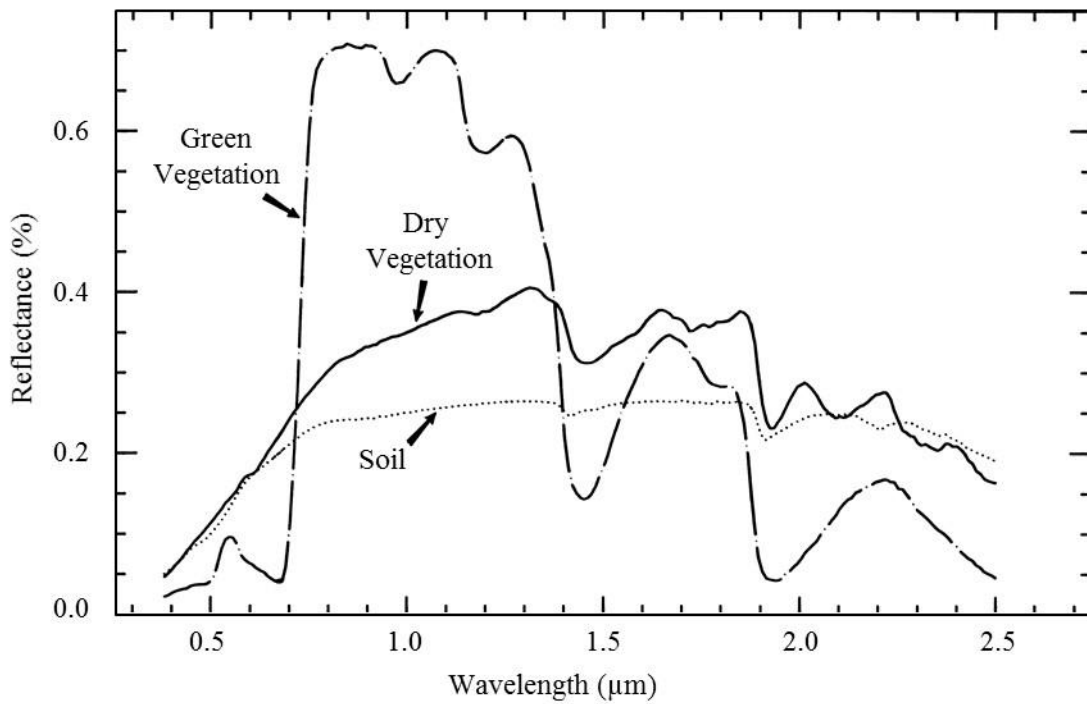


**Figure 3.2: The spectral reflectance curves of green, dry vegetation and soil (after Clark et al., 1999).**

### 3.4.2 Normalized multiband drought index (NMDI)

It was observed that the leaf water content ( $C_w$ ) found to be sensitive to MODIS SWIR bands centered at 1.24, 1.64, and 2.13  $\mu\text{m}$ ; and insensitive at 0.86  $\mu\text{m}$ . Thus, combination of three spectral bands, that is, 0.86  $\mu\text{m}$  as the reference, and two other water absorption bands i.e., 1.64, and 2.13  $\mu\text{m}$  were used for calculating the NMDI. The simulated effect of leaf water content on canopy reflectance shown in Figure 3.3 (Wang and Qu, 2007) illustrated that the MODIS SWIR bands were sensitive to the change of leaf water content considering the values of chlorophyll content,  $C_{ab} = 40$ ; leaf dry matter content,  $C_m = 0.01$ ; leaf internal structure,  $N=1.3$ ; soil moisture,  $\theta = 0.25$ ; and leaf area index,  $LAI = 2$ .

The NMDI is a relatively new index first described by Wang and Qu (2007). Its 8-day composite values at 500-m resolution were computed using the following expression:

$$NMDI = \frac{\rho_{0.86} - (\rho_{1.64} - \rho_{2.13})}{\rho_{0.86} + (\rho_{1.64} - \rho_{2.13})} \quad (3.3)$$

where,

$\rho$  is the surface reflectance values of NIR (centered at 0.86  $\mu\text{m}$ ); and SWIR (centered at 1.64 and 2.13  $\mu\text{m}$ ) spectral bands.

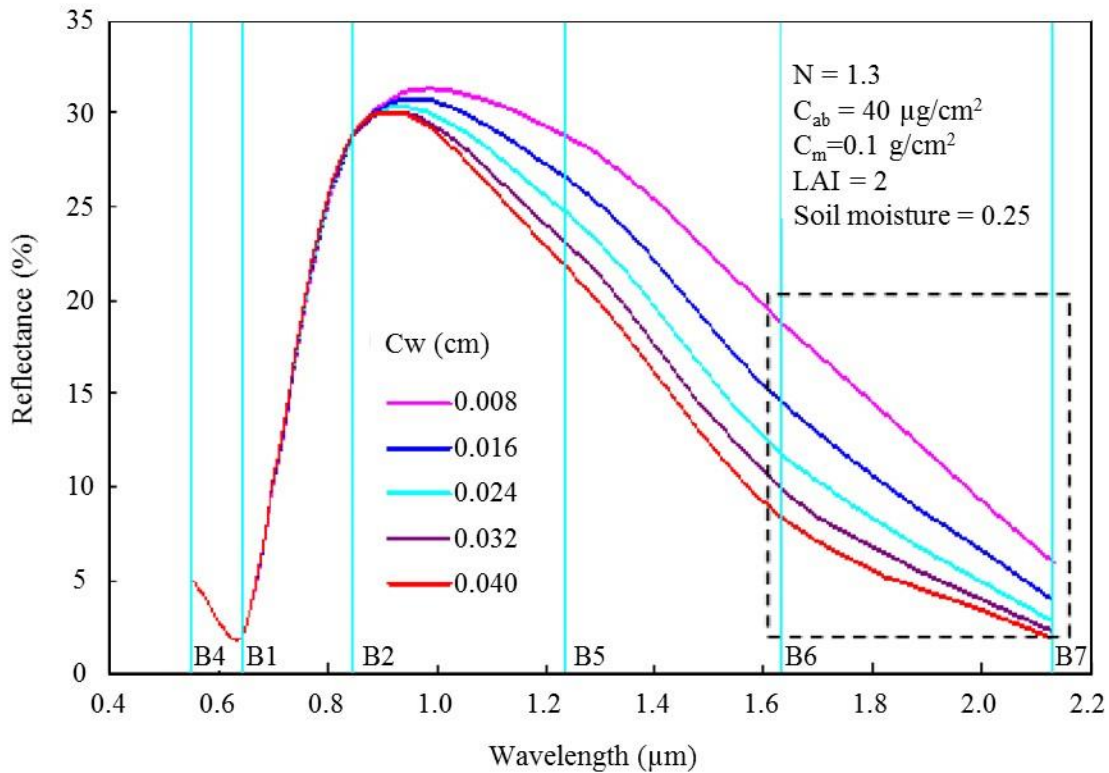


**Figure 3.3: Model simulated canopy spectra at different leaf water content (after Wang and Qu, 2007).**

### 3.5 Constraints in relation to the employed input variables

Here, I employed four MODIS-derived input variables, i.e., 8-day composite of  $T_s$ , NMDI, and NDVI; and daily PW. In general, the 8-day composite MODIS images were composed from the daily scale data as it might reduce the cloud-contamination (that potentially would block the surface reflectance and outgoing thermal radiation reaching to the satellite sensor). The use of these variables was having several issues, e.g.,:

- The 8-day composite of  $T_s$  images were generated by averaging the  $T_s$  images acquired under clear-sky conditions at approximately 10:30 am local time (Wan, 2006). Thus, these values might not represent the daily variations and/or maximum temperature;

- The 8-day composite of MODIS surface reflectance data used to calculate NMDI and NDVI, was generated based on minimum-blue criterion; which coincided with the best clear-sky condition day during the composite of interest (Vermote et al., 2011; Descloitres and Vermote, 1999). As such, two consecutive 8-day composite images might be apart in the range of 2 to 16 days. In addition, NMDI and NDVI variables were less dynamic in temporal dimension, i.e., wetness/greenness condition of forest vegetation might not change over short time period even though the vegetation would experience stresses (Leblon et al., 2001); and
- The daily PW variable was based on total column of water vapor amounts in the atmosphere; and usually found to be very sensitive to boundary-layer water vapor (Gao and Kaufman, 2014). Also, relationships between water vapor at different boundary layers and fire occurrences were reported in the literature, such as (i) Brotak 1977 found that low moisture at 850 mb layer was highly associated with severe fires in the eastern United States (i.e., 93% of the all fire occurrences); and (ii) Price 2000 showed that PW at above 300 mb and 300-500 mb layer was linked to lightning activities, which would be considered as one of the major source of fire ignition. In Canada alone, lightning-caused fire burned more than 1.6 million ha of forested land annually on an average (Stocks et al., 2003). So, it would be worthwhile to investigate the water vapor regimes at different boundary layers and their relationship with fire occurrences. In such cases, one of the viable options would be the use of radiosonde data (Brotak, 1977; Price, 2000).

## CHAPTER 4 : METHODS

The overall methods for forecasting the forest fire danger conditions consisted of three major components, such as (i) developing of the gap-filling algorithm for the input variables of FFDFS and its validation; (ii) calculating the fire danger conditions using  $T_s$ , NMDI, and NDVI variables for mid-term forecasting (i.e., 8-day scale FFDFS) and its validation; and (iii) developing a daily-scale fire danger forecasting system and evaluation of its performance. Their brief descriptions can be found in the following subsections.

### **4.1 Development of a gap-filling algorithm for the input variables of FFDFS system**

#### *4.1.1 Development of data gap-filling algorithm*

In order to quantify the amount of data gaps in  $T_s$ , NMDI, and NDVI images; I calculated the total number of variable-specific pixels where these were not produced due to cloud effects and other reasons by considering: (i) QC image of the respective  $T_s$  images; and (ii) QA image considering both of the MODLAND QA bits and band-specific quality bits of the respective surface reflectance images for calculating both NMDI and NDVI variables. Then, I attempted to fill such gap pixels by considering both of the spatial (i.e., in the range  $3 \times 3$  to  $15 \times 15$  window sizes) and temporal (i.e., considering the images from  $i-1$  and  $i$  periods) dimensions. In the boreal landscape, the spatial extent might vary gradually within similar land cover types and temporal dimension might influence significant changes in temperature, greenness and moisture conditions within the 8-day time period. A schematic diagram illustrating the method employed in gap-filling is shown in Figure 4.1.

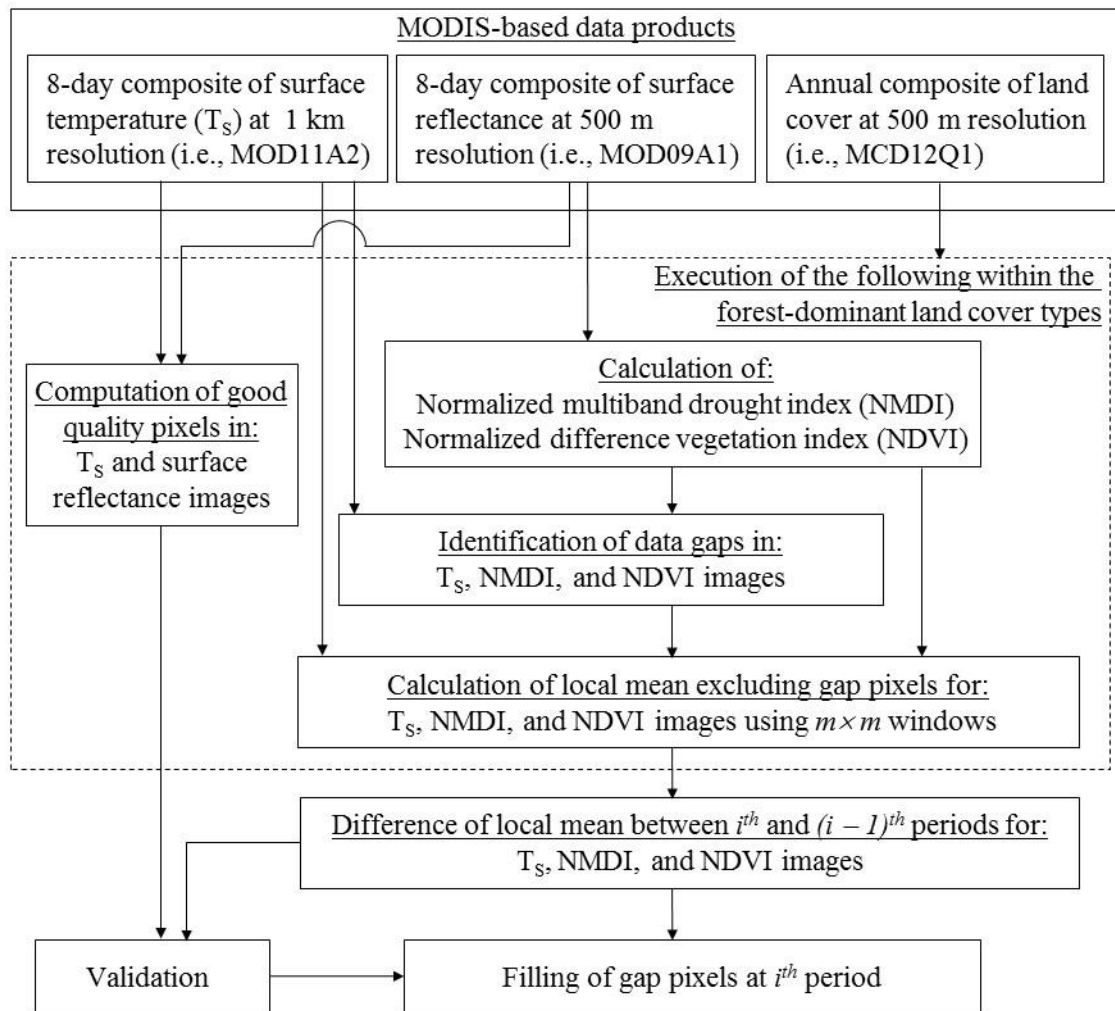


**Figure 4.1: The schematic diagram of the proposed gap-filling method at 8-day scale for  $T_s$ , NMDI, and NDVI variables.**

The proposed gap-filling algorithm was as follows:

$$X(i) = X(i - 1) + [\bar{X}(i)_{m \times m} - \bar{X}(i - 1)_{m \times m}] \quad (4.1)$$

where,

$X(i)$  and  $X(i - 1)$  are the in-filled and non-contaminated values for the variables of Ts, NMDI, and NDVI during  $i$  and  $i - 1$  periods, respectively;

$\bar{X}(i)_{m \times m}$  and  $\bar{X}(i - 1)_{m \times m}$  are the average values of the variables (i.e., Ts, NMDI, and NDVI) of interest within  $m \times m$  window size during  $i$  and  $i - 1$  periods, respectively; and

$m \times m$  is the window size in the range  $3 \times 3$  to  $15 \times 15$ .

The mean values of the variables were computed based on different moving window sizes (i.e., in the range  $3 \times 3$  to  $15 \times 15$ ) within the selected land cover types. So thus, I obtained mean value images for each 8-day period according to different window sizes. The deviation of the mean values of the variables during  $i$  and  $i - 1$  period for  $m \times m$  window size was added with the instantaneous value at  $i - 1$  period. The process would initiate with the smallest window size (i.e.,  $3 \times 3$ ) and then check whether the filling would complete by recalculating the remaining gap pixels in the image. If not, the remaining gap pixels would be filled by increasing the window size to next level (i.e., in the range  $5 \times 5$  to  $15 \times 15$ ). Note that the increment of the window would depend on the status of filling condition and only be performed on the remaining gap pixels. In some instances, the employment of even  $15 \times 15$  window size might unable to fill the gaps. Then, I might consider the window size equivalent to the entire study area of selected land covers. In the implementation of the above gap-filling algorithm, it was assumed that the probability of a

particular pixel having data gap within 16 days would be very rare. In such cases, filling data gap at  $i$  period would not be possible if gap-free pixels at  $i - 1$  period found to be absent.

#### *4.1.2 Validation of data gap-filling method*

In reality, it would not be possible to verify the accuracy of the above described algorithm due to the fact that level and local occurrence of cloud formation and other causes is extremely difficult to measure. However, I performed a validation by synthetically treating good quality pixels as gap ones; and quantified statistically by determining coefficient of determination ( $r^2$ ) and root mean square error (RMSE) (see equations 4.2 and 4.3). Note that such good pixels were retrieved based on the following criterion: (i) for  $T_s$  when the average  $T_s$  errors were found to be either equal or less than 2 K; and (ii) for surface reflectance, I employed a set of parameters, such as MOD35 cloud (i.e., clear), cloud shadow (i.e., no), aerosol quality (i.e., climatology and low), cirrus detected (i.e., none and small), internal cloud algorithm flag (i.e., no cloud), and pixel to adjacent to cloud (i.e., no). We only filled the gaps if the RMSE was less than: (i) 2 K for  $T_s$ , which would be acceptable according to (Wan, 2014; Oyoshi et al., 2014); and (ii) 0.03 for both NMDI and NDVI, which would also be acceptable according to (Gao et al., 2003; Vermote and Kotchenova, 2011).

$$r^2 = \left( \frac{\sum_{i=1}^n (O_i - \bar{O}) (P_i - \bar{P})}{\sqrt{\sum_{i=1}^n (O_i - \bar{O})^2} \sqrt{\sum_{i=1}^n (P_i - \bar{P})^2}} \right)^2 \quad (4.2)$$

$$RMSE = \sqrt{\frac{\sum_{i=1}^n (O_i - P_i)^2}{n}} \quad (4.3)$$

where,

$n$  is the total number of observations;

$O_i$  is the observed Ts, NMDI, and NDVI values;

$\bar{O}$  is the average of the observed Ts, NMDI, and NDVI values;

$P_i$  is the predicted Ts, NMDI, and NDVI values; and

$\bar{P}$  is the average of predicted Ts, NMDI, and NDVI values.

Note that I implemented the above-mentioned algorithm in order to generate in-filled 8-day composite of Ts, NMDI, and NDVI images during 2009–2011 fire seasons. However, I did not attempt to fill the data gaps in daily PW image. Because these data gaps were due to the presence of cloud in most of the instances, which were associated with high moisture content in the atmosphere (Kaufman and Gao, 1992); and also high moisture would decrease the potential of fire occurrences (Haines, 1988).

## 4.2 Enhancement of 8-day scale FFDFS system for mid-term forecasting

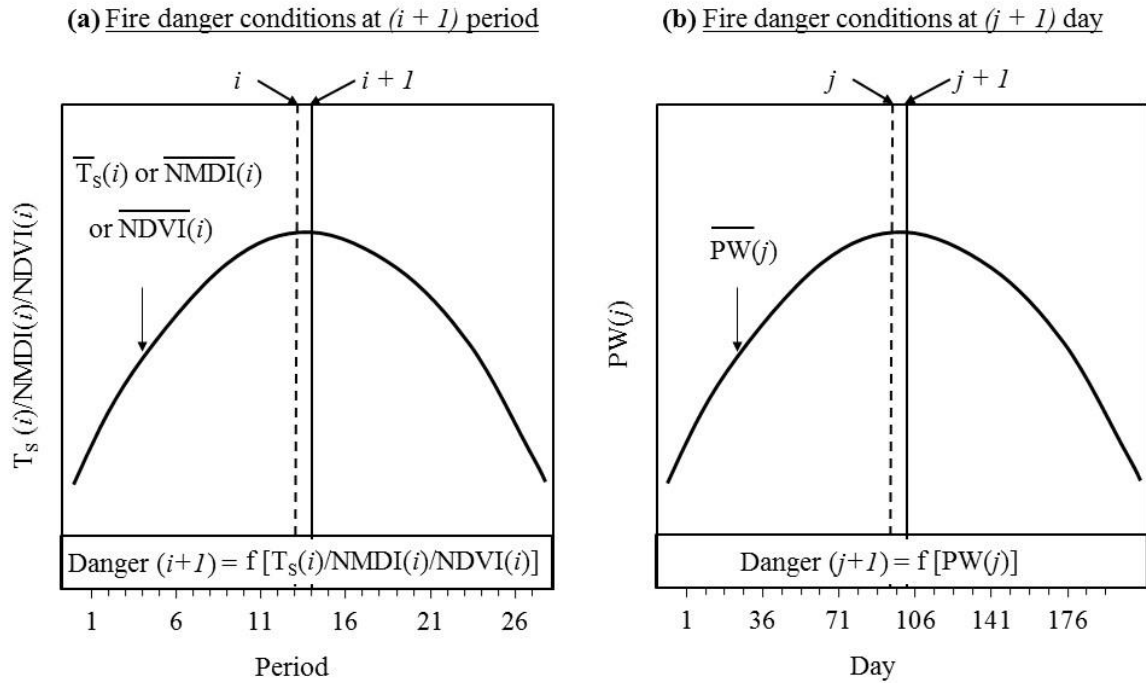
### 4.2.1 Calculation of individual variable-specific fire danger conditions

We employed 8-day composite of MODIS-derived input variables of  $T_s$ , NMDI, and NDVI in the proposed FFDFS framework (see Figure 4.2a for details). The FFDFS consisted of two steps. In first step, I calculated the study area-specific mean values for the input variables during the  $i$  period [i.e.,  $\overline{T_s(i)}$ ,  $\overline{NMDI(i)}$ ,  $\overline{NDVI(i)}$ ]. In second step, I determined the individual input variable-specific danger conditions (either high or low, see Figure 4.2c) during  $i + 1$  period upon comparing the instantaneous values of each of the input variables at a given pixel from  $i$  period [i.e.,  $T_s(i)$  /  $NMDI(i)$  /  $NDVI(i)$ ] with their respective mean-values [i.e.,  $\overline{T_s(i)}$ ,  $\overline{NMDI(i)}$ ,  $\overline{NDVI(i)}$ ] calculated in first step.

### 4.2.2 Generation of combined fire danger maps

We combined the individual input variable-specific fire danger conditions determined in the previous section into four danger categories, such as

- (i) very high: if all the three variables demonstrated that the fire danger would be high;
- (ii) high: if at least two of the three variables demonstrated that the fire danger would be high;
- (iii) moderate: if at least one of the three variables demonstrated that the fire danger would be high; and
- (iv) low: if all of the three variables demonstrated that the fire danger would be low.



(c)

Input variables	Danger ( <i>ij</i> + 1)		Comments
	High	Low	
$T_s(i)$	$\geq \overline{T_s(i)}$	$< \overline{T_s(i)}$	High temperature favor fire
$NMDI(i)$	$\leq \overline{NMDI(i)}$	$> \overline{NMDI(i)}$	Low moisture in vegetation may support fire
$NDVI(i)$	$\leq \overline{NDVI(i)}$	$> \overline{NDVI(i)}$	Low greenness may support to initiate fire as it relates with a set of biophysical variables
$PW(j)$	$\leq \overline{PW(j)}$	$> \overline{PW(j)}$	Low precipitable water in the atmosphere may associate with the flammability of both live and dead fuels

**Figure 4.2: The conceptual diagram of: (a) 8-day scale FFDFS using  $T_s$ , NMDI, and NDVI variables (i.e., between DOY 89 and 265); (b) fire danger conditions of daily PW; and (c) the criterion of describing fire danger conditions for the input variables of  $T_s$ , NMDI, NDVI, and PW.**

The integration of individual input variables (e.g.,  $T_s$ , NMDI, and NDVI) of different spatial resolution was done so that the geometric element and object structure, for example, gridded pixels of the datasets would match to each other. The data integration was done by resampling the  $T_s$  images at 500 m from 1 km prior to integrate with the NMDI and NDVI variables having 500 m spatial resolution. It would be worthwhile to mention that fire will not occur in any danger classes unless there would be an ignition source.

#### *4.2.3 Validation with actual fire spots data*

##### *4.2.3.1 Evaluation of variable-specific fire danger conditions*

In order to investigate the performance of the individual variables, ground-based fire spots data (i.e., Alberta ESRD) were considered as a criteria of fire danger conditions (either high or low). For each individual fire spot (i.e., occurrences of fire during  $i+1$  period), I extracted the corresponding value of the variables of interest (i.e.,  $T_s$ , NMDI, and NDVI) and compared with the study area-specific average value during  $i$  period. As such, I determined how many cases the values of a particular variable of interest in comparison with the study area-specific average during  $i$  period would fall under high or low danger categories. Furthermore, I classified the high and low danger categories into six classes on the basis of study area-specific average and their standard deviation values within ‘average  $\pm$  3 standard deviation’ at one standard deviation of the variable of interest. This analysis would provide information regarding the situation of individual variables which would be revealed to understand whether comparatively higher temperature, low live fuel moisture condition, and less vegetation greenness would favor occurrences of fire.

#### 4.2.3.2 Evaluation of the potential of combined fire danger conditions

Upon generating the fire danger maps (i.e., four danger categories, such as very high, high, moderate, and low), I compared them with the Alberta ESRD ground-based fire spots data during 2009-2011 to evaluate the performance of the 8-day scale FFDFS. In these cases, I overlaid the fire spots (i.e., start of a location-specific fire) over the forecasted fire danger maps over a period of interest; and computed the distribution of the fire danger categories over the fire spots. Finally, I determined the ‘% of each danger classes’ over all of the fire spots during the entire study period.

### 4.3 Development of a remote sensing-based daily-scale FFDFS system

#### 4.3.1 Development of a daily-scale FFDFS

We developed a remote sensing-based FFDFS system at daily-scale using MODIS-derived variables (Figure 4.3). The proposed system comprised of four steps. Firstly, I assimilated all four input variables (i.e.,  $T_s$ , NMDI, NDVI, and PW) within the selected forest-dominant land cover types. Secondly, I computed the study area-specific average values for all input variables during the  $i$  period [i.e.,  $\overline{T_s(i)}$ ,  $\overline{NMDI(i)}$ ,  $\overline{NDVI(i)}$ ] (as mentioned in section 4.2) and  $j$  day [i.e.,  $\overline{PW(j)}$ ]. Thirdly, I calculated fire danger conditions (either high or low; see Figure 4.2c) for each of the input variable during both  $i+1$  period and  $j+1$  day upon comparing the input variable-specific instantaneous values at a given pixel from  $i$  period and  $j$  day [i.e.,  $T_s(i)$ ,  $NMDI(i)$ ,  $NDVI(i)$ , and  $PW(j)$ ] with their respective average values computed in the second step. We assumed that the fire danger condition for the specific variable of interest would be high if following condition would prevail. For example,  $T_s(i) \geq \overline{T_s(i)}$ : high temperature might favor fire;  $NMDI(i) \leq \overline{NMDI(i)}$ : low moisture in vegetation might support fire;  $NDVI(i) \leq \overline{NDVI(i)}$ : low vegetation greenness might

support to initiate fire as it relates with other biophysical variables; and  $PW(j) \leq \overline{PW}(j)$ : low water vapour in the atmosphere might be associated with the flammability of both live and dead fuels.

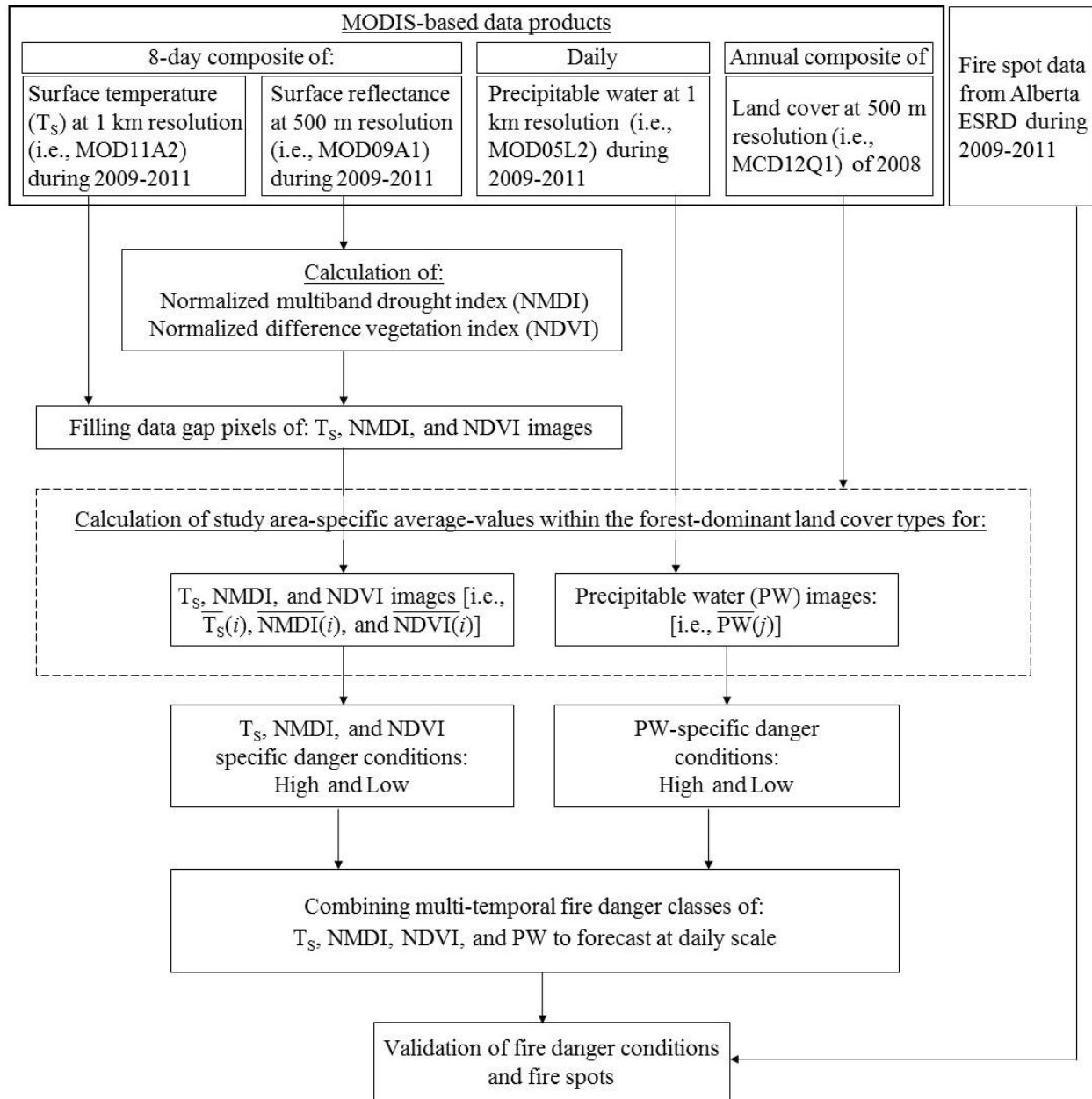


**Figure 4.3: The conceptual diagram of daily-scale FFDFS using  $T_s$ , NMDI, NDVI, and PW variables.**

#### *4.3.2 Generation of fire danger maps at daily-scale*

Finally, I integrated the individual input variable-specific fire danger conditions into five categories, such as:

- (i) extremely high: when all the four variables fell in the high danger class;
- (ii) very high: when at least three of the four variables fell in the high danger class;
- (iii) high: when at least two of the four variables fell in the high danger class;
- (iv) moderate: when at least one of the four variables fell in the high danger class; and
- (v) low: when all four variables fell in the low danger class.

In integrating the individual variable-specific fire danger conditions in the framework of daily-scale FFDFS, I assumed that the impact of 8-day composite of  $T_s$ , NMDI, and NDVI variables would be constant over the following 8-day period.

#### *4.3.3 Validation of daily-scale FFDFS system with ground-based fire spot data*

##### *4.3.3.1 Evaluation of daily PW-based fire danger conditions*

We incorporated the daily PW variable in the 8-day scale FFDFS framework, thus I opted to evaluate its individual impact on the fire danger conditions prior to integrating with other variables.

As part of this process, the study area-specific average values of PW ( $\overline{PW}$ ) during  $j$  day was compared with the ground-based fire spot data during  $j+1$  day. We followed the same procedure to evaluate the performance of PW-based fire danger condition like other variables of interest as illustrated in section 4.2.3.1. This analysis would provide information regarding the water vapor regimes in the atmosphere; and whether relatively less moisture in the atmosphere would favor fire occurrences.

#### 4.3.3.2 Evaluation of the combined fire danger conditions

Upon generating the combined fire danger maps at daily scale (i.e., five danger categories, such as extremely high, very high, high, moderate, and low), I assessed them with ground-based fire spots data to evaluate the enactment of the daily FFDFS system during the periods of 2009-2011. The fire spots data were superimposed on the forecasted fire danger conditions for a particular day; and captured the fire danger categories over the fire spots. Lastly, I calculated the ‘% of fire danger classes’ under each category over the entire study periods.

## CHAPTER 5 : RESULTS & DISCUSSION

### 5.1 Evaluation of gap-filling algorithm

#### 5.1.1 Calculation of data gaps

We employed the MODIS quality assurance information for each variable of interest, and found that the data gaps in the 8-day composite of  $T_s$ , NMDI, and NDVI variables were in the range 0.52-2.82%, 0.001-0.0334%, and 0.00003-0.0034% respectively on an average during 2009-2011 period (see Tables A2.3, A2.4, and A2.5 for details). Subsequently, I filled these gaps using both spatial (i.e., in the range  $3 \times 3$  to  $15 \times 15$  window sizes) and temporal (i.e., considering the images from  $i-1$  and  $i$  periods) dimensions for the variable of interest. Figure 5.1 shows the data gaps in the  $T_s$  images during the entire study period. Relatively high amount of data gaps in the  $T_s$  images were observed due to the fact that the quality of the MODIS-based  $T_s$  product would be often contaminated to a large scale as a matter of inherent limitation of the thermal infrared remote sensors (i.e., retrieved only in clear-sky conditions) (Wan, 2008).

#### 5.1.2 Evaluation of the gap-filling algorithm

Upon implementing the proposed gap-filling algorithm, I used all the imaging periods for each of the  $T_s$ , NMDI, and NDVI images for evaluating its performance. We observed that the gaps were in-filled approximately in the range: (i) 84.70–98.93% for  $T_s$  images (see Table A2.6); and (ii) 100% for NMDI and NDVI images, during 2009–2011 period. During the period of validation, our analyses showed strong agreements of the predicted values for the variable of interest with the observed data (i.e., the good quality pixels which were declared as data gaps). For example, using  $3 \times 3$  window size, the  $r^2$ , RMSE, and slope values were on an average: (i) 0.87, 0.95 K, and 0.92;

(ii) 0.86, 1.10 K, and 0.91; and (iii) 0.89, 0.96 K, and 0.93; respectively, during the period 2009-2011 for  $T_s$  images (see Tables A2.7, A2.8, and A2.9 for details). Figure 5.2 shows the comparison between observed and predicted  $T_s$  upon using  $3 \times 3$  window size for gap-filling for five periods which were well distributed over the entire growing season.

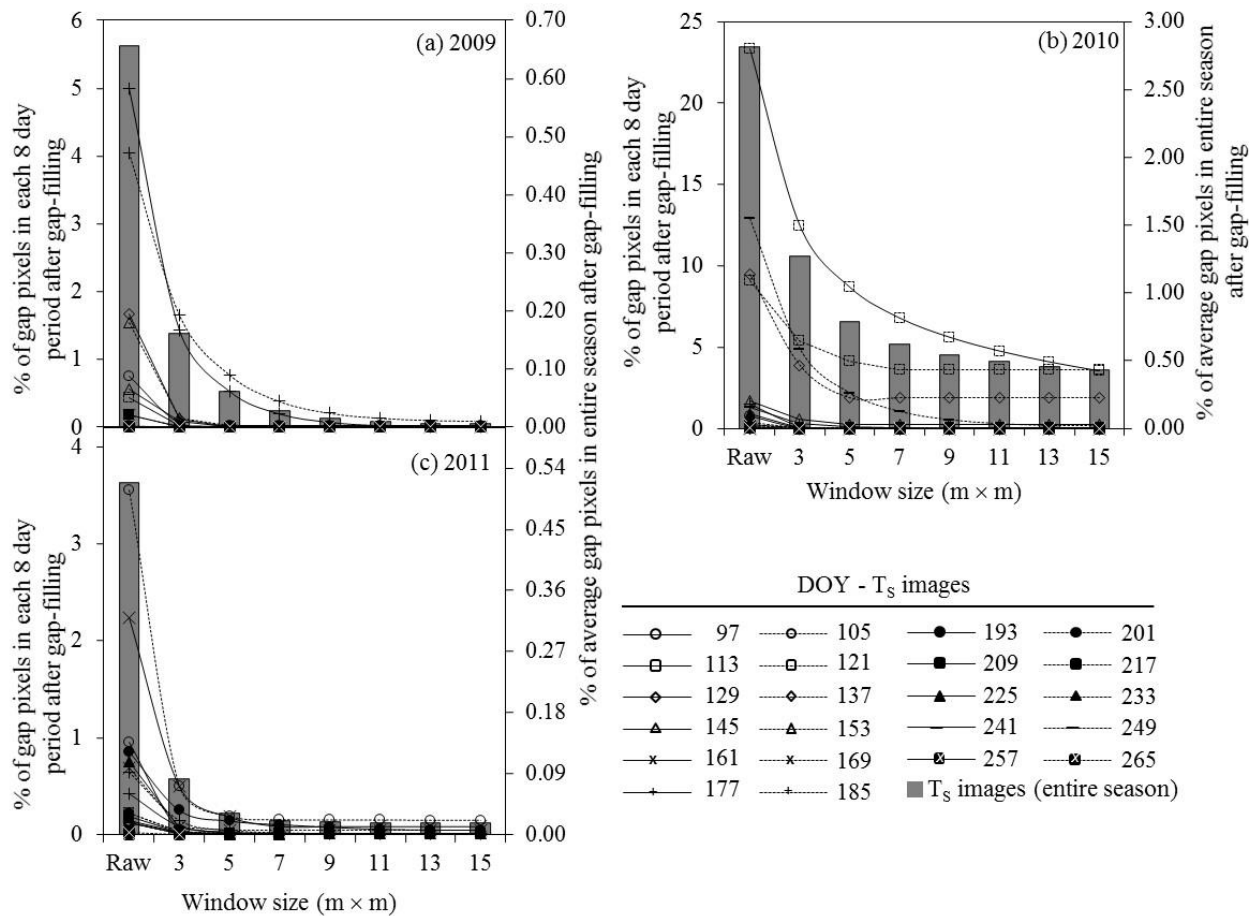


**Figure 5.1: Percentage of gap pixels in  $T_s$  images upon gap-filling using various window sizes during 2009–2011.**

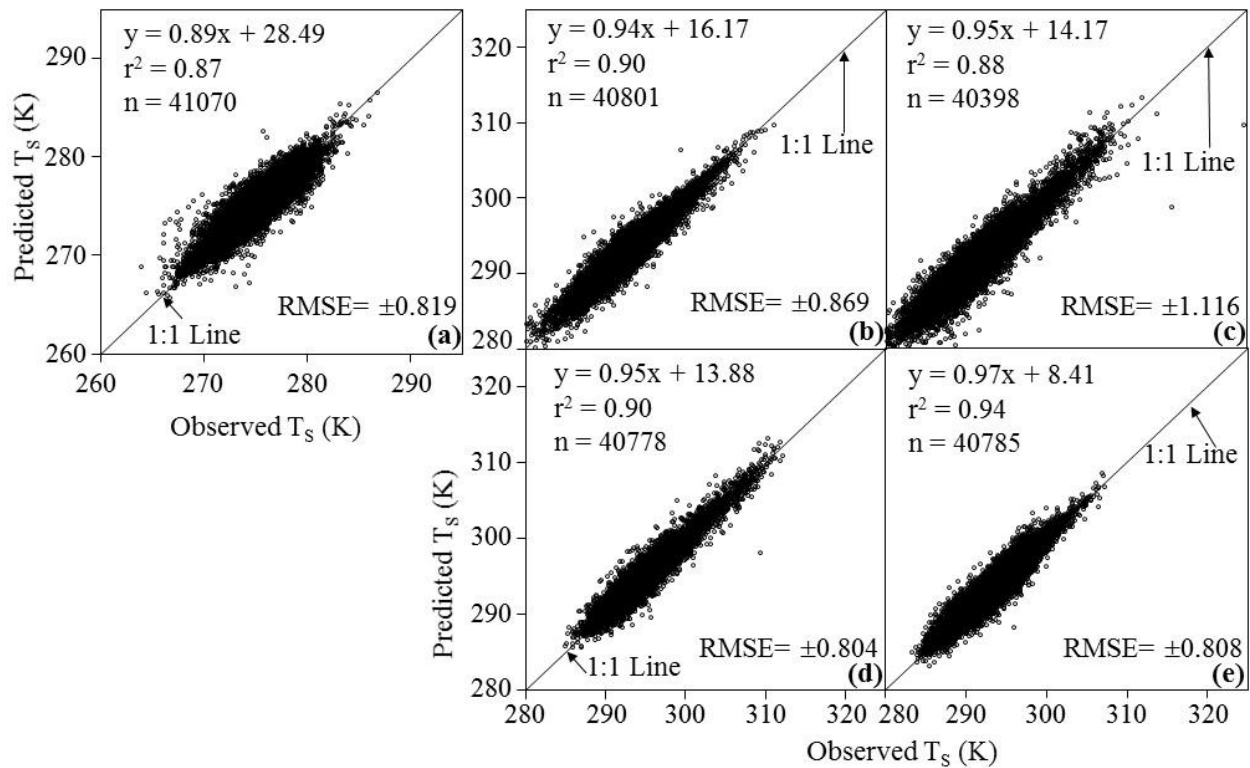


**Figure 5.2: Comparison between observed and predicted  $T_s$  upon using  $3 \times 3$  window size for gap-filling: (a) 97 DOY,  $F = 286507$ ,  $p$  value  $< 0.0001$  (b) 137 DOY,  $F = 368260$ ,  $p < 0.0001$  (c) 177 DOY,  $F = 320805$ ,  $p < 0.0001$ , (d) 217 DOY,  $F = 382576$ ,  $p < 0.0001$ , (e) 249 DOY,  $F = 607077$ ,  $p < 0.0001$**

In addition, I observed the  $r^2$ , RMSE, and slope values (using  $3 \times 3$  window size) were on an average: (i) 0.94, 0.019, and 0.97; (ii) 0.92, 0.019, and 0.96; and (iii) 0.93, 0.019, and 0.97; respectively, during the period 2009-2011 for NMDI images for 90% of the data points (for details see Table A2.10). Figure 5.3 shows the comparison between observed and predicted NMDI upon using  $3 \times 3$  window size for gap-filling during which were well spread over the growing season. Furthermore, I found the  $r^2$ , RMSE, and slope values (using  $3 \times 3$  window size) were on an average: (i) 0.89, 0.021, and 0.95; (ii) 0.86, 0.023, and 0.93; and (iii) 0.87, 0.022, and 0.94; respectively, during the period 2009-2011 for NDVI images for 90% of the data points (see Table A2.10). Figure 5.4 shows the comparison between observed and predicted NDVI upon using  $3 \times 3$  window size

for five periods which were well distributed over the growing season. The observed RMSE values for both  $T_s$  (i.e., 0.51–1.56 K; see Tables A2.7-A2.9) and NDVI (i.e., 0.015–0.030; see Table A2.10) gap-filling were similar to other study, such as

- (i) MODIS-derived  $T_s$  values in comparison with ground-based such measurements over homogeneous rice fields and forested areas yielded a RMSE of 0.70 K (Coll et al., 2009);

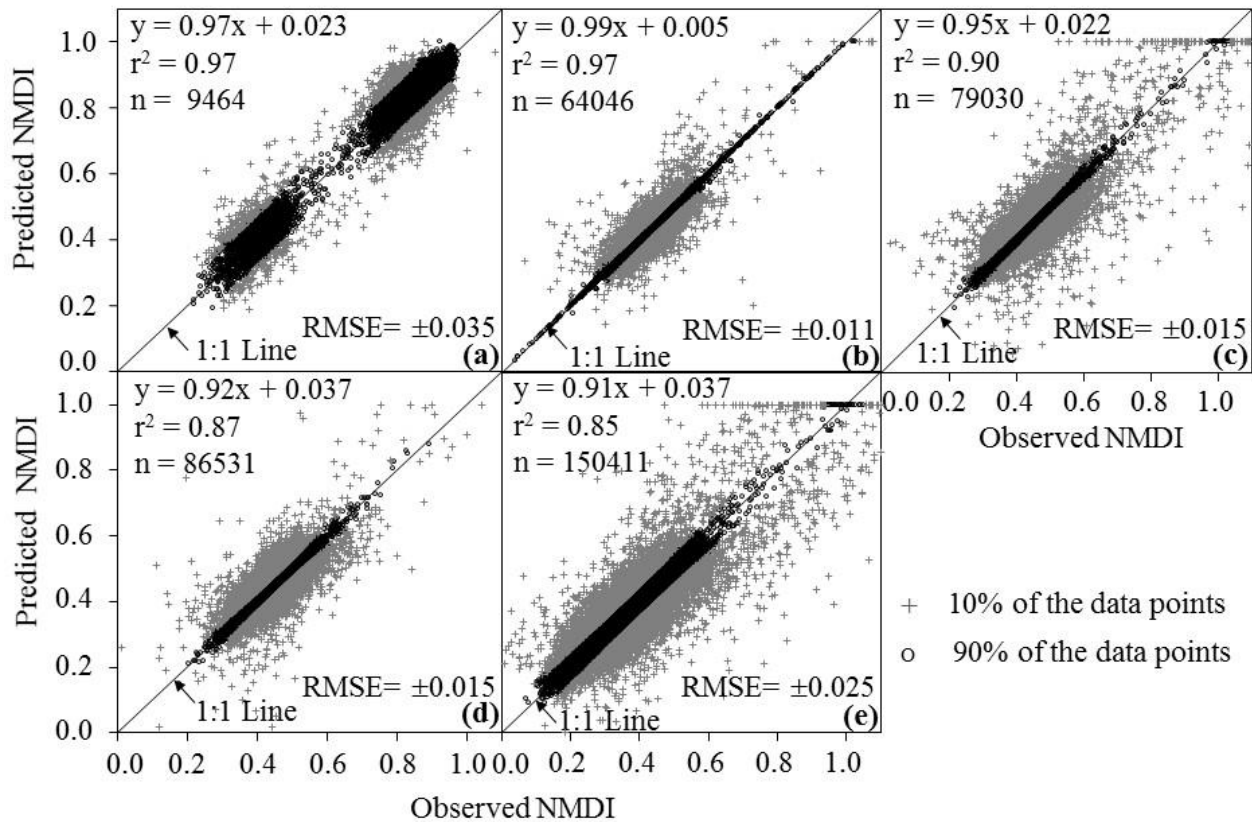


**Figure 5.3: Comparison of observed and predicted NMDI upon using  $3 \times 3$  window size for gap-filling: (a) 113 DOY,  $F = 18880$ ,  $p < 0.0001$ , (b) 153 DOY,  $F = 241571$ ,  $p < 0.0001$ , (c) 193 DOY,  $F = 263602$ ,  $p < 0.0001$ , (d) 233 DOY,  $F = 111437$ ,  $p < 0.0001$ , (e) 265 DOY,  $F = 510446$ ,  $p < 0.0001$**

- (ii) MODIS-derived NDVI values over the good quality pixels were within an error bar of  $\pm(0.02 + 2\% \text{ NDVI})$  for 97.11% of the observations (Vermote and Kotchenova, 2008); and
- (iii) the evaluation of MODIS-derived NDVI over all of the land cover types at Jornada Experimental Range in New Mexico, USA in comparison with MODIS Quick Airborne Looks-based observations showed RMSE values less than 0.03 (Gao et al., 2003).

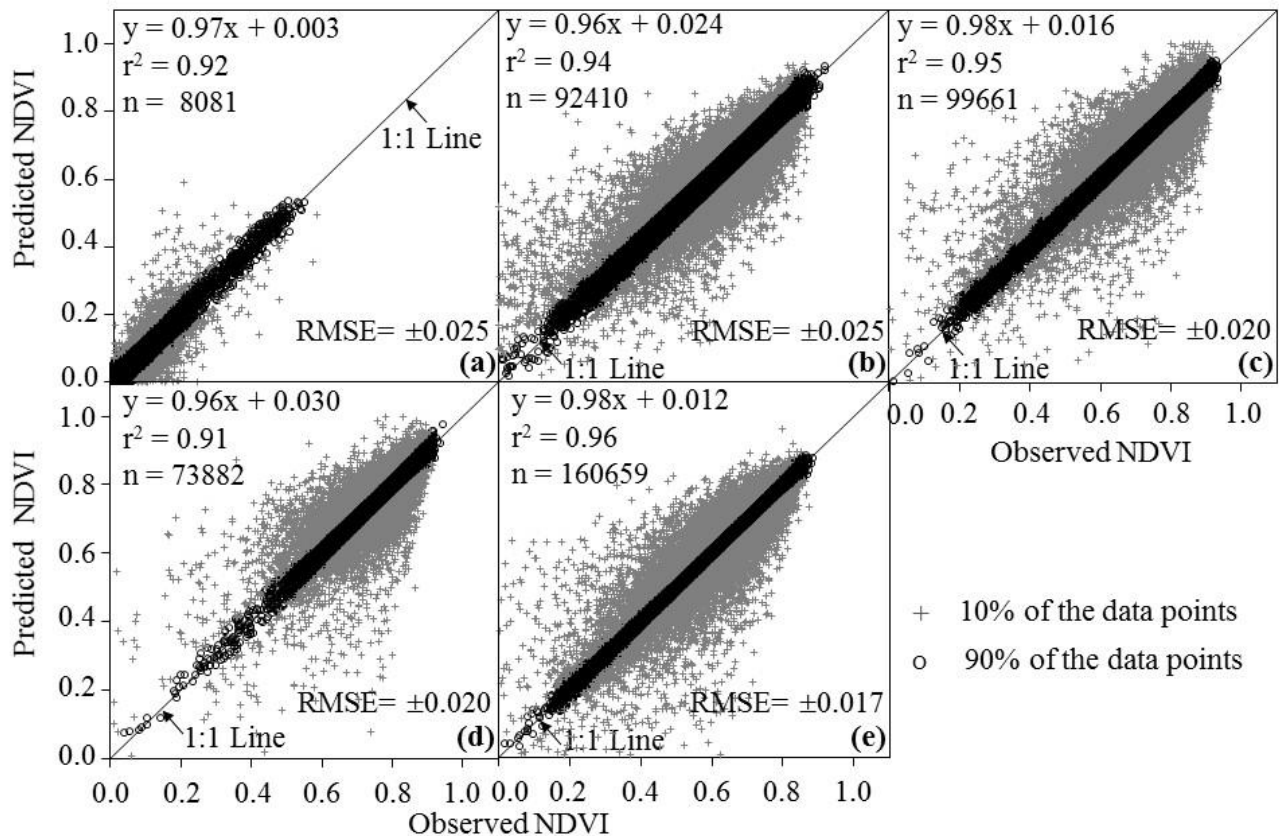


**Figure 5.4: Comparison of observed and predicted NDVI upon using  $3 \times 3$  window size for gap-filling: (a) 105 DOY,  $F = 18880$ ,  $p < 0.0001$ , (b) 145 DOY,  $F = 241571$ ,  $p < 0.0001$ , (c) 185 DOY,  $F = 263602$ ,  $p < 0.0001$ , (d) 225 DOY,  $F = 111437$ ,  $p < 0.0001$ , (e) 257 DOY,  $F = 510446$ ,  $p < 0.0001$**

So far, I did not find studies reporting accuracy information associated with NMDI retrieval or gap-filling. However, I might consider that the observed RMSE values for NMDI (i.e., 0.011–0.040) would be reasonable due to their similarities with that of NDVI. It would be the case as both of the NMDI and NDVI were calculated as a function of surface reflectance.

In the case of  $T_s$  images, it was required to increase the window size (in the range from  $5 \times 5$  to  $15 \times 15$ ; and also entire study area) in order to gap-filling the remaining data gaps (i.e.,  $\sim 0.50$ ,  $1.55$ , and  $0.44\%$ , respectively) for the period of 2009-2011. For each of the window size, I compared the predicted values with the observed data (i.e., the good quality pixels which were declared as data gaps); and calculated  $r^2$  and RMSE average values were shown in Table 5.1. It revealed that both of the  $r^2$  and RMSE values were deteriorating with the increment of the window sizes (e.g.,  $r^2 \approx 0.81$  and  $RMSE \approx 1.25$  K for  $5 \times 5$  window size;  $r^2 \approx 0.68$  and  $RMSE \approx 1.51$  K for  $15 \times 15$  window size; and  $r^2 \approx 0.29$  and  $RMSE \approx 2.77$  K for the window size equal to the study area). These finding would be reasonable due to the fact that the spatial integrity would start to fall apart with the increment of the search window (Girard and Girard, 2003; Li and Heap, 2011).

Also, it would be worthwhile to note that both of the window size (i.e.,  $15 \times 15$  and the study area) were not able to gap-filling similar portion of the data gaps (i.e.,  $\sim 0.154$ ,  $9.485$ ,  $0.370\%$ ; and  $\sim 0.133$ ,  $3.301$ ,  $0.293\%$ , respectively during 2009-2011). Under these circumstances, I considered that the choice of  $15 \times 15$  window size would be appropriate because it produced reasonable agreements (i.e.,  $r^2 \approx 0.68$  and  $RMSE \approx 1.51$  K) in comparison with that of the window size equal to the entire study area (i.e.,  $r^2 \approx 0.29$  and  $RMSE \approx 2.77$  K). The rationale behind the inability to

gap-filling all of the data gaps would be due to the absence of gap-free pixels in both temporal and spatial dimensions (Kang et al., 2005).

**Table 5.1: Average co-efficient of determination ( $r^2$ ) and root mean square error (RMSE) between observed and predicted  $T_s$  variable using different window size during 2009-2011.**

Window size	Year						Average	
	2009		2010		2011		$r^2$	RMSE
	$r^2$	RMSE	$r^2$	RMSE	$r^2$	RMSE		
3 × 3	0.87	0.95	0.86	1.10	0.89	0.96	0.88	1.00
5 × 5	0.81	1.18	0.78	1.38	0.83	1.19	0.81	1.25
7 × 7	0.77	1.31	0.73	1.47	0.80	1.29	0.77	1.36
9 × 9	0.74	1.36	0.70	1.51	0.77	1.34	0.74	1.40
11 × 11	0.72	1.39	0.68	1.58	0.75	1.40	0.72	1.46
13 × 13	0.71	1.43	0.66	1.61	0.74	1.44	0.70	1.49
15 × 15	0.69	1.43	0.64	1.63	0.72	1.48	0.68	1.51
Study area	0.31	2.55	0.22	3.15	0.35	2.62	0.29	2.77

## 5.2 Temporal dynamics of the input variables of FFDFS system

### 5.2.1 Study-area specific average values of 8-day composite $T_s$ , NMDI, and NDVI

During study period, the temporal dynamics of study area-specific average values of the  $T_s$ , NMDI, and NDVI variables showed distinct patterns (Figure 5.5), which were identical to the generalized ones shown in Figure 4.2a. Upon applying quadratic fits to the variable of interest as a function of DOY, I found strong relations having average  $r^2$  values of 0.82, 0.80, and 0.93 for  $T_s$ , NMDI, and NDVI, respectively during 2009-2011 (see Table 5.2 for details).

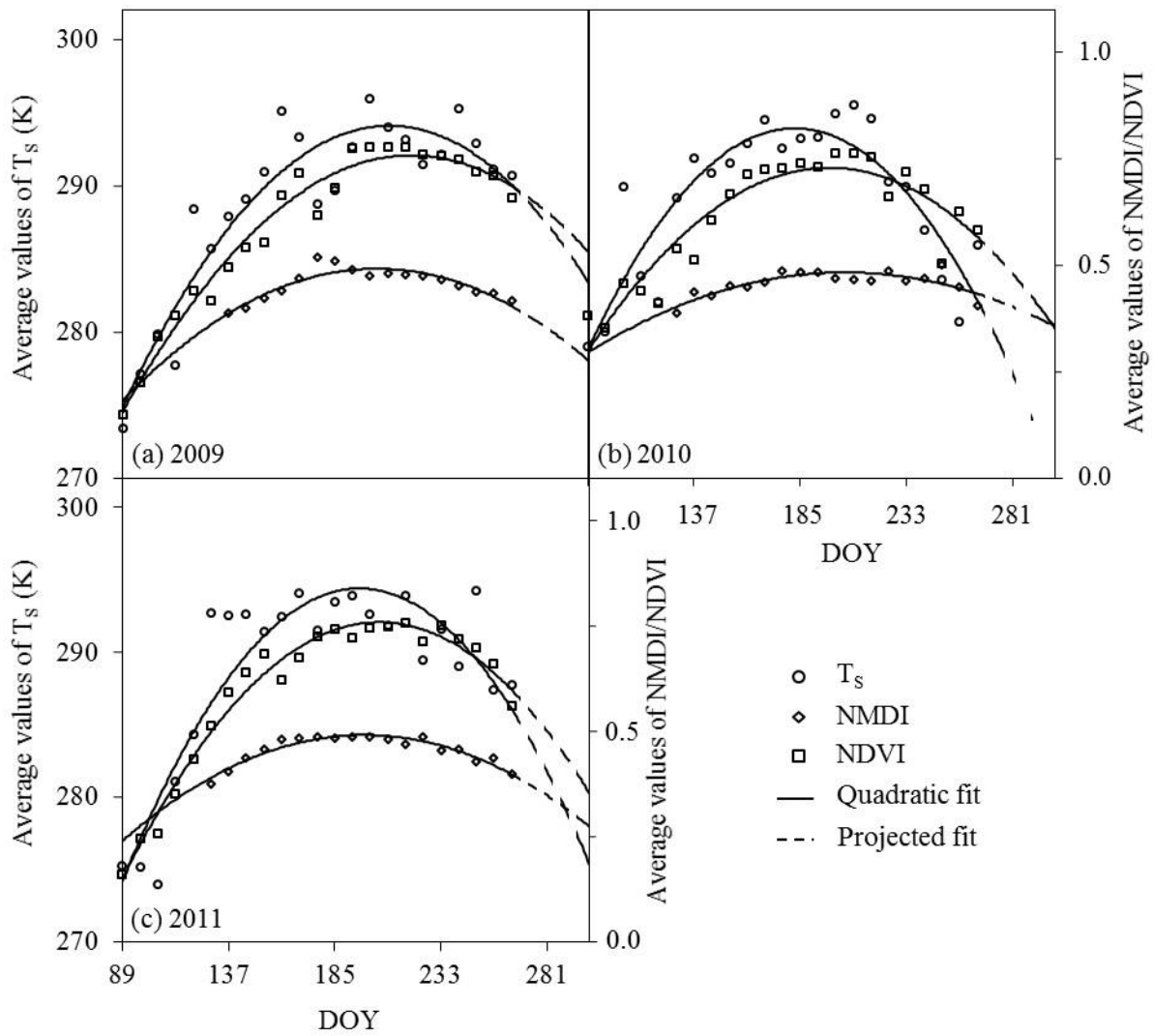


**Figure 5.5: Study-area specific average values for  $T_s$ , NMDI, and NDVI variables for 2009–2011 fire seasons (i.e., between DOY 89 and 265).**

**Table 5.2: Quadratic fits ( $y = ax^2 + bx + c$ ) of the variables  $T_s$ , NMDI, and NDVI variables as a function of DOY for the fire seasons of 2009–2011 (i.e., between DOY 89 and 265).**

Year	Variables	a	b	c	$r^2$
2009	$T_s$	-0.001	0.555	235.93	0.87
	NMDI	-2.40E-05	0.01	-0.485	0.83
	NDVI	-3.50E-05	0.016	-0.948	0.97
2010	$T_s$	-0.002	0.631	236.29	0.77
	NMDI	-1.40E-05	0.006	-0.107	0.67
	NDVI	-3.60E-05	0.014	-0.691	0.86
2011	$T_s$	-0.002	0.688	226.83	0.82
	NMDI	-2.10E-05	0.008	-0.335	0.91
	NDVI	-4.50E-05	0.018	-1.136	0.97

### 5.2.2 Study area-specific average values of daily PW

As I incorporated the daily PW variable in the FFDFS framework, thus I opted to evaluate its individual impact on the fire danger conditions prior to integrating with other variables. As part of this process, I calculated the study area-specific average values of PW ( $\overline{PW}$ ) in order to comprehend its seasonal trends. Then, I performed quadratic fits for the  $\overline{PW}$  as a function of 8-day periods (see Figure 5.6). The  $r^2$ -value for these curves were in the range 0.60-0.71 during 2009-2011 period. Note that the generic shapes of these curves were similar to those illustrated in Figure 4.2b, which proved that our assumed pattern for the PW held quite nicely.

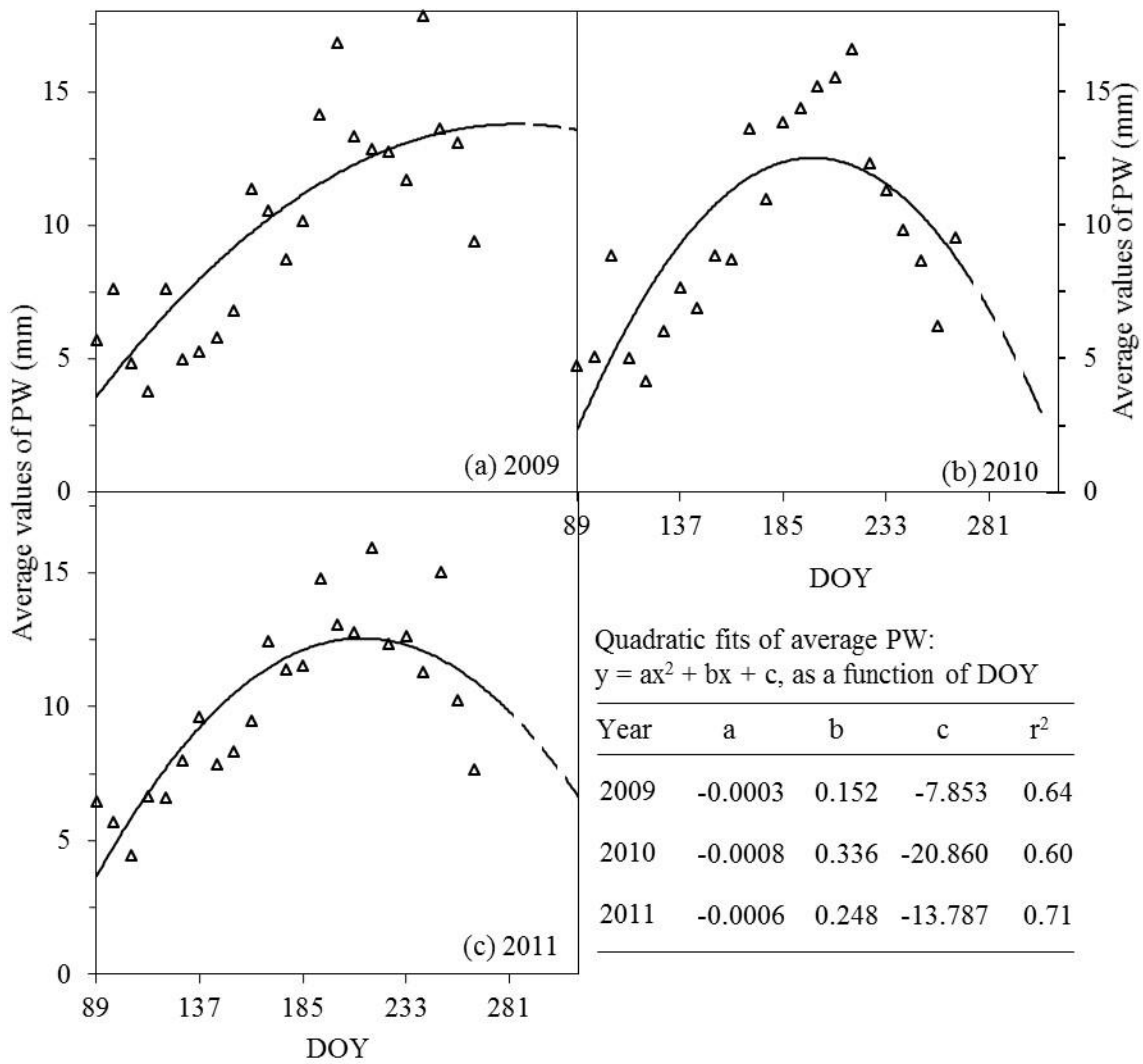


**Figure 5.6: Study area-specific average values of PW (i.e., 8-day average) with DOY for the fire seasons of 2009–2011 (i.e., between DOY 89 and 272).**

### **5.3 Evaluation of FFDFS system at mid-term forecasting**

#### *5.3.1 Assessment of variable-specific $T_s$ , NMDI, and NDVI on fire danger conditions*

We assessed the variable-specific fire danger conditions (i.e., high or low) with the actual fire spot data by capturing the variable-specific values during  $i$  period and comparing with study-area specific average values during the same period while the fire occurred during the  $i+1$  period. We observed that the input variables of the FFDFS (i.e.,  $T_s$ , NMDI, and NDVI) demonstrated 50.60% while  $T_s(i) \geq \overline{T_s(i)}$ ; 65.50% while  $NMDI(i) \leq \overline{NMDI(i)}$ ; and 61.95% while  $NDVI(i) \leq \overline{NDVI(i)}$  of the fire spots fell under ‘high danger’ category during 2009-2011 (see Table 5.3 for details). Our findings were similar to other studies such as 60.59, 72.41, and 54.19% of the fire fell under ‘high danger’ categories for  $T_s$ , NMDI, and TVWI variables (Akther and Hassan, 2011a). The discrepancies observed approximately 49.40, 34.50, and 38.05%, respectively for the  $T_s$ , NMDI, and NDVI which might be attributed due to other environmental factors, such as precipitation, wind speed, topography, fuel types, etc. (Oldford et al., 2003; Ardakani et al., 2011).

**Table 5.3: Percentage of fire spots fell under variable-specific fire danger conditions (i.e., either high or low, extracted one period earlier than the fire occurrence) during the period of 2009-2011.**

Year	Danger conditions	Percentage of data			
		2009	2010	2011	Average
Ts	High	51.66	49.46	50.68	50.60
	Low	48.34	50.54	49.32	49.40
NMDI	High	56.41	69.79	70.29	65.50
	Low	43.59	30.21	29.71	34.50
NDVI	High	58.28	64.06	63.50	61.95
	Low	41.72	35.94	36.50	38.05

Furthermore, I evaluated each fire spot data with study area average and the standard deviation values as shown in Figure 5.7. The figures did not showed a clear connotation of the fire spots with the condition of the variables of interest. However, I observed that most of the fire fell within ‘average  $\pm$  1 standard deviation’ which clearly demonstrated that warmer or less vegetation moisture conditions would favor fires. In similar studies, it has been observed that more dryness didn’t favour the fire occurrences while using the surface temperature, fuel moisture, and soil moisture as a fire danger indicator (Akther and Hassan, 2011a; Bartsch et al., 2009). So, it could be suggested that individual variable might not able to capture the fire danger conditions precisely.

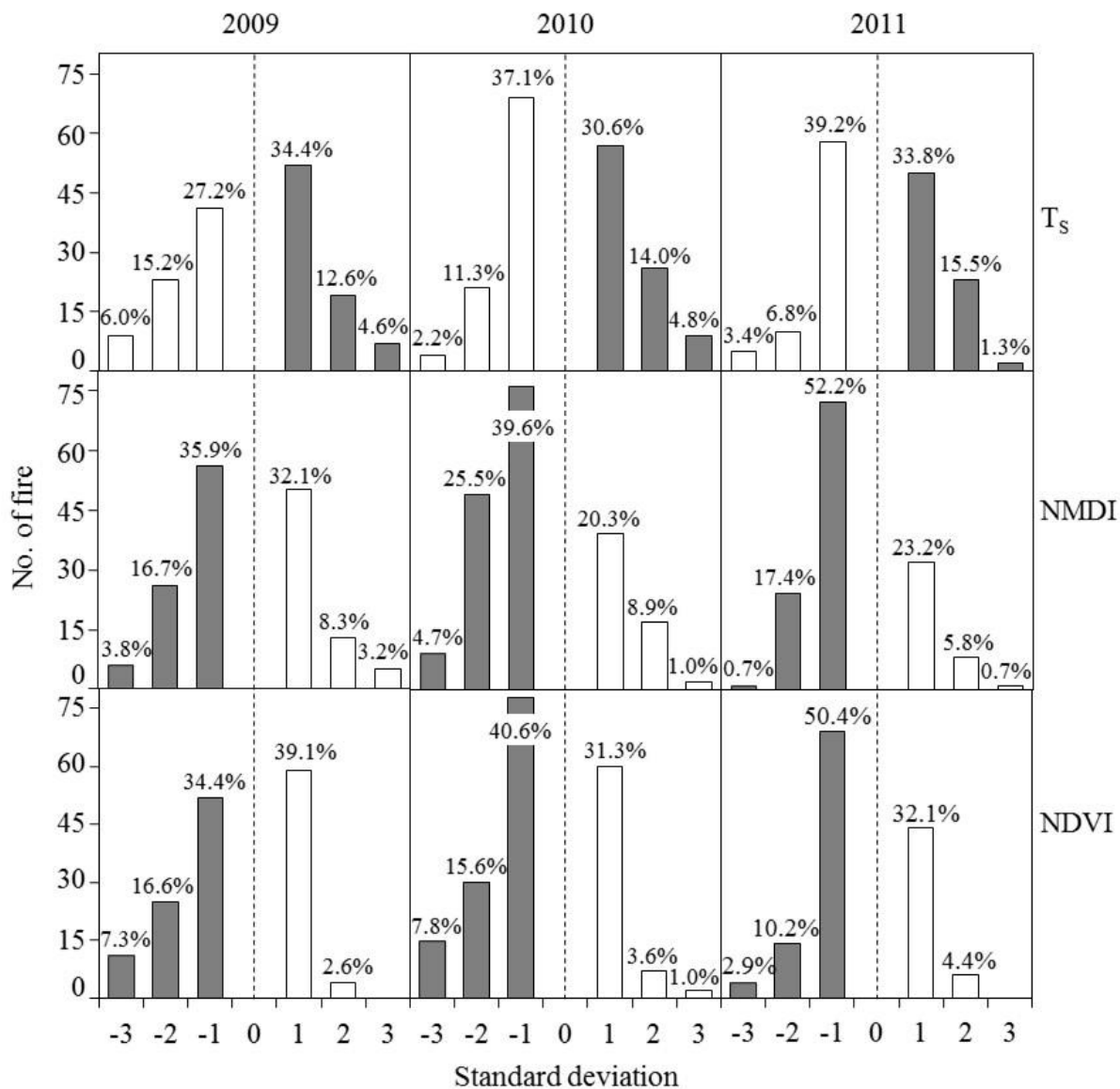


**Figure 5.7: Frequency distribution of the fires with respect to  $T_s$ , NMDI, and NDVI variables and its corresponding study area average values during the  $i$  period when actual fires were taken place in the following  $i+1$  period on the basis of the 'study area-specific average  $\pm$  3 standard deviation' values and percentage of fire spots during 2009-2011.**

### *5.3.2 Evaluation of combined fire danger conditions and its impacts*

Table 5.4 shows the outcomes of the FFDFS using the combinations of input variables (i.e.,  $T_s$ , NMDI, and NDVI) as per the criterion illustrated in Figure 4.2c. These outcomes were compared with the % of pixels represented by the fire spots. The combined variables revealed strong agreements, where 90.94% of fire fell under the categories from ‘very high’ to ‘moderate’ danger classes, respectively. However, the amount of disagreements (i.e., 9.06%) between the predictions and fire spots could be attributed by other factors, as mentioned in section 5.3.1 (Leblon et al., 2001; Desbois and Vidal, 1996; de Angelis et al., 2012), which were beyond the scope of the study. It would be interesting to note that similar results were demonstrated by Akther and Hassan (2011a). For example, the combination of  $T_s$ , NMDI, and TVWI variables revealed 91.60% of the fires spots fell under ‘very high’ to ‘moderate’ danger classes when compared between the fire danger categories and actual fire occurrences data during the period of 2006–2008 fire seasons.

**Table 5.4: Percentage of data fell under each fire danger category using the combined variable of Ts, NMDI, and NDVI in comparison with the fire spot.**

Year	No of variables satisfying the fire danger condition	Fire danger categories	% of data	Cumulative % of data
2009	All	Very High	22.92	22.92
	At least 2	High	31.94	54.86
	At least 1	Moderate	34.03	<b>88.89</b>
	None	Low	11.11	100.00
2010	All	Very High	30.77	30.77
	At least 2	High	35.16	65.93
	At least 1	Moderate	24.73	<b>90.66</b>
	None	Low	9.34	100.00
2011	All	Very High	32.84	32.84
	At least 2	High	31.34	64.18
	At least 1	Moderate	29.10	<b>93.28</b>
	None	Low	6.72	100.00
Average (2009-2011)	All	Very High	28.84	28.84
	At least 2	High	32.81	61.66
	At least 1	Moderate	29.29	<b>90.94</b>
	None	Low	9.06	100.00

### 5.3.3 Fire danger maps for each period of interest

We produced fire danger maps for the whole fire seasons of 2009-2011. For example, Figures 5.8-5.10 show the forecasted fire danger maps during different periods of interest along with the fire spots data. They revealed that 84.7, 72.0, and 87.1% of the fire danger categories fell under ‘very high’ to ‘moderate’ danger classes during the three periods of interest. The fires (i.e., June 13, 2009; June 20, 2010; and May 14, 2011) which were started within these periods and burned more than 36,000; 33,310; and 119,375 ha of the forested land. Furthermore, individual fire spot demonstrated that most of the fire fell under ‘high’ to ‘very high’ danger classes.

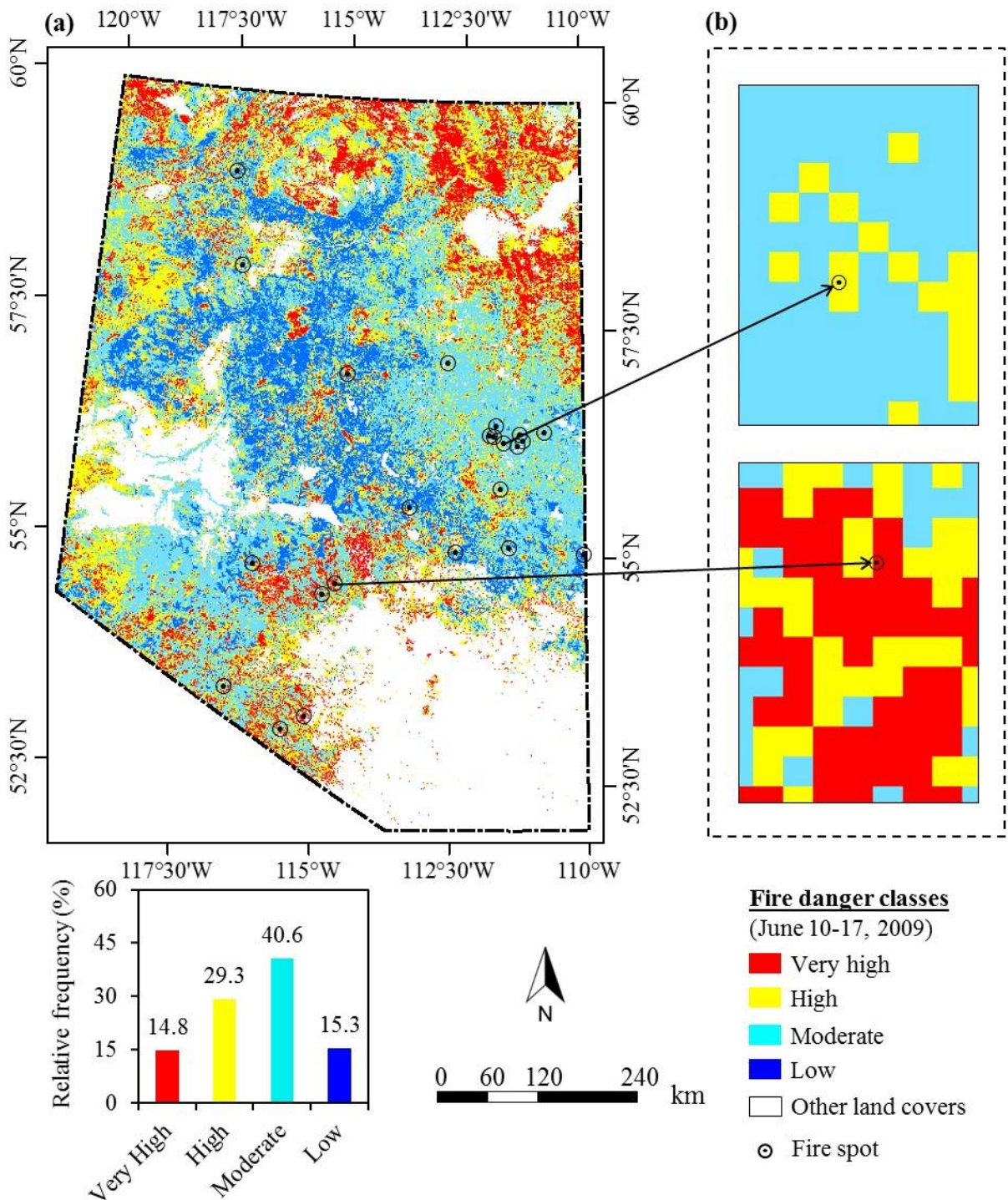


**Figure 5.8: (a) Fire danger map for the period June 10-17, 2009 forecasted by combining the  $T_s$ , NMDI, and NDVI variables exploited during the immediate preceding period i.e., June 2-9, 2009; and actual fire spots during the June 13, 2009 (i.e., 164 DOY); (b) fire danger classes with actual fire spots.**

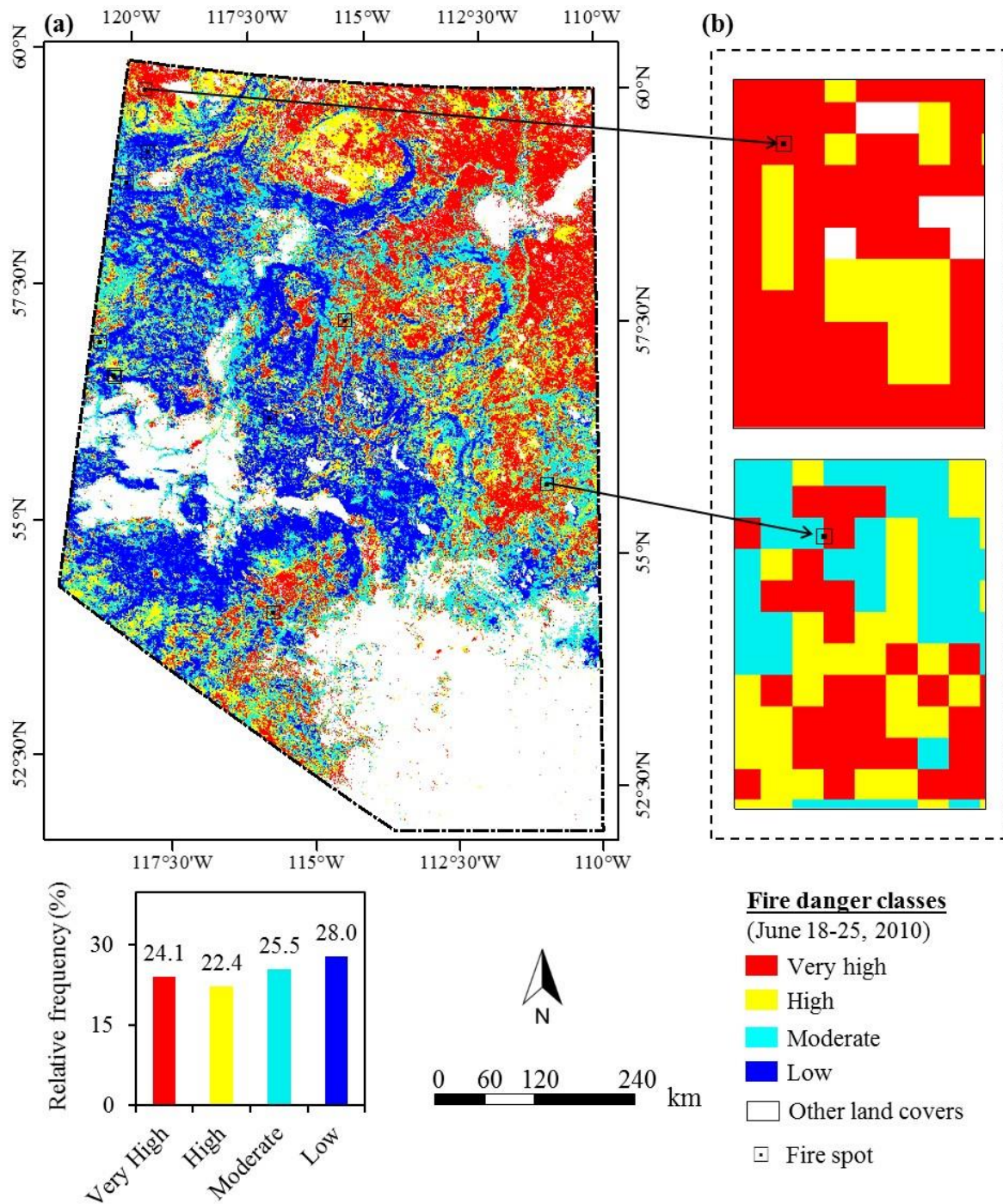


**Figure 5.9: (a) Fire danger map for the period June 18-25, 2010 forecasted by combining the  $T_s$ , NMDI, and NDVI variables exploited during the immediate preceding period i.e., June 10-17, 2010; and actual fire spots during the June 20, 2010 (i.e., 171 DOY); (b) fire danger classes with actual fire spots.**

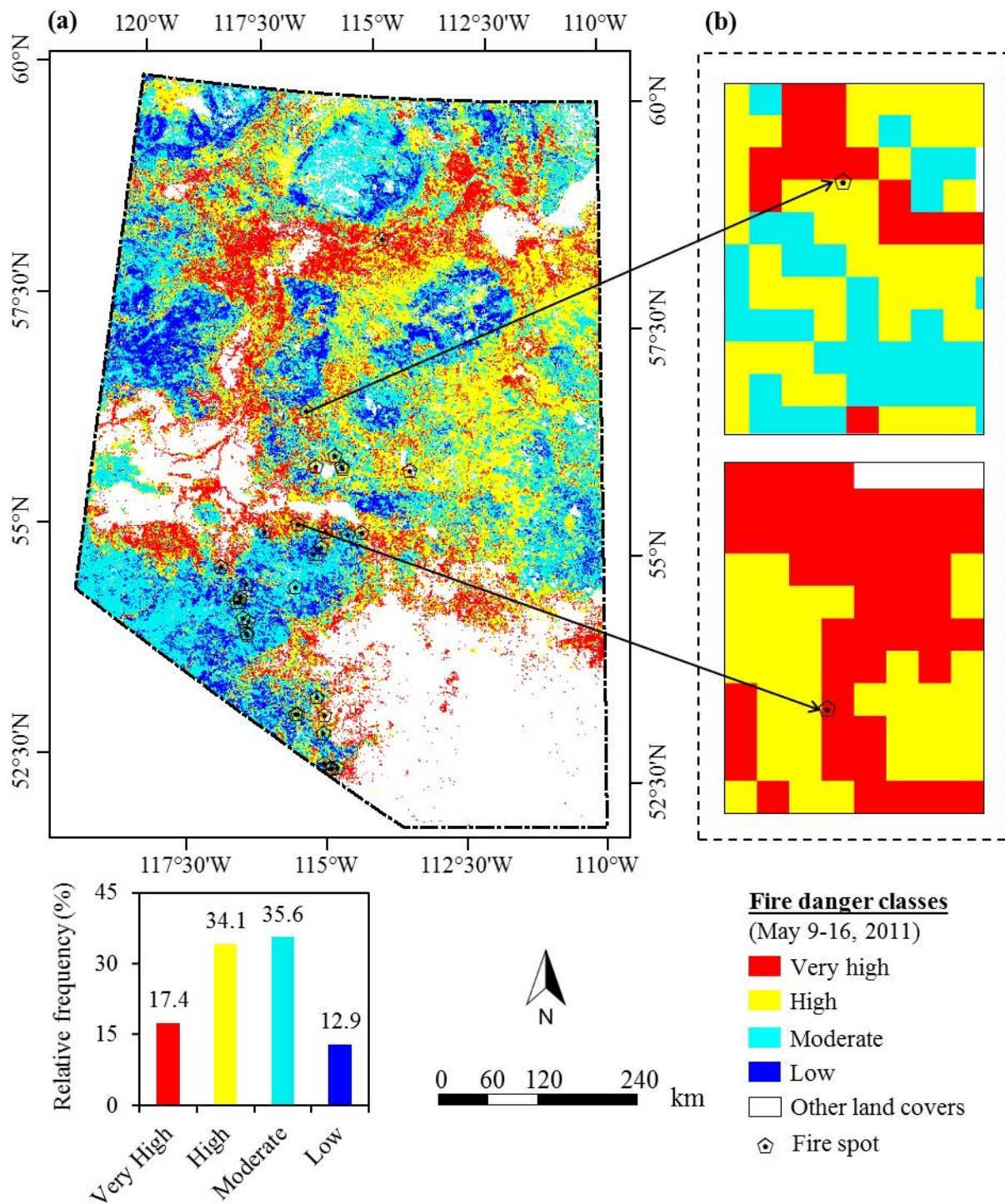


**Figure 5.10: (a) Fire danger map for the period May 9-16, 2011 forecasted by combining the  $T_s$ , NMDI, and NDVI variables exploited during the immediate preceding period i.e., May 1-8, 2011; and actual fire spots during the May 14, 2011 (i.e., 134 DOY); (b) fire danger classes with actual fire spots.**

## 5.4 Evaluation of FFDFS system at daily-scale forecasting

### 5.4.1 Assessment of the impact of daily PW on fire danger conditions

Upon getting the study area-specific daily ( $\overline{PW}$ ) during  $j$  day; I computed the daily PW-specific fire danger conditions (i.e., high and low) during  $j+1$  day, and compared them against the ground-based fire spots. It revealed that fair amount (i.e., 53.54% on an average during 2009-2011 period; see Figure 5.11 for details) of fire spots fell under high danger category [i.e.,  $PW(j) \leq \overline{PW}(j)$ ]. These findings were quite reasonable as the fire occurrences would not only depend on the PW but also other factors, e.g., temperature, precipitation, wind regimes, topography, fuel types, source of ignitions, etc. (van Wagner, 1987; Leblon et al., 2001; Lecina-Diaz et al., 2014; Adab et al., 2013; Ardakani et al., 2011). Furthermore, I analyzed the actual fire occurrence in the context of the study area-specific average and standard deviations associated with PW (see Figure 5.11); and observed two major issues. Firstly, I didn't find whether relatively lower amount of PW (i.e., less than 'average - 1 standard deviation') was related to more fire occurrences. In fact, similar situations were also observed for the variables of  $T_s$ , NMDI, and TVWI over boreal forested regions of Alberta in (Akther and Hassan, 2011a). Also, Bartsch et al. 2009 noticed that more dryness didn't always favor the fire occurrences while investigating soil moisture anomalies as a fire danger indicator over Siberia. Secondly, I found that approximately 70.44% of the fires fell within 'average  $\pm$  1 standard deviation'; and similar results were also reported in other studies. For example: (i) Clabo and Bunkers (2011) found that most of the fires occurred in South Dakota when the PW in 800-700 mb layer (i.e., ~1.8-2.7 km above the ground surface) was below or around the monthly  $\overline{PW}$ -levels; (ii) Sitnov and Mokhov (2013) observed the daily PWs were highly anomalous (i.e., water vapor content was low compare to that of the ten years average-values)

during July 23 to August 18, 2010 over European Russia when more than 60% of the fires were taken place; and (iii) Akther and Hassan (2011a) reported that most of the fire occurrences were found within the ‘average  $\pm 1$  standard deviation’ for the variables of  $T_s$ , NMDI, and TVWI over boreal forested regions of Alberta.

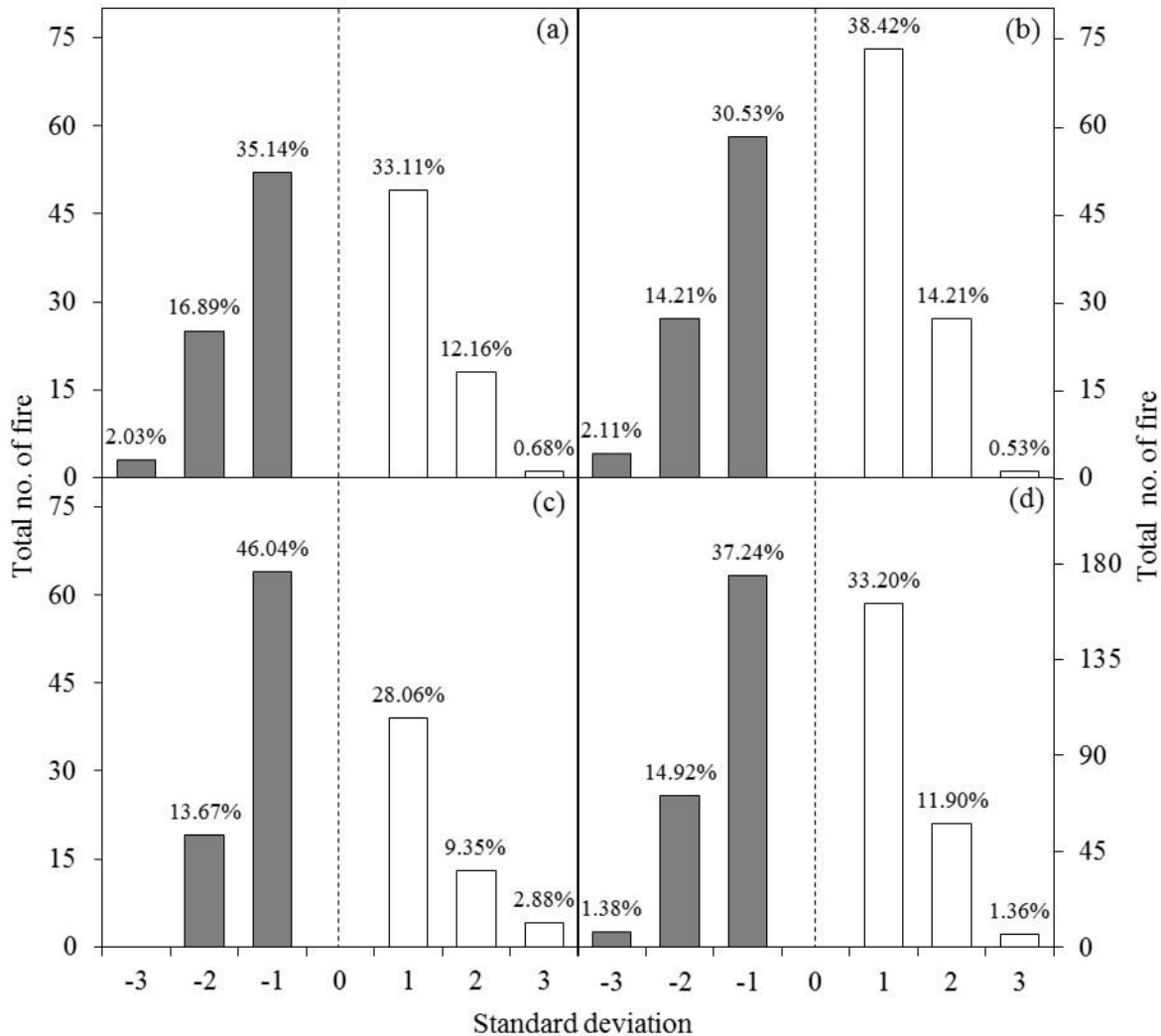


**Figure 5.11: Frequency distribution of the fires with respect to PW and its corresponding study area average values during the  $j$  day when actual fires were taken place in the following  $j+1$  day on the basis of the ‘study area-specific average  $\pm 3$  standard deviation’ values and percentage of fire spots during (a) 2009, (b) 2010, (c) 2011, and (d) 2009-2011.**

#### 5.4.2 Evaluation of daily-scale FFDFS system

Once the variable-specific (i.e., Ts, NMDI, NDVI, and PW) fire danger conditions (i.e., either high or low) were generated, I combined all the variables of interest to forecast the fire danger conditions at daily-scale. The combined fire danger conditions demonstrated excellent results, i.e., on an average 95.51% of the fires fell under ‘extremely high’ to ‘moderate’ danger classes during 2009-2011 period (see Table 5.5).

**Table 5.5: Percentage of data fell under each fire danger category using the combined variable of Ts, NMDI, NDVI, and PW in comparison with the fire spot.**

Year	No of variables satisfying the fire danger condition	Fire danger categories	% of data	Cumulative % of data
2009	All	Extremely High	8.96	8.96
	At least 3	Very High	28.36	37.31
	At least 2	High	36.57	73.88
	At least 1	Moderate	20.90	<b>94.78</b>
	None	Low	5.22	100.00
2010	All	Extremely High	14.88	14.88
	At least 3	Very High	30.95	45.83
	At least 2	High	30.36	76.19
	At least 1	Moderate	19.64	<b>95.83</b>
	None	Low	4.17	100.00
2011	All	Extremely High	15.45	15.45
	At least 3	Very High	36.59	52.03
	At least 2	High	30.08	82.11
	At least 1	Moderate	13.82	<b>95.93</b>
	None	Low	4.07	100.00
Average (2009-2011)	All	Extremely High	13.09	13.09
	At least 3	Very High	31.97	45.06
	At least 2	High	32.34	77.39
	At least 1	Moderate	18.12	<b>95.51</b>
	None	Low	4.49	100.00

In particular to 2011 fire season, several catastrophic fires (i.e., Slave Lake and Fort McMurray regional fires in mid-May) were observed within the study area. The Slave Lake fires were responsible for burning approximately 22,000 ha of forest (FTCWRC, 2012); on the other hand, 595,000 ha of muskeg and bush was burned within Fort McMurray region (Treenotic, 2011). Thus, I opted to evaluate the performance of the FFDFS during mid-May, 2011, which were calculated as a function of the combined input variables of  $T_s$ , NMDI, NDVI, and PW acquired during the prior day (i.e., May 9 and 13, 2011 for PW; and May 1-8, 2011 for  $T_s$ , NMDI, and NDVI) (see Figure 5.12 for details). The fire danger conditions were analyzed over both of Slave Lake and Fort McMurray regions (where the worst fires were occurred during the recent history). It revealed that 100 and 94% of the fire spots fell under ‘extremely high’ to ‘high’ danger classes for Slave Lake and Fort McMurray regions, respectively while comparing with MODIS fire spot data. Thus, the effectiveness of the daily-scale FFDFS in forecasting the devastating fires was also proved.

#### *5.4.3 Generation of fire danger forecasting map at daily-scale*

Upon combining the four input variables of the FFDFS, I produced fire danger map on daily basis to forecast the fire danger conditions into five categories. Figures 5.13-5.15 show the combined fire danger maps at 500 m spatial resolution for June 13, 2009; June 20, 2010; and May 14, 2011 respectively while the input variables were acquired during the immediate preceding days for PW, and period (i.e., June 2-9, 2009; June 10-17, 2010; and May 1-8, 2011) for  $T_s$ , NMDI, and NDVI images. The fire danger map shown in Figure 5.13 revealed that approximately 91.50% of the pixels fell in ‘extremely high’ to ‘moderate’ danger categories. In addition, I observed that the

actual fires that started during June 13, 2009 (i.e., 23 number of fires that burned more than 36,000 ha); and their specific danger conditions demonstrated that

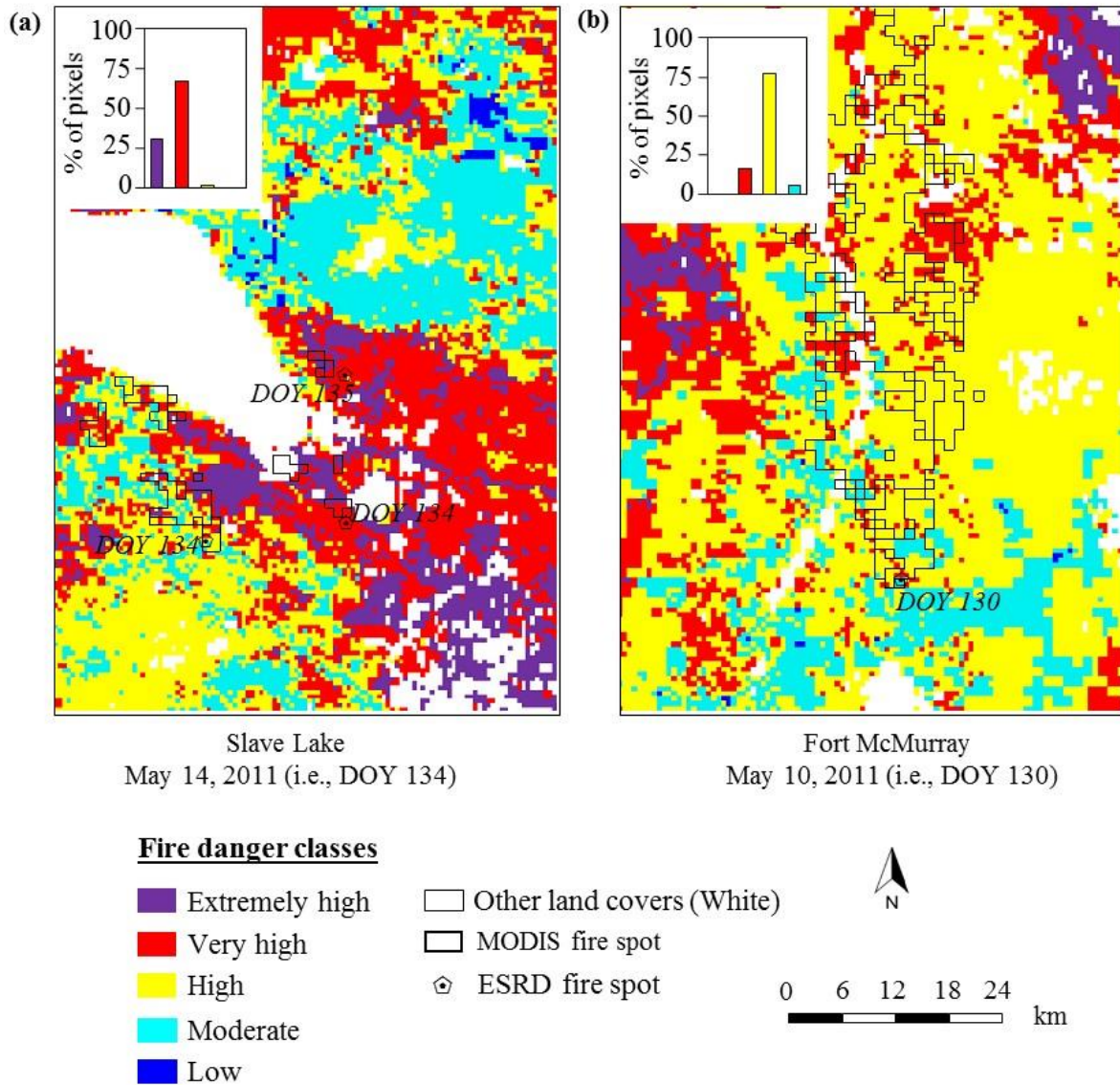


**Figure 5.12: Fire danger maps for mid-May, 2011 forecasted by combining the  $T_s$ , NMDI, NDVI, and PW variables exploited during the immediate preceding day at: (a) Slave lake (May 13, 2011), and (b) Fort McMurray (May 9, 2011) regions.**

95.24% of fire fell under ‘extremely high’ to ‘moderate’ danger classes (sample fire spots along with the danger conditions were shown in Figure 5.13b). Similarly, I observed from Figure 5.14 that 83.10% of the pixels fell under ‘extremely high’ to ‘moderate danger’ classes. The fire danger map in Figure 5.15 revealed that ~8.1, 25.7, 39.0, and 22.9% (i.e., in total 95.70%) of the pixels fell under danger categories of ‘extremely high’, ‘very high’, ‘high’, and ‘moderate’ for the entire study area.

### **5.5 Enhancement of forecasting capability of daily-scale over the 8-day scale FFDFS**

We combined the variables of interest (i.e.,  $T_s$ , NMDI, NDVI, and PW) to forecast the fire danger conditions at daily-scale. The combined fire danger conditions demonstrated on an average 95.51% of the fires fell under ‘extremely high’ to ‘moderate’ danger classes during 2009-2011 period (Table 5.5). We also observed very good results using the combined variables of  $T_s$ , NMDI, and NDVI at 8-day scale; while on an average 90.94% of the fires fell in ‘very high’ to ‘moderate’ danger classes during the same periods of interest (Table 5.4). In both cases, the fire danger conditions were compared with the Alberta ESRD fire spot data. So, it was clearly evident that the daily-scale FFDFS performed better than the 8-day scale FFDFS; i.e., improvement over 4.57% during the period of 2009-2011. However, the major enhancement of the new FFDFS system was the forecasting capability of fire danger conditions at daily-scale, which would be a pre-requisite in the context of operational perspective.

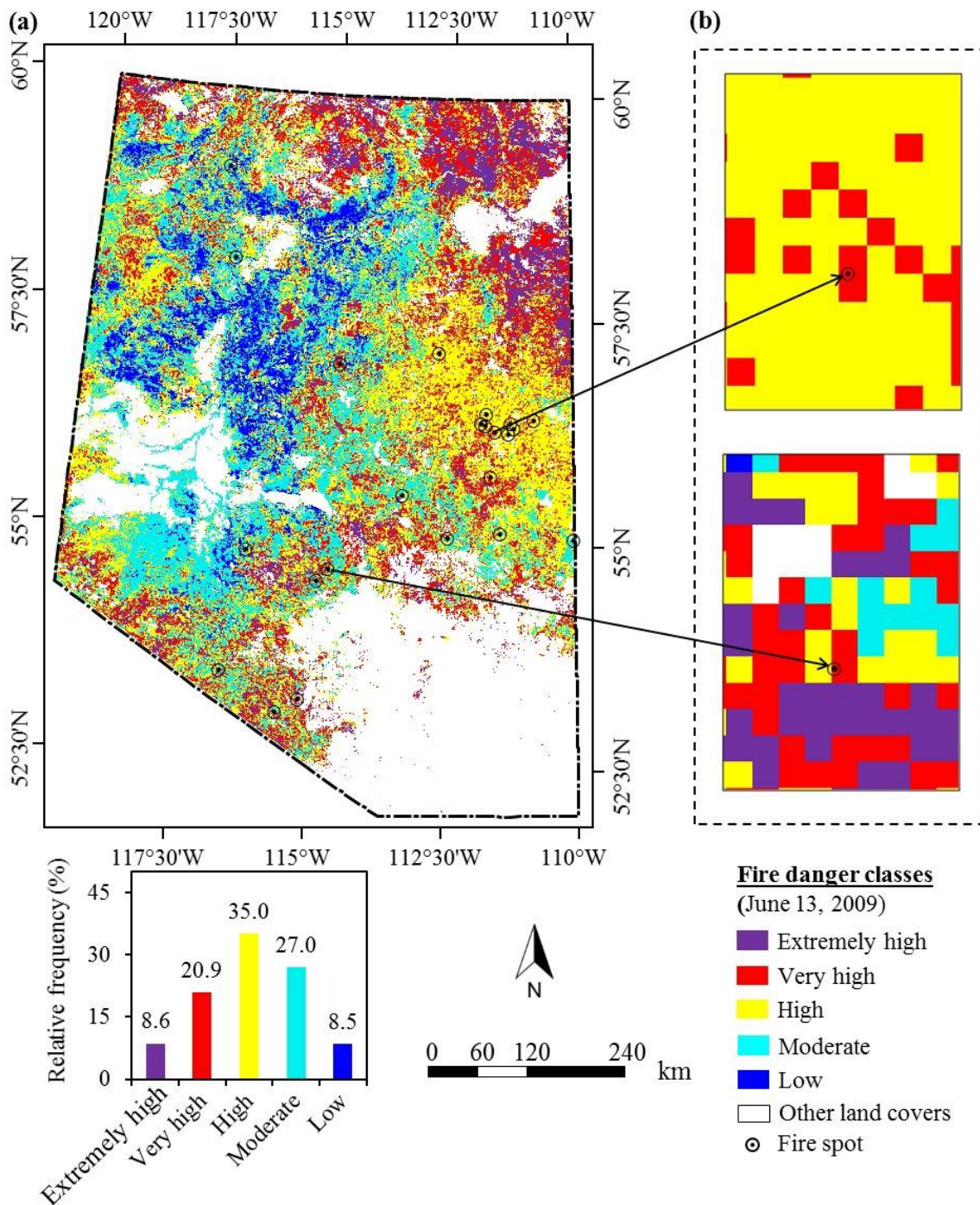


**Figure 5.13: (a) Fire danger map for June 13, 2009 forecasted by combining the  $T_s$ , NMDI, NDVI, and PW variables exploited during the immediate preceding day i.e., June 12, 2009; and actual fire spots during the June 13, 2009 (i.e., 164 DOY); (b) fire danger classes with actual fire spots.**

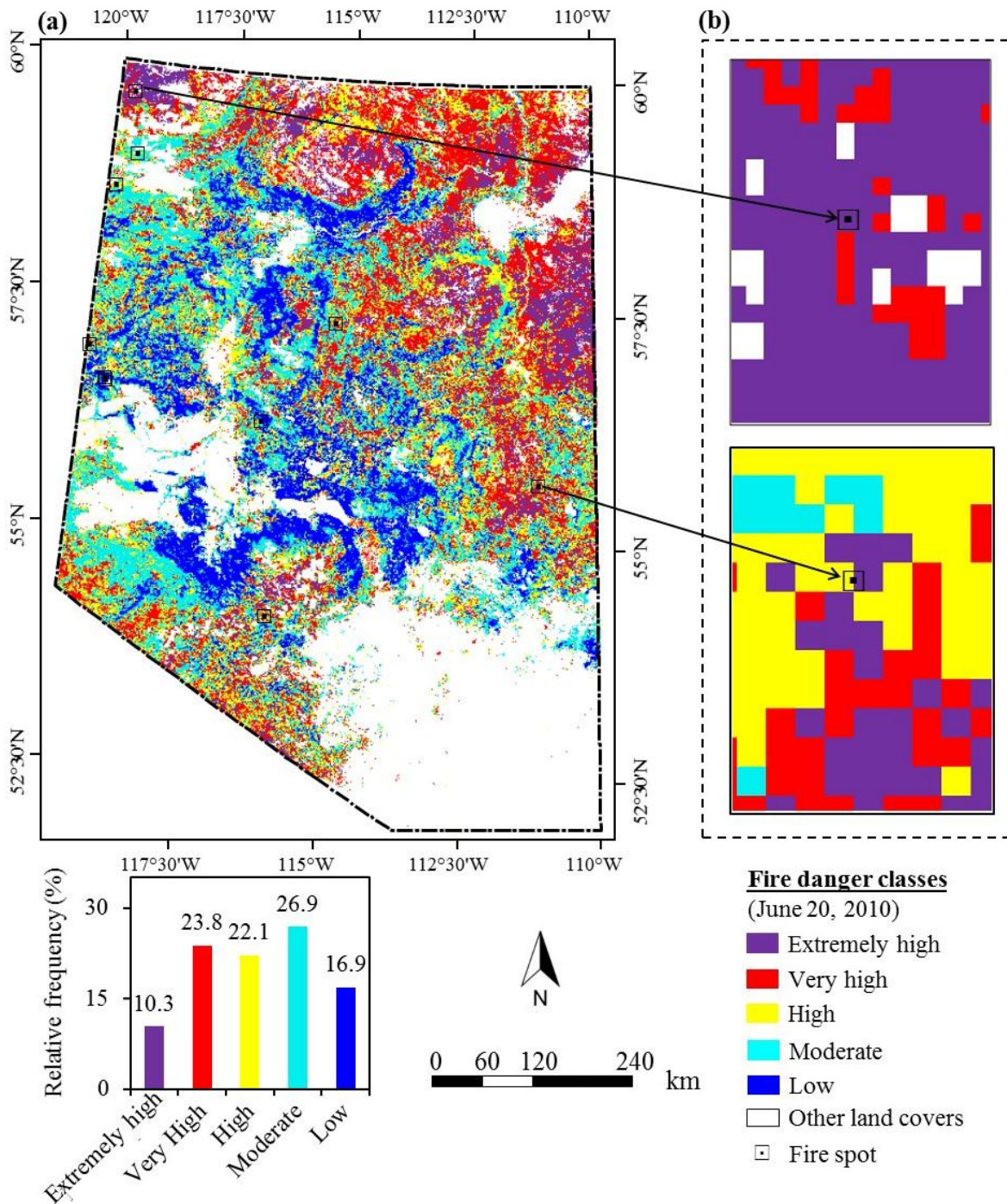


**Figure 5.14: (a) Fire danger map for June 20, 2010 forecasted by combining the  $T_s$ , NMDI, NDVI, and PW variables exploited during the immediate preceding day i.e., June 19, 2010; and actual fire spots during the June 20, 2010 (i.e., 171 DOY); (b) fire danger classes with actual fire spots.**

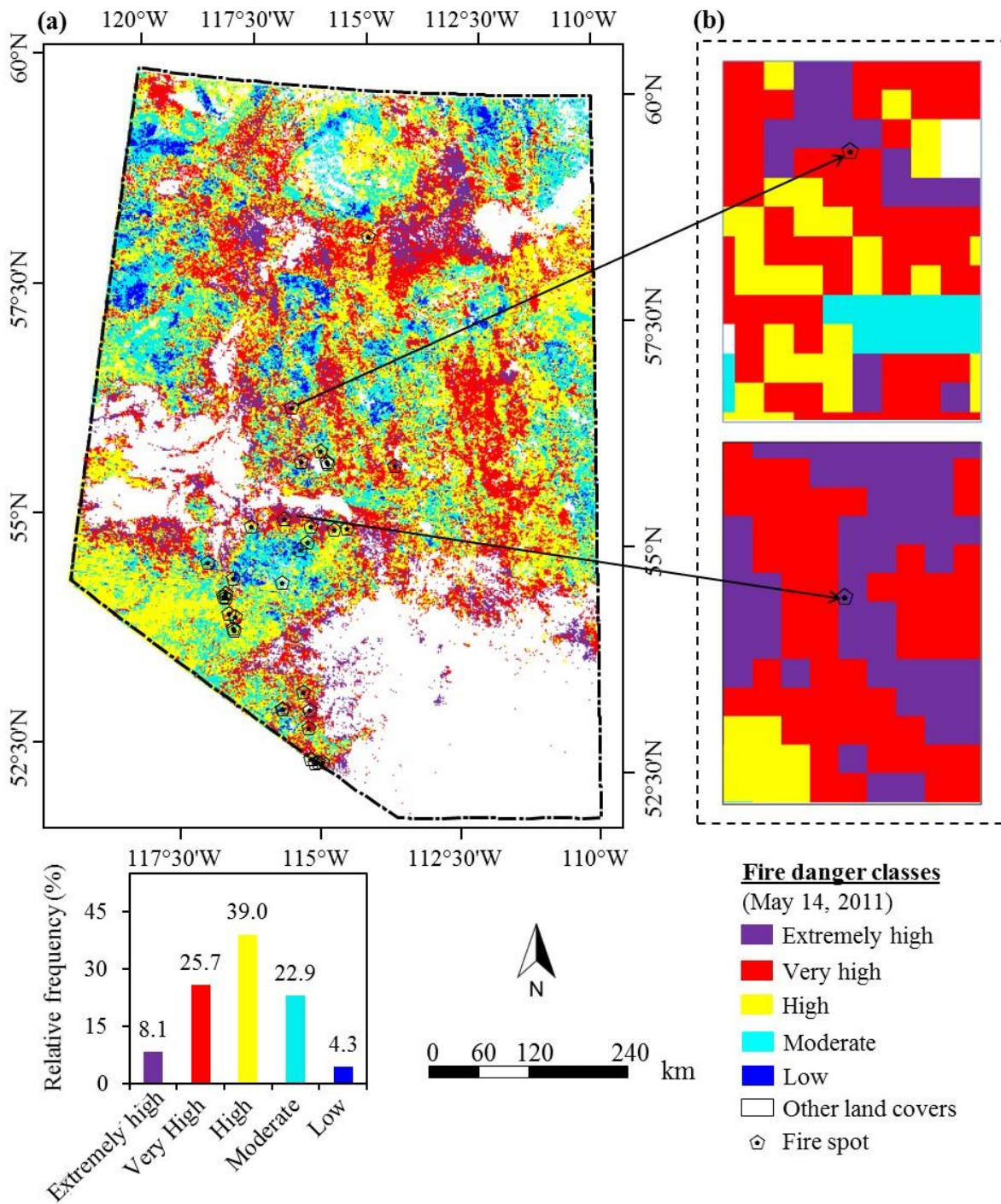


**Figure 5.15: (a) Fire danger map for May 14, 2011 forecasted by combining the  $T_s$ , NMDI, NDVI, and PW variables exploited during the immediate preceding day i.e., May 13, 2011; and actual fire spots during the May 14, 2011 (i.e., 134 DOY); (b) fire danger classes with actual fire spots.**

## CHAPTER 6 : CONCLUSIONS & RECOMMENDATIONS

### 6.1 Summary

In this thesis, I reviewed the most prominent operational fire danger rating systems and their limitations; and effectiveness of remote sensing-based methods for monitoring and forecasting fire danger conditions and their implications in operational perspective. The operational fire danger rating systems are mainly based on the meteorological variables and easily obtainable from ground-based observations. However, these systems have several weaknesses, such as (i) fire danger ratings are derived from sparsely located point-source meteorological data; (ii) spatial dynamics of the variable of interest generated by employing interpolation methods, which are highly dependable on density of observation network, topography, and the type of interpolation method used; (iii) function of dead fuel moisture only; (iv) limited number of fuel types are used, as determination of fuel parameters are time-consuming, cost intensive, and dynamic over different climatic conditions; (iv) the parameters and relationships are determined empirically using field and laboratory experiments; and (v) complex rules in operational perspective. So thus, it is essential to investigate the fire danger ratings in each ecosystem independently, as it depends on the interactions between biotic and abiotic components. The changing climate conditions also urge of revisiting the parameters of the operational systems for making them more reliable and acceptable.

The fire danger conditions are the most important part in integrated fire management due to their wide applicability (e.g., pre-fire forest conditions, delineating prescribe burning area, reduce intensive survey operations, quick detection of fire starts and deployment of firefighting units, etc.). Over the last several decades, the remote sensing-based methods have been investigated for fire danger management activities. These methods are categorized into two major groups: fire danger monitoring and fire danger forecasting systems. In particular for monitoring the fire danger conditions, several environmental variables are derived from optical, thermal, and radar images, and explored individually and/or in combination. As the fire danger conditions define the likelihood of fire occurrence, these methods are found to be unsuccessful because they attempt to capture danger conditions during and/or after the fire occurrence. However, for monitoring the forest fire related disaster, MODIS-based fire detection data are available at a daily temporal scale which is under full operation and used by the fire managers for fire behavior and suppression strategy.

The use of remote sensing-based methods for forecasting fire danger conditions are found in the literature though limited. Most of the fire danger forecasting systems are in the moderate range and coarse spatial resolution. An NDVI-based operational system was proposed by Burgan et al., 1998 to compute the fire potential maps, but it could not be considered as a fully remote sensing based method as it combines satellite data, meteorological observations and fuel models (detail in section 2.4). The methods illustrated above have the potential to functioning by incorporating some adjustments and improvements, such as enhancement of temporal resolution; acquisition of cloud free imagery by the sensors; development of enhanced gap-filling methods that would improve

quality of optical and thermal images; and better understanding of the vegetation characteristics those are closely related to fire danger conditions. It is interesting to note that, the radar data has the potential to capture in the microwave spectral bands that penetrates cloud, canopy and interacts with the tree structure, and theoretically in any weather, but has greater limitations in temporal scale and operates under the commercial operating mode.

Due to the limitations of the meteorological-based operational systems; and remote sensing-based methods illustrated, I opted to develop a fully remote sensing-based fire danger forecasting systems which could be utilized as an operational one. In this thesis, I proposed a simple protocol in order to filling the data gaps in the 8-day composite of MODIS-derived  $T_s$ , NMDI, and NDVI on the basis of both spatial and temporal connotations. It revealed that the use of the  $3 \times 3$  window size would infill approximately 71.52 and 100% of the data gaps for  $T_s$  and both NMDI and NDVI images during 2009-2011, respectively. In these cases, I also observed strong agreements between the predicted values for the variable of interest with the observed data (i.e., the good quality pixels which were declared as data gaps), such as  $r^2$ , and RMSE values were on an average: (i) 0.87 and 1.003 K, respectively for  $T_s$  images; (ii) 0.93 and 0.019, respectively, for NMDI images; and (iii) 0.88 and 0.022, respectively, for NDVI images during 2009-2011. In order to filling the remaining data gaps (i.e., ~ 0.50, 1.55, and 0.44%, respectively) for the period of 2009-2011 for  $T_s$  images, I increased window size (in the range from  $5 \times 5$  to  $15 \times 15$ ); and both of the  $r^2$  and RMSE values were still found to be in the reasonable bounds (i.e.,  $r^2 \approx 0.81$  and RMSE  $\approx 1.25$  K for  $5 \times 5$  window size;  $r^2 \approx 0.68$  and RMSE  $\approx 1.51$  K for  $15 \times 15$  window size).

In this thesis, the earlier developed method of forest fire danger forecasting system was enhanced by incorporating several remote sensing-derived variables (i.e.,  $T_s$ , NMDI, and NDVI). We observed very good results using the combined variables of  $T_s$ , NMDI, and NDVI at 8-day scale while comparing with the Alberta ESRD fire data during 2009-2011. It shows that on an average 90.94% of the fires fell in 'very high' to 'moderate' danger classes. Furthermore, I developed a simple framework for forecasting forest fire danger conditions at daily-scale using only remote sensing-derived variables for the first time according to our best knowledge. This proposed system consisted of four steps: (i) calculation of input variables (i.e.,  $T_s$ , NMDI, NDVI, and PW) of the FFDFS system; (ii) computation of study-area specific average values for each variable of interest; (iii) determination of variable-specific fire danger conditions (either high or low); and (iv) integration of all the four variable-specific fire danger conditions into five fire danger categories (i.e., extremely high, very high, high, moderate, and low). The integrated daily-scale FFDFS system revealed excellent results in forecasting the forest fire danger conditions, i.e., 94.78–95.93% of the fires fell under 'extremely high' to 'moderate' danger classes during 2009–2011 period. Thus, the proposed daily-scale FFDFS system would be effective in the operational perspective. We also believe that the proposed system would be useful in supplementing the currently operational meteorological-based forecasting systems in particular to the remote areas of the landscape and in between two weather stations. In addition, the proposed system could potentially be adopted in other jurisdictions and/or globally; however, I strongly recommend that it should be thoroughly evaluated prior to its implementation.

## 6.2 Contribution to science

The expected contributions of forest fire danger forecasting system using remote sensing technology can be summarized as follows:

- (i) The proposed gap filling algorithm will enhance the quality of the images (i.e., the input variables of FFDFS) as gaps are commonly found in optical and thermal remote sensing data due to the presence of cloud, aerosol, viewing geometry of the satellite platforms, etc.;
- (ii) The four variables of interest such as  $T_s$ , NMDI, NDVI, and PW were used in forecasting the fire danger conditions for the first time according to best of my knowledge;
- (iii) The daily scale FFDFS system has greater advantage over the meteorological based Canadian FWI system in regards to capturing the spatial variability of the forecasted danger conditions. In addition, the FWI system has variable thresholds for fire danger conditions in different jurisdictions while the FFDFS system can be used globally depending on the conditions of the variables in the area of interest;
- (iv) In view of operational perspective, a simplified modelling approach is proposed by combining the environmental variables for fire danger forecasting at daily scale; thus such a system will help the fire managers for better understanding the conditions of forest areas those are potential to fire ignition, and therefore supports in both prescribed fire and wildfire; and
- (v) The FFDFS approach developed using remote sensing variables has operational value and can potentially be incorporated into meteorological-based fire danger forecasting systems.

### **6.3 Recommendations for future work**

Our proposed remote sensing-based daily-scale FFDFS system demonstrated its excellent abilities in forecasting the forest fire danger conditions. Despite the overall performance of the FFDFS, I observed a small percentage of the fire spots (i.e., 4.49%) fell in the low danger category, which could be enhanced upon considering other fire related variables. Those might include the incorporation of: (i) spatially dynamic but temporally static (e.g., topographic parameters such as slope, elevation, and aspect, proximity to road networks, and vicinity to urban areas) (Adab et al., 2013), and spatially static but temporally dynamic (e.g., the effect of long weekends would attract more people for camping in forest) variables; (ii) other meteorological variables, such as incident solar radiation, amount and duration of precipitation, wind regimes, etc. as these factors are commonly used in meteorological-based operational systems (Burgan et al., 1997); (iii) lightning as a source of ignition; (iv) vegetation phenology as it might play an important role in defining the water stress so thus fire occurrence (Bajocco et al., 2010); (v) comparison of the outcomes of the FFDFS system with that of Canadian FWI system; (vi) leaf area index (as it increases with the increase of vegetation greenness) could be used in the framework of FFDFS system; (vii) further exploration is needed in regards to determine inter-relationship among the variables of interest (i.e.,  $T_s$ , NMDI, NDVI, and PW); and (viii) relatively higher spatial resolution (e.g., 250 m) for the input variables in delineating the landscape in more detail (Wing et al., 2014). Among these, wind regimes are commonly used in most of the operational systems; however, I was unable to incorporate such a variable in our proposed FFDFS as remote sensing-based estimates of wind regimes would be extremely difficult.

## References

- Abbott, K.N.; Leblon, B.; Staples, G.C.; Maclean, D.A.; Alexander, M.E., 2007. Fire danger monitoring using RADARSAT-1 over northern boreal forests. *International Journal of Remote Sensing* 28 (6), 1317-1338.
- Adab, H.; Kanniah, K.D.; Solaimani, K., 2013. Modeling forest fire risk in the northeast of Iran using remote sensing and GIS techniques. *Natural Hazards* 65, 1723-1743.
- Aguado, I.; Chuvieco, E.; Martin, P.; Salas, J., 2003. Assessment of forest fire danger conditions in southern Spain from NOAA images and meteorological indices. *International Journal of Remote Sensing* 24, 1653-1668.
- Akther, M.S.; Hassan, Q.K., 2011a. Remote sensing based assessment of fire danger conditions over boreal forest. *IEEE Journal of Selected Topics in Applied Earth Observations and Remote Sensing* 4 (4), 992-999.
- Akther, M.S.; Hassan, Q.K., 2011b. Remote sensing based estimates of surface wetness conditions and growing degree days over northern Alberta, Canada. *Boreal Environment Research* 16 (5), 407-416.
- Albini, F.A., 1976. Estimating wildfire behavior and effects. Department of Agriculture, Forest Service, Intermountain Forest and Range Experiment Station, Ogden, UT, 91p.
- Alexander, M.E.; Cole, F.V., 2001. Rating fire danger in Alaska ecosystems: CFFDRS provides an invaluable guide to systematically evaluating burning conditions. U.S. Department of Interior, Bureau of Land Management, Alaska Fire Service, Fort Wainwright, Alaska, *Fireline* 12 (4), 2-3.

- Alexander, M.E.; Fogarty, L.G., 2002. A pocket card for predicting fire behavior in grasslands under severe burning conditions. Natural Resources Canada, Canadian Forest Service, Ottawa, Ontario, Forest Research, Rotorua, New Zealand, and National Rural Fire Authority, Wellington, New Zealand, Fire Technology Transfer Note No. 25, 8p.
- Allgöwer, B.; Carlson, J.D.; van Wagendonk, J.W., 2003. Introduction to fire danger rating and remote sensing – Will remote sensing enhance wildland fire danger rating? In: Wildland Fire Danger Estimation and Mapping, The Role of Remote Sensing Data, Chuvieco Ed., World Scientific Publishing Co. Pte. Ltd., 5 Toh Tuck Link, Singapore, 4, pp. 1-19.
- Amiro, B.D.; Cantin, A.; Flannigan, M.D.; de Groot, W.J., 2009. Future emissions from Canadian boreal forest fires. *Canadian Journal of Forest Research* 39, 383-395.
- Andrews, P.L.; Bevins, C.D.; Seli, R.C., 2005. BehavePlus fire modeling system version 3.0, User's guide Rocky mountain research station, USDA Forest Service, 142p.
- Ardakani, A.S.; Zoj, M.J.V.; Mohammadzadeh, A.; Mansourian, A., 2011. Spatial and temporal analysis of fires detected by MODIS data in northern Iran from 2001 to 2008. *IEEE Journal of Selective Topics in Applied Earth Observations and Remote Sensing* 4, 216-225.
- Bajocco, S.; Rosati, L.; Ricotta, C., 2010. Knowing fire incidence through fuel phenology, A remotely sensed approach. *Ecological Modelling* 221, 59-66.
- Bartsch, A.; Balzter, H.; George, C., 2009. The influence of regional surface soil moisture anomalies on forest fires in Siberia observed from satellites. *Environmental Research Letter* 4, p.045021. doi:10.1088/1748-9326/4/4/045021

- Beck, J.A.; Alexander, M.E.; Harvey, S.D.; Beaver, A.K. 2001. Forecasting diurnal variation in fire intensity for use in wildland fire management applications. Fourth Symposium on Fire and Forest Meteorology Meeting, 13-15 November 2001, Reno Nevada, USA.
- Bisquert, M.; Sanchez, J.M.; Caselles, V., 2014. Modeling fire danger in Galicia and Asturias (Spain) from MODIS images. *Remote Sensing* 6, 540-554.
- Bisquert, M.M.; Sanchez, J.M.; Caselles, V., 2011. Fire danger estimation from MODIS Enhanced Vegetation Index data: application to Galicia region (North-west Spain). *International Journal of Wildland Fire* 20, 465-473.
- Bleken, E.; Mysterud, I.; Mysterud, I., 1997. Forest fire and environmental management: A technical report on forest fire as an ecological factor, Contracted report, Directorate for Fire and Explosion Prevention and Department of Biology, University of Oslo, 266p.
- BLM (Bureau of Land Management) Wyoming Wildland Fire Glossary, U.S. Department of the Interior. Available online: <http://www.blm.gov/wy/st/en/programs/Fire/glossary.2.html> (Accessed on: November 9, 2012).
- Bond, W.J.; Woodward, F.I.; Midgley, G.F., 2005. The global distribution of ecosystems in a world without fire. *New Phytologist* 165, 525–538.
- Bourgeau-Chavez, L.L.; Garwood, G.; Riordann, K.; Cella, B.; Alden, S.; Kwart, M.; Murphy, K., 2007. Improving the prediction of wildfire potential in boreal Alaska with satellite imaging radar. *Polar Record* 43 (4), 321-330.
- Bradshaw, L.S.; Deeming, J.E.; Burgan, R.E.; Cohen, J.D., 1983. The 1978 national fire-danger rating system, Tech Doc INT-169, USDA Forest Service, Ogden, Ut., 46p.

- Brotak, E.A., 1977. An investigation of the synoptic situations associated with major wildland fire. *Journal of Applied Meteorology* 16, 867-870.
- Burgan, R.E., 1988. 1988 revisions to the 1978 national fire-danger rating system. Research Paper SE-273, Asheville, NC: U.S. Department of Agriculture, Forest Service, Southeastern Forest Experiment Station, 39p.
- Burgan, R.E.; Andrews, P.L.; Bradshaw, L.S.; Chase, C.H.; Hartford, R.A.; Latham, D.J., 1997. Current status of the wildland fire assessment system (WFAS). *Fire Management Notes* 57, 14-17.
- Burgan, R.E.; Hartford, R.A., 1993. Monitoring vegetation greenness with satellite data. Gen. Tech. Rep. INT-297. Ogden, UT: U.S. Department of Agriculture, Forest Service, Intermountain Research Station, 13p.
- Burgan, R.E.; Hartford, R.A.; Eidenshink, J.C., 1996. Using NDVI to assess departure from average greenness and its relation to fire business. Gen. Tech. Rep. INT-GTR-333, Ogden, UT: U.S. Department of Agriculture, Forest Service, Intermountain Research Station, 8p.
- Burgan, R.E.; Klaver, R.W.; Klaver, J.M., 1998. Fuel models and fire potential from satellite and surface observations. *International Journal of Wildland Fire* 8, 159-170.
- Byram, G.M., 1963. An analysis of the drying process in forest fuel material. In: *International Symposium on Humidity and Moisture*. Washington D.C., 38p.
- Carlson, J.D.; Burgan, R.E., 2003. Review of users' needs in operational fire danger estimation: the Oklahoma example. *International Journal of Remote Sensing* 24 (8), 1601-1620.

- Carlson, T., 2007. An overview of the "triangle method" for estimating surface evapotranspiration and soil moisture from satellite imagery. *Sensors* 7, 1612-1629.
- CBS news, Edmonton, Fire destroys 40% of Slave Lake. Available online: <http://www.cbc.ca/news/canada/edmonton/story/2011/05/16/slave-lake-fire-evacuation.html>, First posted: May 16, 2011 03:58 PM MT. Last visited May 18, 2013.
- Ceccato P.; Flasse, S.; Gregoire, J-M., 2002a. Designing a spectral index to estimate vegetation water content from remote sensing data: Part 2. Validation and applications. *Remote Sensing of Environment* 82, 198-207.
- Ceccato P.; Gobron, N.; Flasse, S.; Pinty, B.; Tarantola, S., 2002b. Designing a spectral index to estimate vegetation water content from remote sensing data: Part 1. Theoretical approach. *Remote Sensing of Environment* 82, 188-197.
- Ceccato, P.; Flasse, S.; Tarantola, S.; Jacquemoud, S.; Grégoire. J-M., 2001. Detecting vegetation leaf water content using reflectance in the optical domain. *Remote Sensing of Environment* 77, 22-33.
- CFS (Canadian Forestry Service), 1984. Tables for the Canadian forest fire weather index system, 4<sup>th</sup> edition, Canadian Forestry Service, Ottawa, Ontario, Forestry Technical Report 25, 48p.
- Chatenoux, B.; Peduzzi, P., 2012. Biomass fires: preliminary estimation of ecosystem global economic losses. UNEP/GRID-Geneva, The United Nations Office for Disaster Risk Reduction and Global Assessment Report, Geneva, Switzerland, 12p.
- Chilès, J-P.; Delfiner, P. 2012. *Geostatistics Modeling Spatial Uncertainty*. Second edition, John Wiley & Sons Inc.: Hoboken, New Jersey, USA; 699p.

- Chu, T.; Guo, X., 2014. Remote sensing techniques in monitoring post-fire effects and patterns of forest recovery in Boreal forest regions: A review. *Remote Sensing* 6, 470-520.
- Chuvieco, E.; Aguado, I.; Cocero, D.; Riano, D., 2003. Design of an empirical index to estimate fuel moisture content from NOAA-AVHRR images in forest fire danger studies. *International Journal of Remote Sensing* 24 (8), 1621-1637.
- Chuvieco, E.; Aguado, I.; Dimitrakopoulos, A.P., 2004a. Conversion of fuel moisture content values to ignition potential for integrated fire danger assessment. *Canadian Journal of Forest Research* 34, 2284-2293.
- Chuvieco, E.; Aguado, I.; Yebra, M.; Nieto, H.; Salasa, J.; Martínez, M.P.; Vilar, L.; Martínez, J.; Martín, S.; Ibarra, P.; de la Riva, J.; Baeza, J.; Rodríguez, F.; Molina, J.R.; Herrero, M.A.; Zamora, R., 2010. Development of a framework for fire risk assessment using remote sensing and geographic information system technologies. *Ecological Modelling* 221, 46-58.
- Chuvieco, E.; Cocero, D.; Aguado, I.; Palacios, A.; Prado, E., 2004b. Improving burning efficiency estimates through satellite assessment of fuel moisture content. *Journal of Geophysical Research* 109, 1–8. <http://dx.doi.org/10.1029/2003JD003467>
- Chuvieco, E.; Cocero, D.; Riaño, D.; Martín, P.; Martínez-Vega, J.; De la Riva, J.; Pérez, F., 2004c. Combining NDVI and surface temperature for the estimation of live fuel moisture content in forest fire danger rating. *Remote Sensing for Environment* 92, 332-331.
- Chuvieco, E.; Giglio, L.; Justice, C., 2008. Global characterization of fire activity: toward defining fire regimes from Earth observation data. *Global Change Biology* 14, 1488-1502.

- Clabo, D.R.; Bunkers, M.J., 2011. Using variable column precipitable water as a predictor for large fire potential. In *Weather and Climate Impacts*, proceedings of the Ninth Symposium on Fire and Forest Meteorology, Palm Springs, CA, USA, October 20, 2011, Publisher: American Meteorological Society: Boston, MA, USA, 11.6.
- Clark, R. N., 1999. Spectroscopy of Rocks and Minerals, and Principles of Spectroscopy. In A. N. Rencz (Ed.), *Manual of Remote Sensing, Volume 3, Remote Sensing for the Earth Sciences* (pp. 3-58), New York: John Willey and Sons.
- Coll, C.; Wan, Z.; Galve, J.M., 2009. Temperature-based and radiance-based validations of the V5 MODIS land surface temperature product. *Journal of Geophysical Research*, 114: D20102, doi:10.1029/2009JD012038
- De Angelis, A.; Bajocco, S.; Ricotta, C., 2012. Phenological variability drives the distribution of wildfires in Sardinia. *Landscape Ecology* 27, 1535-1545.
- de Groot, W.J.; Bothwell, P.M.; Carlsson, D.H.; Logan, K.A., 2003. Simulating the effects of future fire regimes on western Canadian boreal forests. *Journal of Vegetation Science* 14, 355–364.
- de Groot, W.J.; Field, R.D.; Brady, M.A.; Roswintiarti, O.; Mohamad, M., 2007. Development of the Indonesian and Malaysian Fire Danger Rating Systems. *Mitigation and Adaptation Strategies for Global Change* 12, 165-180.
- Deeming, J.E.; Burgan, R.E.; Cohen, J.D., 1978. The national fire-danger rating system-1978, Gen. Tech. Rep. INT-39, USDA Forest Service, Ogden, Ut., 63p.

- Deeming, J.E.; Lancaster J.W.; Fosberg, M.A.; Furman, W.R.; Schroeder, M.J., 1972. The national fire-danger rating system, Res. Pap. RM-84, USDA Forest Service, Fort Collins, CO., 165p.
- Dennison, P.E.; Roberts, D.A.; Peterson, S.H.; Rechel, J., 2005. Use of normalized difference water index for monitoring live fuel moisture. *International Journal of Remote Sensing* 26 (5), 1035-1042.
- Desbois, N.; Vidal, A., 1996. Real time monitoring of vegetation flammability using NOAA-AVHRR thermal infrared data. *EARSel Advances in Remote Sensing* 4(4-XI), 25–32.
- Descloitres, J.; Vermote, E., 1999. Operational retrieval of the spectral surface reflectance and vegetation index at global scale from SeaWiFS data. *Proceedings of the International Conference and Workshops on Ocean Color, Land Surfaces, Radiation and Clouds, Aerosols, ALPS.99: The contribution of POLDER and new generation spaceborne sensors to global change studies*, Meribel, France, 18-22 January 1999, CNES: Toulouse, France, Land surfaces-O-02, pp. 1-4.
- Dominguez, L.; Lee, B.S.; Chuvieco, E.; Cihlar, J., 1994. Fire danger estimation using AVHRR images in the prairie provinces of Canada. In *Proceedings of the 2<sup>nd</sup> International Conference on Forest Fire Research*, Coimbra, Portugal, pp. 679-690.
- Downing D.J.; Pettapiece W.W., 2006. *Natural Regions and Subregions of Alberta*. Pub. No. T/852. Natural Regions Committee: Government of Alberta, Alberta, Canada, [http://tpr.alberta.ca/parks/heritageinfocentre/docs/NRSRcomplete%20May\\_06.pdf](http://tpr.alberta.ca/parks/heritageinfocentre/docs/NRSRcomplete%20May_06.pdf) (Accessed on April 10, 2012)

EOSDIS (Earth Observing System Data and Information System), 2011. Reverb ECHO, The Next Generation Earth Discovery Tool [online application]. National Aeronautics and Space Administration (NASA). Available online:  
[http://reverb.echo.nasa.gov/reverb/#utf8=%E2%9C%93&spatial\\_map=satellite&spatial\\_type=rectangle&keywords=mod](http://reverb.echo.nasa.gov/reverb/#utf8=%E2%9C%93&spatial_map=satellite&spatial_type=rectangle&keywords=mod) (Accessed on: September 20, 2011 & January 10, 2014).

ERDAS, 2011. Hexagon Geospatial. Available online:  
<http://www.hexagongeospatial.com/products/remote-sensing/erdas-imagine>. (Accessed on: September 15, 2011).

ESRD (Environment and Sustainable Resource Development), 10-Year Wildfire Statistics Available online:  
<http://www.srd.alberta.ca/Wildfire/WildfireStatus/HistoricalWildfireInformation/10-YearStatisticalSummary.aspx> (Accessed on June 23, 2014).

FAO (Food and Agriculture Organization of the United Nations), 2007. Fire management – global assessment 2006. FAO Forestry Paper 151, ISBN 978-92-5-1056666-0, Rome, Italy, 135p.

Flannigan, M.; Stocks, B.; Turetsky, M.; Wotton, M., 2009. Impact of climate change on fire activity and fire management in the circumboreal forest. *Global Change Biology* 15, 549-560.

FTCWRC (Flat Top Complex Wildfire Review Committee), 2012. Flat top complex, Submitted to the Minister of Alberta Environment and Sustainable Resource Development.  
<http://www.srd.alberta.ca/Wildfire/WildfirePreventionEnforcement/>

WildfireReviews/documents/FlatTopComplex-WildfireReviewCommittee-May18-2012.pdf, (Last visited 25 June, 2012).

Gao, B., 1996. NDWI-A normalized difference water index for remote sensing of vegetation liquid water from space. *Remote Sensing of Environment* 58, 257-266.

Gao, B.-C.; Kaufman, Y. J., 2014. Algorithm Technical Background Document, The MODIS Near-IR Water Vapor Algorithm, Product ID: MOD05 – Total Precipitable Water. Available online: [http://modis-atmos.gsfc.nasa.gov/\\_docs/atbd\\_mod03.pdf](http://modis-atmos.gsfc.nasa.gov/_docs/atbd_mod03.pdf) (accessed on 10 January 2014).

Gao, X.; Huete, A.R.; Didan, K., 2003. Multisensor comparisons and validation of MODIS vegetation indices at the semiarid Jordana experimental range. *IEEE Transaction of Geoscience and Remote Sensing* 41, 2368-2381.

GBA (Global Burnt Area)-2000 initiative, International strategy for disaster reduction. Available online: <http://www.fire.uni-freiburg.de/inventory/burnt%20area.html> (Accessed on: November 29, 2014).

Girard, M-C.; Girard C.M., 2003. Processing of remote sensing data. A.A. Balkema, India, 291p.

Gitelson, A.A.; Stark, R.; Grits, U.; Rundquist, D.; Kaufman, Y.; Derry, D., 2002. Vegetation and soil lines in visible spectral space: a concept and technique for remote estimation of vegetation fraction. *International Journal of Remote Sensing* 23 (13), 2537-2562.

González-Cabán, A., 2013. The economic dimension of wildland fires. *Vegetation Fires and Global Change – Challenges for Concentrated International Action*. Global Fire Monitoring Center (GFMC). ISBN 978-3-941300-1.

- Govind, A.; Chen, J.M.; Bernier, P.; Margolis, H.; Guindon, L.; Beaudoin, A., 2011. Spatially distributed modeling of the long-term carbon balance of a boreal landscape, *Ecological Modelling* 222, 2780-2795.
- Goward, S.N.; Markham, B.; Dye, D.G.; Dulaney, W.; Yang, J., 1990. Normalized difference vegetation index measurements from the Advanced Very High Resolution Radiometer. *Remote Sensing of Environment* 35, 257-277.
- Granstrom, A.; Schimmel, J., 1998. Assessment of the Canadian forest fire danger system for Swedish fuel conditions (in Swedish). Rescue Services Agency, Stockholm, Sweden, 34p.
- Guangmeng, G.; Mei, Z., 2004. Using MODIS land surface temperature to evaluate forest fire risk of northeast China. *IEEE Geoscience and Remote Sensing Letters* 1 (2), 98-100.
- Haines, D.A., 1988. A lower atmospheric severity index for wildland fires. *National Weather Digest* 13, 23-27.
- Han, K.; Viay, A.A.; Anctil, F., 2003. High-resolution forest fire weather index computations using satellite remote sensing. *Canadian Journal of Forest Research* 33, 1134-1143.
- Hardisky, M. A.; Klemas, V.; Smart, R.M., 1983. The influences of soil salinity, growth form, and leaf moisture on the spectral reflectance of *Spartina Alterniflora* canopies. *Photogrammetric Engineering and Remote Sensing* 49, 77-83.
- Hassan, Q.K.; Bourque, C.P.A.; Meng, F.; Cox, R.M., 2007. A wetness index using terrain-corrected surface temperature and normalized difference vegetation index derived from standard MODIS products: An evaluation of its use in a humid forest-dominated region of eastern Canada. *Sensors* 7, 2028-2048.

- Hassan, Q.K.; Bourque, C.P.A., 2009. Potential species distribution of Balsam Fir based on the integration of biophysical variables derived with remote sensing and process-based methods. *Remote Sensing* 1, 393-407.
- Hernandez-Leal, P.A.; Arbelo, M.; Gonzalez-Calvo, A., 2006. Fire risk assessment using satellite data. *Advances in Space Research* 37, 741-746.
- Hijmans, R.J.; Cameron, S.E.; Parra J.L.; Jones, P.G.; Jarvis, A., 2005. Very high resolution interpolated climate surfaces for global land areas. *International Journal of Climatology* 25, 1965-2005.
- Huesca, M.; Litago, J.; Palacios-Orueta, A.; Montes, F.; Sebastián-López, A.; Escribano, P., 2009. Assessment of forest fire seasonality using MODIS fire potential: A time series approach. *Agricultural and Forest Meteorology* 149, 1946–1955.
- Huete, A., 1988. A soil-adjusted vegetation index (SAVI). *Remote Sensing of Environment* 25, 295–309.
- Huete, A.; Didan, K.; Miura, T.; Rodriguez, E.P.; Gao, X.; Ferreira, L.G., 2002. Overview of the radiometric and biophysical performance of the MODIS vegetation indices. *Remote Sensing for Environment* 83, 195-213.
- Hunt, E.R.; Rock, B.N., 1989. Detection of changes in leaf water content using near and middle-infrared reflectance. *Remote Sensing Environment* 30, 43–54.
- Illera, P.; Fernandez, A.; Delgado, A., 1996. Temporal evolution of the NDVI as an indicator of forest fire danger. *International Journal of Remote Sensing* 17 (6), 1093-1105.
- Jain, A.; Ravan, S.A.; Singh, R.K.; Das, K.K.; Roy, P.S., 1996. Forest fire risk modelling using remote sensing and geographic information system. *Current Science* 70 (10), 928-932.

- Jiang, M.; Hu, Z.; Ding, D.; Fang, D.; Li, Y.; Wei, L.; Guo, M.; Zhang, S., 2012. Estimation of vegetation water content based on MODIS: Application on forest fire risk assessment. 20<sup>th</sup> International Conference on Geoinformatics, IEEE Conference Publications. pp. 1-4.
- Joyce, K.E.; Belliss, S.E.; Samsonov, S.V.; McNeill, S.J.; Glassey, P.J., 2009. A review of the status of satellite remote sensing and image processing techniques for mapping natural hazards and disasters. *Progress in Physical Geography* 33 (2), 183-207.
- Kales, S. N.; Soteriades, E.S.; Christophi, C.A.; Christiani, D.C., 2007. Emergency duties and deaths from heart disease among firefighters in the United States. *The New England Journal of Medicine* 356 (12), 1207-1215.
- Kang, S.; Running, S.W.; Zhao, M.; Kimball, J.S.; Glassy, J., 2005. Improving continuity of MODIS terrestrial photosynthesis products using an interpolation scheme for cloudy pixels. *International Journal of Remote Sensing* 26, 1659-1676.
- Kaufman, Y.K.; Gao, B-O., 1992. Remote sensing of water vapor in the Near IR from EOS/MODIS. *IEEE Transaction of Geoscience and Remote Sensing* 30 (5), 871-884.
- Keetch, J.J.; Byram, G.M., 1968. A drought index for forest fire control, Research Paper SE-38, USDA Forest Service, Southeastern forest experiment station, Asheville, NC, 32p.
- Khan, V.M., 2012. Long-term forecasting of forest fire danger based on the SLAV model seasonal ensemble forecasts, *Russian Meteorology and Hydrology* 37 (8), 505-513.
- King, R.M.; Furman, R.W., 1976, Fire danger rating network density, USDA Forest Service, Research Paper RM-117, Rocky Mountain Forest and Range Experimental Station, Fort Collins, Colorado 80521, 4p.

- Kogan, F.N., 1990. Remote sensing of weather impacts on vegetation in non-homogeneous areas. *International Journal of Remote Sensing* 11 (8), 1405-1419.
- Lawler, M., 2004. Analysis of the American national fire danger rating system vs. the Canadian fire weather index system for the Superior National Forest, US Forest Service, Tofte Ranger District, Superior National Forest, Technical Fire Management-17. (Tofte, MN), Available on request at <http://www.washingtoninstitute.net/showtfm17.php>
- Leblon, B., 2005. Monitoring forest fire danger with remote sensing, *Natural Hazards* 35, 343-359.
- Leblon, B.; Alexander, M.; Chen, J.; White, S., 2001. Monitoring fire danger of northern boreal forests with NOAA-AVHRR NDVI images. *International Journal of Remote Sensing* 22, 2839-2846.
- Leblon, B.; Bourgeau-Chavez, L.; San-Miguel-Ayanz, J., 2012. Sustainable development - authoritative and leading edge content for environmental management. In *Use of Remote Sensing in Wildfire Management*. Curkovic, S, editor. InTech: Croatia; pp. 55-81.
- Leblon, B.; García, P.A.F.; Oldford, S.; Maclean, D.A.; Flannigan, M., 2007. Using cumulative NOAA-AVHRR spectral indices for estimating fire danger codes in northern boreal forests. *International Journal of Applied Earth Observation and Geoinformation* 9, 335-342.
- Leblon, B.; Kasischke, E.S.; Alexander, M.E.; Doyle, M.; Abbott, M., 2002. Fire danger monitoring using ERS-1 SAR images in the case of northern boreal forests. *Natural Hazards* 27, 231-255.

- Lecina-Diaz, J.; Alvarez, A.; Retana, J., 2014. Extreme fire severity patterns in topographic, convective and wind-driven historical wildfires of Mediterranean pine forests. PLoS ONE 9, e85127. doi:10.1371/journal.pone.0085127
- Lee, B.S.; Alexander, M.E.; Hawkes, B.C.; Lynham, T.J.; Stocks, B.J.; Englefield, P., 2002. Information systems in support of wildland fire management decision making in Canada. Computers and Electronics in Agriculture 37, 185–198.
- Li, J.; Heap, A.D., 2011. A review of comparative studies of spatial interpolation methods in environmental sciences: Performance and impact factors. Ecological Information 6, 228–241.
- Loehman, R.A.; Clark, J.A.; Keane, R.E., 2011. Modeling effects of climate change and fire management on western white pine (*Pinus monticola*) in the Northern Rocky Mountains, USA. Forests 2, 832-860.
- Longley, P.A.; Goodchild, M.; Maguire, D.J.; Rhind, D.W., 2010. Geographic Information Systems and Science, 3rd edition. ISBN 978-0-470-72144-5. John Wiley & Sons Inc., Hoboken, NJ, 560p.
- Loveland, T.R.; Merchant, J.W.; Ohlen, D.O.; Brown, J.F., 1991. Development of a land characteristics database for the conterminous U.S., Photogrammetric Engineering and Remote Sensing 57 (11), 1453-1463.
- Luke, R.H.; McArthur, A.G., 1978. Bushfires in Australia, Australian Government Publishing Service, Canberra, 359p.

- Malone, S.L.; Kobziar, L.N.; Staudhammer, C.L.; Abd-Elrahman, A., 2011. Modeling relationships among 217 fires using remote sensing of burn severity in southern pine forests. *Remote Sensing* 3, 2005-2028.
- Manzo-Delgado, L.; Aguirre-Gómez, R.; Álvarez, R., 2004. Multitemporal analysis of land surface temperature using NOAA-AVHRR: preliminary relationships between climate anomalies and forest fires. *International Journal of Remote Sensing* 25 (20), 4471-4423.
- Martell, D.L., 2011. The development and implementation of forest fire management decision support systems in Ontario, Canada: Personal reflections on past practices and emerging challenges. *Mathematical and Computational Forestry & Natural-Resource Sciences* 3 (1), 18-26.
- McArthur, A.G., 1958. The preparation and use of fire danger tables, In *Proceedings, Fire Weather Conference*, Bureau of Meteorology, Melbourne, Australia, 18p.
- McArthur, A.G., 1967. Fire behavior in Eucalypt forests. Leaflet No. 107. Commonwealth of Australia, Department of National Development, Forest and Timber Bureau, Forestry Research Institute, Canberra, A.C.T. 36p.
- McVicar, T.; Jupp, D., 1998. The current and potential uses of remote sensing to aid decisions on drought exceptional circumstances in Australia: A review. *Agricultural Systems* 57, 399-46.
- Merrill, D.F.; Alexander, M.E., 1987. Glossary of forest fire management terms. 4th edition, Canadian Committee on Forest Fire Management, National Research Council of Canada, Ottawa, 91p.

- Mildrexler, D.J.; Zhao, M.; Heinsch, F.A.; Running, S.W., 2007. A new satellite-based methodology for continental-scale disturbance detection. *Ecological Application* 17, 235-250.
- Montealegre, A.L.; Lamelas, M.T.; Tanase, M.A.; Riva, J. de la., 2014. Forest fire severity assessment using ALS data in a Mediterranean environment. *Remote Sensing* 6, 4240-4265.
- Moreira, A.; Prats-Iraola, P.; Younis, M.; Krieger, G.; Hajnsek, I.; Papathanassiou, K.P., 2013. A tutorial on synthetic aperture radar. *IEEE Geoscience and Remote Sensing Magazine* 1 (1), 6-43.
- MRT (MODIS Reprojection Tool, version 4.1), 2011. USGS Earth Resources Observation and Science Center, Sioux Falls, SD, USA. Available online: [https://lpdaac.usgs.gov/tools/modis\\_reprojection\\_tool](https://lpdaac.usgs.gov/tools/modis_reprojection_tool) (Accessed on: September 30, 2011).
- MRT Swath (MODIS Reprojection Tool Swath, version 2.2), 2010. USGS Earth Resources Observation and Science Center, Sioux Falls, SD, USA. Available online: [https://lpdaac.usgs.gov/tools/modis\\_reprojection\\_tool\\_swath](https://lpdaac.usgs.gov/tools/modis_reprojection_tool_swath) (Accessed on: September 30, 2011).
- NASA (National Aeronautics and Space Administration), 2011. Available online: <http://modis.gsfc.nasa.gov/about/> (Accessed on: June 30, 2012).
- Nelson R.M.Jr., 1984. A method for describing equilibrium moisture content of forest fuels. *Canadian Journal of Forest Research* 14 (4), 597-600.

- Nesterov, V.G., 1949. Forest fire danger and methods of its determination. USSR State Industry Press: Goslesbumizdat, Moscow, 76p [In Russian].
- Nieto, H.; Aguadoa, I.; Chuvieco, E.; Sandholt, I., 2010. Dead fuel moisture estimation with MSG-SEVIRI data. Retrieval of meteorological data for the calculation of equilibrium moisture content. *Agricultural and Forest Meteorology* 150, 861-870.
- NRCAN (Natural Resources Canada), Fire. Available online: <http://www.nrcan.gc.ca/forests/fire/13143> (Accessed on: November 29, 2014).
- Oldford, S.; Leblon, B.; Gallant, L., 2003. Mapping pre-fire forest conditions with NOAA-AVHRR images in northern boreal forests. *Geocarto International* 18, 21-32.
- Oldford, S.; Leblon, B.; Maclean, D.; Flannigan, M., 2006. Predicting slow-drying fire weather index fuel moisture codes with NOAA-AVHRR images in Canada's northern boreal forests. *International Journal of Remote Sensing* 27, 3881-3902.
- Oyoshi, K.; Akatsuka, S.; Takeuchi, W.; Sobue, S., 2014. Hourly LST monitoring with the Japanese geostationary satellite MTSAT-1R over the Asia-Pacific region. *Asian Journal of Geoinformatics* 14, 1-13.
- Page, S.S.; Siegert, F.; Rieley, J.O.; Boehm, H.V.; Jaya, A., 2002. The amount of carbon released from peat and forest fires in Indonesia during 1997, *Nature* 420, 61–65.
- Pausas, J.G.; Paula, S., 2012. Fuel shapes the fire–climate relationship: evidence from Mediterranean ecosystems. *Global Ecology and Biogeography* 21, 1074–1082.
- Peñuelas, J.; Piñol, J.; Ogaya, R., 1997. Estimation of plant water concentration by the reflectance water index WI (R900/R970). *International Journal of Remote Sensing* 18, 2869–2875.

- Peterson, S.H.; Roberts, D.A.; Dennison, P.E., 2008. Mapping live fuel moisture with MODIS data: A multiple regression approach. *Remote Sensing of Environment* 112, 4272-4284.
- Pinty, B.; Verstraete, M.M., 1992. GEMI: A non-linear index to monitor global vegetation from satellites. *Vegetation* 101, 15–20.
- Preisler, H.K.; Burgan, R.E.; Eidenshink, J.C.; Klaver, J.M.; Klaver, R.W., 2009. Forecasting distributions of large federal-lands fires utilizing satellite and gridded weather information, *International Journal of Wildland Fire* 18, 508-516.
- Price, C., 2000. Evidence for a link between global lightning activity and upper tropospheric water vapour. *Nature* 406, 290-293.
- Qi, Y.; Dennison, P.E.; Spencer, J.; Riano, D., 2012. Monitoring live fuel moisture using soil moisture and remote sensing proxies. *Fire Ecology* 8 (3), 71-87.
- Rahimzadeh-Bajgiran, P.; Omasa, K.; Shimizu, Y., 2012. Comparative evaluation of the vegetation dryness index (VDI), the temperature vegetation dryness index (TVDI), and the improved TVDI (iTVDI) for water stress detection in semi-arid regions of Iran. *ISPRS Journal of Photogrammetry and Remote Sensing* 68, 1-12.
- Realmuto, V.; Hook, S.; Foote, M.; Csiszar, I.; Dennison, P.; Giglio, L.; Ramsey, M.; Vaughan, R.G.; Wooster, M.; Wright, R., 2011. HypsIRI high-temperature saturation study, Jet Propulsion Laboratory, California Institute of Technology, National Aeronautics and Space Agency 11-2, 51p.
- Roberts, D.A.; Dennison, P.E.; Peterson, S.; Sweeney, S.; Reche, J., 2006. Evaluation of Airborne Visible/Infrared Imaging Spectrometer (AVIRIS) and Moderate Resolution Imaging

- Spectrometer (MODIS) measures of live fuel moisture and fuel condition in a shrubland ecosystem in southern California. *Journal of Geophysical Research* 111, 1-16.
- Rothermel, R.C., 1972. A mathematical model for predicting fire spread in wildland fuels, Research Paper INT-115, USDA Forest Service, Intermountain Forest and Range Experiment Station, 40p.
- Rothermel, R.C.; Wilson, R.A.; Morris, G.A.; Sckett, S.S., 1986. Modeling moisture content of fine dead wildland fuels: input to the BEHAVE fire prediction system. Forest Service, Intermountain Research Station, Missoula, MT.
- Rouse, J.W.; Hass, R.H.; Schell, J.A.; Deering, D.W., 1973. Monitoring vegetation systems in the Great Plains with ERTS. Third ERTS-1 Symposium, NASA SP-351, U.S. Gov. Printing Office, Washington D.C., 1, 309-317.
- Running, S.W.; Coughlan, J.C., 1988. A general model of forest ecosystem processes for regional applications, I. Hydrologic balance, canopy gas exchange and primary production processes. *Ecological Modelling* 42, 125-154.
- Ruokolainen, L.; Salo, K., 2009. The effect of fire intensity on vegetation succession on a sub-xeric heath during ten years after wildfire. *Ann. Bot. Fennici*, 46, 30-42.
- Saglam, B.; Bilgili, E.; Dincdurmaz, B.; Kadiogulari, A.I.; Küçük, Ö., 2008. Spatio-temporal analysis of forest fire risk and danger using LANDSAT imagery. *Sensors* 8, 3970-3987.
- Sandholt, I.; Rasmussen, K.; Andersen, J., 2002. A simple interpretation of the surface temperature/vegetation index space for assessment of surface moisture status. *Remote Sensing of Environment* 79, 213-224.

- San-Miguel-Ayanz, J.; Barbosa, P.; Liberta G, Schmuck, G.; Schulte, E.; Bucella, P., 2003a. The European forest fire information system: a European strategy towards forest fire management. Proceedings of the 3<sup>rd</sup> International Wildland Fire Conference, Sydney, Australia, Washington, DC, US Dep Interior, Bur Land Management CD-ROM.
- San-Miguel-Ayanz, J.; Carlson, J.D.; Alexander, M.E.; Tolhurst, K.; Morgan, G.; Sneeuwjagt, R.; Dudfield, M., 2003b. Current methods to assess fire danger potential. In: Wildland fire danger estimation and mapping - the role of remote sensing data. E. Chuvieco, editor. World Scientific Publishing Co. Pte. Ltd., Singapore, pp. 21-61.
- Schneider, P.; Roberts, D.A.; Kyriakidis, P.C., 2008. A VARI-based relative greenness from MODIS data for computing the fire potential index. *Remote Sensing of Environment* 112, 1151-1167.
- Sebastián-López, A.; Salvador-Civil, R.; Gonzalo-Jiménez, J.; SanMiguel-Ayanz, J., 2008. Integration of socio-economic and environmental variables for modelling long-term fire danger in Southern Europe. *European Journal of Forest Research* 127, 149–163.
- Sifakis, N.I.; Iossifidis, C.; Kontoes, C.; Keramitsoglou, I., 2011. Wildfire detection and tracking over Greece using MSG-SEVIRI satellite data. *Remote Sensing* 3, 524-538.
- Sitnov, S.A.; Mokhov, I.I., 2013. Water-vapor content in the atmosphere over European Russia during the summer 2010 fires. *Atmospheric and Oceanic Physics* 49, 380-394.
- Souza, C.M. Jr.; Siqueira, J.V.; Sales, M.H.; Fonseca, A.V.; Ribeiro, J.G.; Numata, I.; Cochrane, M.A.; Barber, C.P.; Roberts, D.A.; Barlow, J., 2013. Ten-year Landsat classification of deforestation and forest degradation in the Brazilian Amazon. *Remote Sensing* 5, 5493-5513.

- Sow, M.; Mbow, C.; Hély, C.; Fensholt, R.; Sambou, B., 2013. Estimation of herbaceous fuel moisture content using vegetation indices and land surface temperature from MODIS data. *Remote Sensing* 5, 2617-2638.
- Stefanidou, M.; Athanaselis, S.; Spiliopoulou, C., 2008. Health impacts of fire smoke inhalation. *Inhalation Toxicology* 20, 761-766.
- Stocks, B.J.; Lawson, B.D.; Alexander, M.E.; van Wagner, C.E.; McAlpine, R.S.; Lynham, T.J.; Dube, D.E., 1989. Canadian forest fire danger rating system: an overview. *Forestry Chronicle* 65, 450–457.
- Stocks, B.J.; Mason, J.A.; Todd, J.B.; Bosch, E.M.; Wotton, B.M.; Amiro, B.D.; Flannigan, M.D.; Hirsch, K.G.; Logan, K.A.; Martell, D.L.; Skinner, W.R., 2003. Large forest fires in Canada, 1959-1997. *Journal of Geophysical Research* 108, 8149. doi:10.1029/2001JD000484.
- Stow, D.; Niphadkar, M.; Kaiser, J., 2005. MODIS-derived visible atmospherically resistant index for monitoring chaparral moisture content. *International Journal of Remote Sensing* 26, 3867-3873.
- Taylor, S.W., 2001. Considerations of applying the Canadian Forest Fire Danger Rating System in Argentina. Unpublished report, Canadian Forest Service, Pacific Forestry Centre, Victoria, BC, 25p.
- Treenotic Inc., 2011. Alberta firefighters fighting biggest fire they've ever fought. <http://foresttalk.com/index.php/2011/06/16/alberta-firefighters-fighting-biggest-fire-theyve-ever-fought/> (Last visited May 18, 2012)

- Vadrevu, K.P.; Csiszar, I.; Ellicott, E.; Giglip, L.; Badarinath, K.V.S.; Vermote, E.; Justice, C., 2013. Hotspot analysis of vegetation fires and intensity in the Indian region. *IEEE Journal of Selected Topics in Applied Earth Observations and Remote Sensing* 6, 224-238.
- van Wagner, C.E., 1987. Development and Structure of the Canadian Forest Fire Weather Index, Government of Canada: Ottawa, Canada, 37p.
- Vasilakos, C.; Kalabokidis, K.; Hatzopoulos, J.; Matsinos, I., 2009. Identifying wildland fire ignition factors through sensitivity analysis of a neural network. *Natural Hazards* 50, 125–143.
- Vermote, E.F.; Kotchenova, S., 2008. Atmospheric correction for the monitoring of land surfaces. *J of Geophys Res*, 113: D23S90. doi:10.1029/2007JD009662
- Vermote, E.F.; Kotchenova, S.Y.; Ray, J.P., 2011. MODIS Surface Reflectance User`s Guide, Version 1.3. University of Maryland: College Park, Maryland, 40p. Available online: [http://modis-sr.ltdri.org/products/MOD09\\_UserGuide\\_v1\\_3.pdf](http://modis-sr.ltdri.org/products/MOD09_UserGuide_v1_3.pdf) (accessed 15 January 2011).
- Vermote, E.F.; Vermeulen, A., 1999. MODIS Algorithm Theoretical Basis Document, Atmospheric Correction Algorithm: Spectral Reflectances (MOD09), Version 4.0, University of Maryland: College Park, Maryland, 107p. Available online: [http://modis.gsfc.nasa.gov/data/atbd/atbd\\_mod08.pdf](http://modis.gsfc.nasa.gov/data/atbd/atbd_mod08.pdf) (Accessed on: January 15, 2011).
- Vicente-Serrano, S.M.; Gouveia, C.; Camarero, J.J.; Begueria, S.; Trigo, R.; López-Moreno, J.I.; Azorín-Molina, C.; Pasho, E.; Lorenzo-Lacruz, J.; Revuelto, J.; Morán-Tejeda, E.;

- Sanchez-Lorenzo, A., 2012. Response of vegetation to drought time-scales across global land biomes. *Proceedings of the National Academy of Sciences* 110 (1), 52-57.
- Vidal, A.; Devaux-Ros, C., 1995. Evaluating forest fire hazard with a Landsat TM derived water stress index. *Agricultural and Forest meteorology* 77, 207-224.
- Viegas, D.X.; Bovio, G.; Ferreira, A.; Nosenzo, A.; Sol, B., 1999. Comparative study of various methods of fire danger evaluation in southern Europe. *International Journal of Wildland Fire* 9 (4), 235–246.
- Vonsky, S.M.; Zhdanko, V.A., 1976. Principles for elaboration of forest fire danger meteorological indices. Leningrad, LenNILH, 48p [In Russian].
- Wan, Z., 1999. MODIS Land-Surface Temperature Algorithm Theoretical Basis Document, Version 3.3. University of California: Santa Barbara, CA; 77p. Available online: [http://modis.gsfc.nasa.gov/data/atbd/atbd\\_mod11.pdf](http://modis.gsfc.nasa.gov/data/atbd/atbd_mod11.pdf) (Accessed on: January 15, 2011).
- Wan, Z., 2006. MODIS Land Surface Temperature Products User`s Guide, Collection 5. University of California: Santa Barbara, CA, 30p. Available online: [http://www.icess.ucsb.edu/modis/LstUsrGuide/MODIS\\_LST\\_products\\_Users\\_guide\\_C5.pdf](http://www.icess.ucsb.edu/modis/LstUsrGuide/MODIS_LST_products_Users_guide_C5.pdf) (Accessed on: December 10, 2011).
- Wan, Z., 2008. New refinements and validation of the MODIS land-surface temperature/emissivity products. *Remote Sensing of Environment*, 112: 59-74.
- Wan, Z., 2014. New refinements and validation of the collection-6 MODIS land-surface temperature/ emissivity product. *Remote Sensing of Environment* 140, 36-45.

- Wang, L.; Qu, J.J., 2007. NMDI: A normalized multi-band drought index for monitoring soil and vegetation moisture with satellite remote sensing. *Geophysical Research Letters*, 34: L20405
- Wang, L.; Qu, J.J.; Hao, X., 2008. Forest fire detection using normalized multi-band drought index (NMDI) with satellite measurements. *Agricultural and Forest Meteorology* 148, 1767-1776.
- Wang, L.; Zhou, Y.; Zhou, W.; Wang, S., 2013. Fire danger assessment with remote sensing: a case study in Northern China. *Natural Hazards* 65, 819-834.
- Wilson, R.A.Jr., 1985. Observations of extinction and marginal burning states in free burning porous fuel beds. *Combustion, Science and Technology* 44,179-193.
- Wilson, R.A.Jr., 1990. Reexamination of Rothermel's fire spread equations in no-wind and no slope conditions. USDA, Forest Service, Intermountain Forest and Range Experimental Station, Research Paper. INT-434, 13p.
- Wing, M.G.; Burnett, J.D.; Sessions, J., 2014. Remote sensing and unmanned aerial system technology for monitoring and quantifying forest fire impacts. *International Journal of Remote Sensing and Applications* 4 (1), 18-35.
- Wotton, B.M., 2009. Interpreting and using outputs from the Canadian Forest Fire Danger Rating System in research applications. *Environmental and Ecological Statistics* 16, 107-131.
- Yebra, M.; Dennison, P.E.; Chuvieco, E.; Riaño, D.; Zylstra, P.; Hunt, E.R.Jr.; Danson, F.M.; Qi, Y.; Jurado, S., 2013. A global review of remote sensing of live fuel moisture content for fire danger assessment: moving towards operational products. *Remote Sensing of Environment* 136, 455-468.

Zarco-Tejada, P. J.; Rueda, C. A.; Ustin, S. L., 2003. Water content estimation in vegetation with MODIS reflectance data and model inversion methods. *Remote Sensing of Environment*, 85: 109–124.

Zhang, J.; Yao, F.; Liu, C.; Yang, L.; Boken, B. K., 2011. Detection, emission estimation and risk prediction of forest fires in China using satellite sensors and simulation models in the past three decades – an overview. *International Journal of Environmental Research and Public Health* 8, 3156-3178.

## **APPENDIX**

## **Appendix A1: Copyright related information**

## A.1 Copyright permissions

The certificates for permissions/licenses to use the copyrighted material are organized as follows:

- *Certificate(s) of Published Journal Articles:*

Obtained through Copyright Clearance Center of Publishers, as agreements of usage for three articles (figures from which were used after modifications) namely:

1. Sandholt et al., 2002;
2. McVicar and Jupp, 1998; and
3. Wang and Qu, 2007.

- *Certificate of a Book Chapter:*

Title page of the book chapter, Clark et al. (1999), showing that content is not copyrighted and is in the public domain.

- *Certificate from Publications:*

Published journal papers:

- (a) Chowdhury, E.H., Hassan, Q.K., 2013. Use of remote sensing-derived variables in developing a forest fire danger forecasting system. *Natural Hazards* 67, 321-334;
- (b) Chowdhury, E.H., Hassan, Q.K., 2014. Operational perspective of remote sensing-based forest fire danger forecasting systems. *ISPRS Journal of Photogrammetry and Remote Sensing*. doi:10.1016/j.isprsjprs.2014.03.011; and
- (c) Chowdhury, E.H., Hassan, Q.K., 2015. Development of a new daily-scale forest fire danger forecasting system using remote sensing data. *Remote Sensing*. 7(3), 2431-2448; showing that the copyrights are owned by authors.

### *A.1.1 Certificate for published journal articles*

(a) Sandholt et al., 2002

#### **ELSEVIER LICENSE TERMS AND CONDITIONS**

Feb 09, 2015

---

This is a License Agreement between Ehsan Chowdhury ("You") and Elsevier ("Elsevier") provided by Copyright Clearance Center ("CCC"). The license consists of your order details, the terms and conditions provided by Elsevier, and the payment terms and conditions.

**All payments must be made in full to CCC. For payment instructions, please see information listed at the bottom of this form.**

<i>Supplier</i>	<i>Elsevier Limited The Boulevard, Langford Lane Kidlington, Oxford, OX5 1GB, UK</i>
<i>Registered Company Number</i>	<i>1982084</i>
<i>Customer name</i>	<i>Ehsan Chowdhury</i>
<i>Customer address</i>	<i>1505-3500 Varsity Drive NW Calgary, AB T2L1Y3</i>
<i>License number</i>	<i>3564881223905</i>
<i>License date</i>	<i>Feb 09, 2015</i>
<i>Licensed content publisher</i>	<i>Elsevier</i>
<i>Licensed content publication</i>	<i>Remote Sensing of Environment</i>
<i>Licensed content title</i>	<i>A simple interpretation of the surface temperature/vegetation index space for assessment of surface moisture status</i>
<i>Licensed content author</i>	<i>Inge Sandholt, Kjeld Rasmussen, Jens Andersen</i>
<i>Licensed content date</i>	<i>February 2002</i>
<i>Licensed content volume number</i>	<i>79</i>
<i>Licensed content issue number</i>	<i>2-3</i>
<i>Number of pages</i>	<i>12</i>
<i>Start Page</i>	<i>213</i>
<i>End Page</i>	<i>224</i>
<i>Type of Use</i>	<i>reuse in a thesis/dissertation</i>
<i>Intended publisher of new work</i>	<i>other</i>
<i>Portion</i>	<i>figures/tables/illustrations</i>
<i>Number of figures/tables/illustrations</i>	<i>2</i>
<i>Format</i>	<i>electronic</i>

(b) McVicar and Jupp, 1998

**ELSEVIER ORDER DETAILS**

Feb 09, 2015

---

---

**This is an Agreement between Ehsan Chowdhury ("You") and Elsevier ("Elsevier"). It consists of your order details, the terms and conditions provided by Elsevier ("Elsevier"), and the payment terms and conditions.**

<i>Order Number</i>	500967517
<i>Order Date</i>	Feb 09, 2015
<i>Licensed content publisher</i>	Elsevier
<i>Licensed content publication</i>	Agricultural Systems
<i>Licensed content title</i>	The current and potential operational uses of remote sensing to aid decisions on drought exceptional circumstances in Australia: a review
<i>Licensed content author</i>	Tim R. McVicar, David L.B. Jupp
<i>Licensed content date</i>	July 1998
<i>Licensed content volume number</i>	57
<i>Licensed content issue number</i>	3
<i>Number of pages</i>	70
<i>Start Page</i>	399
<i>End Page</i>	468
<i>Type of Use</i>	reuse in a thesis/dissertation
<i>Intended publisher of new work</i>	other
<i>Portion</i>	figures/tables/illustrations
<i>Number of figures/tables/illustrations</i>	>10
<i>Actual number of figures/tables/illustrations</i>	17
<i>Format</i>	electronic

(c) Wang and Qu, 2007

**JOHN WILEY AND SONS LICENSE  
TERMS AND CONDITIONS**

Feb 09, 2015

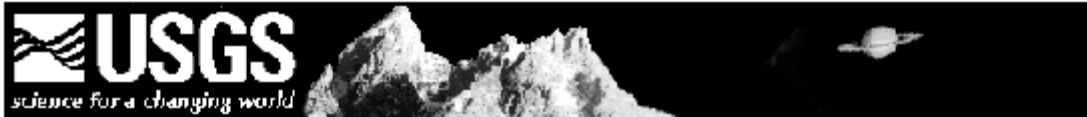
---

This Agreement between Ehsan Chowdhury ("You") and John Wiley and Sons ("John Wiley and Sons") consists of your license details and the terms and conditions provided by John Wiley and Sons and Copyright Clearance Center.

<i>License Number</i>	3564880280300
<i>License date</i>	Feb 09, 2015
<i>Licensed Content Publisher</i>	John Wiley and Sons
<i>Licensed Content Publication</i>	Geophysical Research Letters
<i>Licensed Content Title</i>	NMDI: A normalized multi-band drought index for monitoring soil and vegetation moisture with satellite remote sensing
<i>Licensed Content Author</i>	Lingli Wang, John J. Qu
<i>Licensed Content Date</i>	Oct 23, 2007
<i>Pages</i>	1
<i>Type of use</i>	Dissertation/Thesis
<i>Requestor type</i>	University/Academic
<i>Format</i>	Electronic
<i>Portion</i>	Figure/table
<i>Number of figures/tables</i>	1
<i>Original Wiley figure/table number(s)</i>	Figure 1 (right)
<i>Will you be translating?</i>	No
<i>Title of your thesis / dissertation</i>	Development of a satellite-based forest fire danger forecasting system and implement over the forest dominant region of Alberta
<i>Expected completion date</i>	Mar 2015
<i>Expected size (number of pages)</i>	150
<i>Requestor Location</i>	Ehsan Chowdhury 1505-3500 Varsity Drive NW

Calgary, AB T2L1Y3  
Canada  
Attn: Ehsan Chowdhury

A.1.2 Certificate of a book chapter



**Spectroscopy of Rocks and Minerals, and  
Principles of Spectroscopy**

by  
Roger N. Clark

U.S. Geological Survey, MS 964  
Box 25046 Federal Center  
Denver, CO 80225-0046

(303) 236-1332  
(303) 236-1371 FAX

**<http://speclab.cr.usgs.gov>**

[rclark@speclab.cr.usgs.gov](mailto:rclark@speclab.cr.usgs.gov)

Derived from Chapter 1 in:  
*Manual of Remote Sensing*

John Wiley and Sons, Inc  
A. Rencz, Editor  
New York  
1999

This book chapter was produced by personnel of the US Government  
therefore it can not be copyrighted and is in the public domain

This Web Page last revised June 25, 1999

**How to Reference:**

**Clark, R. N., Chapter 1: Spectroscopy of Rocks and Minerals, and Principles of Spectroscopy, in  
*Manual of Remote Sensing, Volume 3, Remote Sensing for the Earth Sciences*, (A.N. Rencz, ed.) John  
Wiley and Sons, New York, p 3- 58, 1999.**

### A.1.3 Certificate from publications

(a) Chowdhury and Hassan, 2013

Nat Hazards (2013) 67:321–334  
DOI 10.1007/s11069-013-0564-7

ORIGINAL PAPER

## Use of remote sensing-derived variables in developing a forest fire danger forecasting system

Ehsan H. Chowdhury · Quazi K. Hassan

Received: 2 November 2012 / Accepted: 15 January 2013 / Published online: 26 January 2013  
© The Author(s) 2013. This article is published with open access at Springerlink.com

**Abstract** Our aim was to develop a remote sensing-based forest fire danger forecasting system (FFDFS) and its implementation in forecasting 2011 fire season in the Canadian province of Alberta. The FFDFS used Moderate Resolution Imaging Spectroradiometer (MODIS)-derived 8-day composites of surface temperature, normalized multiband drought index, and normalized difference vegetation index as input variables. In order to eliminate the data gaps in the input variables, we propose a gap-filling technique by considering both of the spatial and temporal dimensions. These input variables were calculated during the  $i$  period and then integrated to forecast the fire danger conditions into four categories (i.e., very high, high, moderate, and low) during the  $i + 1$  period. It was observed that 98.19 % of the fire fell under “very high” to “moderate” danger classes. The performance of this system was also demonstrated its ability to forecast the worst fires occurred in Slave Lake and Fort McMurray region during mid-May 2011. For example, 100 and 94.0 % of the fire spots fell under “very high” to “high” danger categories for Slave Lake and Fort McMurray regions, respectively.

**Keywords** MODIS · Normalized difference vegetation index · Normalized multiband drought index · Surface temperature · Fire spot

### 1 Introduction

Forest fire is one of the natural hazards over many forested ecosystems across the world including boreal ones. Over the boreal forested region in the Canadian province of Alberta, the annual average fire incidences were 1,541 in numbers that caused burning of approximately 220 thousand ha during the period 2002–2011 (ASRD 2012). In particular to 2011 fire season, several catastrophic fires (i.e., Slave Lake and Fort McMurray regional fires in mid-May) were observed. The Slave Lake fires were responsible for burning

E. H. Chowdhury · Q. K. Hassan (✉)  
Department of Geomatics Engineering, Schulich School of Engineering, University of Calgary, 2500  
University Dr NW, Calgary, AB T2N 1N4, Canada  
e-mail: qhassan@ucalgary.ca

temporal connotations. It revealed that the use of the  $3 \times 3$  window size would infill approximately 84.14 and 100 % of the data gaps for  $T_S$  and both NMDI and NDVI images, respectively. In these cases, we also observed strong agreements between the predicted values for the variable of interest with the observed data (i.e., the good quality pixels which were declared as data gaps), such as  $r^2$ , and RMSE values were on an average: (i) 0.88 and 0.883 K, respectively, for  $T_S$  images; (ii) 0.91 and 0.021, respectively, for NMDI images; and (iii) 0.93 and 0.021, respectively, for NDVI images. In order to filling the remaining data gaps (i.e.,  $\sim 15.86$  %) for  $T_S$  images, we increased window size (in the range from  $5 \times 5$  to  $15 \times 15$ ); and both of the RMSE and  $r^2$  values were still found to be in the reasonable bounds (i.e., RMSE  $\approx 1.096$  K and  $r^2 \approx 0.85$  for  $5 \times 5$  window size; RMSE  $\approx 1.444$  K and  $r^2 \approx 0.75$  for  $15 \times 15$  window size). In addition, the combination of  $T_S$ , NMDI, and NDVI also produced good results (i.e., 98.19 % of the fire fell under “very high” to “moderate” danger classes). Thus, the proposed methods would be an effective operational framework of FFDFS.

**Acknowledgments** The study was funded by a NSERC Discovery Grant to Dr. Hassan. We are indebted to NASA for providing the MODIS data at free of cost. In addition, we would like to acknowledge the anonymous reviewers for commenting on our paper.

**Open Access** This article is distributed under the terms of the Creative Commons Attribution License which permits any use, distribution, and reproduction in any medium, provided the original author(s) and the source are credited.

## References

- Akther MS, Hassan QK (2011a) Remote sensing based assessment of fire danger conditions over boreal forest. *IEEE J Sel Top Appl Earth Obs Remote Sens* 4:992–999
- Akther MS, Hassan QK (2011b) Remote sensing based estimates of surface wetness conditions and growing degree days over northern Alberta, Canada. *Boreal Environ Res* 16:407–416
- Ardakani AS, Zoj MJV, Mohammadzadeh A, Mansourian A (2011) Spatial and temporal analysis of fires detected by MODIS data in northern Iran from 2001 to 2008. *IEEE J Sel Topics Appl Earth Obs Remote Sens* 4(1):216–225
- ASRD (Alberta Sustainable Resource Development) (2012) 10-Year Wildfire Statistics. <http://www.srd.alberta.ca/Wildfire/WildfireStatus/HistoricalWildfireInformation/10-YearStatisticalSummary.aspx> (Last visited 25 June, 2012)
- Chilès J-P, Delfiner P (2012) Geostatistical modeling spatial uncertainty, 2nd edn. Wiley, Hoboken 699p
- Coll C, Wan Z, Galve JM (2009) Temperature-based and radiance-based validations of the V5 MODIS land surface temperature product. *J Geophys Res* 114:D20102. doi:10.1029/2009JD012038
- De Angelis A, Bajocco S, Ricotta C (2012) Phenological variability drives the distribution of wildfires in Sardinia. *Landsc Ecol*. doi:10.1007/s10980-012-9808-2
- Desbois N, Vidal A (1996) Real time monitoring of vegetation flammability using NOAA-AVHRR thermal infrared data. *EARSel Adv Remote Sens* 4(4-XI):25–32
- Downing DJ, Pettapiece WW (2006) Natural Regions and Subregions of Alberta. Pub. No. T/852. Natural Regions Committee: Government of Alberta, Alberta, Canada, [http://tpr.alberta.ca/parks/heritagenfocentre/docs/NRSRcomplete%20May\\_06.pdf](http://tpr.alberta.ca/parks/heritagenfocentre/docs/NRSRcomplete%20May_06.pdf) (Last visited 10 April, 2012)
- FTCWRC (Flat Top Complex Wildfire Review Committee) (2012) Flat top complex, Submitted to the Minister of Alberta Environment and Sustainable Resource Development. <http://www.srd.alberta.ca/Wildfire/WildfirePreventionEnforcement/WildfireReviews/documents/FlatTopComplex-WildfireReviewCommittee-May18-2012.pdf> (Last visited 25 June, 2012)
- Gao X, Huete AR, Didan K (2003) Multi sensor comparisons and validation of MODIS vegetation indices at the semiarid Jornada experimental range. *IEEE Trans Geosci Remote Sens* 41(10):2368–2381
- Girard M-C, Girard CM (2003) Processing of remote sensing data. A.A. Balkema, India 291p
- Govind A, Chen JM, Bemier P, Margolis H, Guindon L, Beaudoin A (2011) Spatially distributed modeling of the long-term carbon balance of a boreal landscape. *Ecol Model* 222(2011):2780–2795

(b) Chowdhury and Hassan, 2014

**ELSEVIER LICENSE  
TERMS AND CONDITIONS**

*Feb 09, 2015*

---

---

This is a License Agreement between Ehsan Chowdhury ("You") and Elsevier ("Elsevier") provided by Copyright Clearance Center ("CCC"). The license consists of your order details, the terms and conditions provided by Elsevier, and the payment terms and conditions.

***All payments must be made in full to CCC. For payment instructions, please see information listed at the bottom of this form.***

<i>Supplier</i>	<i>Elsevier Limited The Boulevard, Langford Lane Kidlington, Oxford, OX5 1GB, UK</i>
<i>Registered Company Number</i>	<i>1982084</i>
<i>Customer name</i>	<i>Ehsan Chowdhury</i>
<i>Customer address</i>	<i>1505-3500 Varsity Drive NW Calgary, AB T2L1Y3</i>
<i>License number</i>	<i>3564841450335</i>
<i>License date</i>	<i>Feb 09, 2015</i>
<i>Licensed content publisher</i>	<i>Elsevier</i>
<i>Licensed content publication</i>	<i>ISPRS Journal of Photogrammetry and Remote Sensing</i>
<i>Licensed content title</i>	<i>Operational perspective of remote sensing-based forest fire danger forecasting systems</i>
<i>Licensed content author</i>	<i>None</i>
<i>Licensed content date</i>	<i>Available online 18 April 2014</i>
<i>Licensed content volume number</i>	<i>n/a</i>
<i>Licensed content issue number</i>	<i>n/a</i>
<i>Number of pages</i>	<i>1</i>
<i>Start Page</i>	<i>None</i>
<i>End Page</i>	<i>None</i>
<i>Type of Use</i>	<i>reuse in a thesis/dissertation</i>
<i>Portion</i>	<i>full article</i>

*Article*

## Development of a New Daily-Scale Forest Fire Danger Forecasting System Using Remote Sensing Data

Ehsan H. Chowdhury and Quazi K. Hassan \*

Department of Geomatics Engineering, Schulich School of Engineering, University of Calgary, 2500 University Dr NW, Calgary, AB T2N 1N4, Canada ; E-Mail: echowdhu@ucalgary.ca

\* Author to whom correspondence should be addressed; E-Mail: qhassan@ucalgary.ca; Tel.: +1-403-210-9494; Fax: +1-403-284-1980.

Academic Editors: Ioannis Gitas and Prasad S. Thenkabail

Received: 23 December 2014 / Accepted: 17 February 2015 / Published: 2 March 2015

---

**Abstract:** Forest fires are a critical natural disturbance in most of the forested ecosystems around the globe, including the Canadian boreal forest where fires are recurrent. Here, our goal was to develop a new daily-scale forest fire danger forecasting system (FFDFS) using remote sensing data and implement it over the northern part of Canadian province of Alberta during 2009–2011 fire seasons. The daily-scale FFDFS was comprised of Moderate Resolution Imaging Spectroradiometer (MODIS)-derived four-input variables, *i.e.*, 8-day composite of surface temperature ( $T_s$ ), normalized difference vegetation index (NDVI), and normalized multiband drought index (NMDI); and daily precipitable water (PW). The  $T_s$ , NMDI, and NDVI variables were calculated during  $i$  period and PW during  $j$  day and then integrated to forecast fire danger conditions in five categories (*i.e.*, extremely high, very high, high, moderate, and low) during  $j + 1$  day. Our findings revealed that overall 95.51% of the fires fell under “extremely high” to “moderate” danger classes. Therefore, FFDFS has potential to supplement operational meteorological-based forecasting systems in between the observed meteorological stations and remote parts of the landscape.

**Keywords:** fire spot; normalized multiband drought index; normalized difference vegetation index; operational perspective; precipitable water; surface temperature

60. Kang, S.; Running, S.W.; Zhao, M.; Kimball, J.S.; Glassy, J. Improving continuity of MODIS terrestrial photosynthesis products using an interpolation scheme for cloudy pixels. *Int. J. Remote Sens.* **2005**, *26*, 1659–1676.
61. Lecina-Diaz, J.; Alvarez, A.; Retana, J. Extreme fire severity patterns in topographic, convective and wind-driven historical wildfires of Mediterranean pine forests. *PLoS One* **2014**, *9*, e85127.
62. Adab, H.; Kanniah, K.D.; Solaimani, K. Modeling forest fire risk in the northeast of Iran using remote sensing and GIS techniques. *Nat. Hazards* **2013**, *65*, 1723–1743.
63. Ardakani, A.S.; Zoej, M.J.V.; Mohammadzadeh, A.; Mansourian, A. Spatial and temporal analysis of fires detected by MODIS data in northern Iran from 2001 to 2008. *IEEE J. Sel. Top. Appl. Earth Obs. Remote Sens.* **2011**, *4*, 216–225.
64. Bartsch, A.; Balzter, H.; George, C. The influence of regional surface soil moisture anomalies on forest fires in Siberia observed from satellites. *Environ. Res. Lett.* **2009**, *4*, 045021, doi:10.1088/1748-9326/4/4/045021
65. Clabo, D.R.; Bunkers, M.J. Using variable column precipitable water as a predictor for large fire potential. In *Weather and Climate Impacts*, Proceedings of the Ninth Symposium on Fire and Forest Meteorology, Palm Springs, CA, USA, 20 October 2011; American Meteorological Society: Boston, MA, USA.
66. Gao, B.-C.; Kaufman, Y.J. Algorithm Technical Background Document, The MODIS Near-IR Water Vapor Algorithm, Product ID: MOD05—Total Precipitable Water. Available online: [http://modis-atmos.gsfc.nasa.gov/\\_docs/atbd\\_mod03.pdf](http://modis-atmos.gsfc.nasa.gov/_docs/atbd_mod03.pdf) (accessed on 10 January 2014).
67. Brotak, E.A. An investigation of the synoptic situations associated with major wildland fire. *J. Appl. Meteorol.* **1977**, *16*, 867–870.
68. Price, C. Evidence for a link between global lightning activity and upper tropospheric water vapour. *Nature* **2000**, *406*, 290–293.
69. Stocks, B.J.; Mason, J.A.; Todd, J.B.; Bosch, E.M.; Wotton, B.M.; Amiro, B.D.; Flannigan, M.D.; Hirsch, K.G.; Logan, K.A.; Martell, D.L.; *et al.* Large forest fires in Canada, 1959–1997. *J. Geophys. Res.* **2003**, *108*, 8149.
70. Wing, M.G.; Burnett, J.D.; Sessions, J. Remote sensing and unmanned aerial system technology for monitoring and quantifying forest fire impacts. *Int. J. Remote Sens. Appl.* **2014**, *4*, 18–35.

© 2015 by the authors; licensee MDPI, Basel, Switzerland. This article is an open access article distributed under the terms and conditions of the Creative Commons Attribution license (<http://creativecommons.org/licenses/by/4.0/>).

## **Appendix A2: Data Tables**

**Table A2.1: Quality control (QC) SDS of MOD11A2 ver. 005 surface temperature and emissivity 8-day L3 Global 1 km (NASA, 2011).**

<b>Bit No.</b>	<b>Long Name</b>	<b>Bit Combination</b>	<b>Description</b>
0-1	Mandatory QA Flags	00	T <sub>s</sub> produced, good quality, not necessary to examine more detailed QA
		01	T <sub>s</sub> produced, other quality, recommend examination of more detailed QA
		10	T <sub>s</sub> not produced due to cloud effects
		11	T <sub>s</sub> not produced primarily due to reasons other than cloud
2-3	Data Quality Flag	00	Good data quality of L1B in 7 TIR bands
		01	Other quality data
		10	TBD
		11	TBD
4-5	Emissivity Error Flag	00	Average emissivity error <= 0.01
		01	Average emissivity error <= 0.02
		10	Average emissivity error <= 0.04
		11	Average emissivity error > 0.04
6-7	T <sub>s</sub> Error Flag	00	Average T <sub>s</sub> error <= 1K
		01	Average T <sub>s</sub> error <= 2K
		10	Average T <sub>s</sub> error <= 3K
		11	Average T <sub>s</sub> error > 3K

**Table A2.2: Quality assurance SDS of MOD09A1 ver. 005 surface reflectance 8-day L3 Global 500 m (NASA, 2011).**

Bit No.	Parameter	Bit Combination	Surface reflectance state
15	Internal snow algorithm flag	1	yes
		0	no
14	BRDF correction performed	1	yes
		0	no
13	Pixel is adjacent to cloud	1	yes
		0	no
12	MOD35 snow/ice flag	1	yes
		0	no
11	Internal fire algorithm flag	1	fire
		0	no fire
10	Internal cloud algorithm flag	1	cloud
		0	no cloud
8–9	Cirrus detected	00	none
		01	small
		10	average
		11	high
6–7	Aerosol quantity	00	climatology
		01	low
		10	average
		11	high
3–5	Land/water flag	000	shallow ocean
		001	land
		010	ocean coastlines and lake shorelines
		011	shallow inland water
		100	ephemeral water
		101	deep inland water
		110	continental/moderate ocean
		111	deep ocean
2	Cloud shadow	1	yes
		0	no
0–1	MOD35 cloud	00	clear
		01	cloudy
		10	mixed
		11	not set, assumed clear

**Table A2.3: Percentage of gap pixels in Ts images during 2009-2011.**

DOY	Year								
	2009			2010			2011		
	Good Pixel	Cloud Pixel	Percent	Good Pixel	Cloud Pixel	Percent	Good Pixel	Cloud Pixel	Percent
89	367382	5966	1.598	373097	251	0.07	372898	450	0.12
97	370549	2799	0.750	370501	2847	0.76	373325	23	0.01
105	373273	75	0.020	373348		0.00	372640	708	0.19
113	371700	1648	0.441	286304	87044	23.31	373313	35	0.01
121	373324	24	0.006	339480	33868	9.07	373317	31	0.01
129	367114	6234	1.670	373331	17	0.00	373348		
137	373302	46	0.012	337984	35364	9.47	373346	2	
145	371225	2123	0.569	367030	6318	1.69	373324	24	0.01
153	367606	5742	1.538	372696	652	0.17	373331	17	
161	373343	5	0.001	373347	1	0.00	372663	685	0.18
169	372645	703	0.188	373308	40	0.01	373176	172	0.05
177	354696	18652	4.996	367667	5681	1.52	373270	78	0.02
185	358236	15112	4.048	373242	106	0.03	373204	144	0.04
193	373341	7	0.002	372932	416	0.11	372824	524	0.14
201	373348		0.000	373333	15	0.00	373317	31	0.01
209	372647	701	0.188	373257	91	0.02	373314	34	0.01
217	373335	13	0.003	373072	276	0.07	373348		
225	373293	55	0.015	369885	3463	0.93	373309	39	0.01
233	373342	6	0.002	372002	1346	0.36	373348		
241	373346	2	0.001	368583	4765	1.28	373344	4	
249	373346	2	0.001	325257	48091	12.88	373348		
257	373346	2	0.001	372391	957	0.26	373348		
265	373344	4	0.001	373298	50	0.01	373347	1	
<b>Average</b>			<b>0.66</b>			<b>2.82</b>			<b>0.52</b>
<b>Total</b>			<b>14.45</b>			<b>61.98</b>			<b>11.41</b>

**Table A2.4: Percentage of gap pixels in NMDI images during 2009-2011.**

DOY	Year								
	2009			2010			2011		
	Good Pixel	Cloud Pixel	Percent	Good Pixel	Cloud Pixel	Percent	Good Pixel	Cloud Pixel	Percent
89	1493095	22	0.001	1491797	21	0.001	1491797	1844	0.123
97	1492821	17	0.001	1492831	7	0.000	1492831	807	0.054
105	1493095	8	0.001	1493218			1493218	422	0.028
113	1493447	4	0.000	1493359	4	0.000	1493359	278	0.019
121	1493484	3	0.000	1493410	4	0.000	1493410	119	0.008
129	1493166	16	0.001	1493495	9	0.001	1493495	63	0.004
137	1493172	6	0.000	1493258	3	0.000	1493258	139	0.009
145	1493245	5	0.000	1493310	6	0.000	1493310	209	0.014
153	1493368	3	0.000	1493115	8	0.001	1493115	374	0.025
161	1493288	5	0.000	1492948	4	0.000	1492948	572	0.038
169	1493143	11	0.001	1492769	16	0.001	1492769	793	0.053
177	1492762	48	0.003	1493252	77	0.005	1493252	329	0.022
185	1493160	24	0.002	1493098	15	0.001	1493098	454	0.030
193	1493135	19	0.001	1492842	20	0.001	1492842	728	0.049
201	1492965	19	0.001	1492674	25	0.002	1492674	931	0.062
209	1493037	17	0.001	1492728	21	0.001	1492728	848	0.057
217	1493221	12	0.001	1492926	16	0.001	1492926	657	0.044
225	1493090	18	0.001	1492646	31	0.002	1492646	914	0.061
233	1493081	20	0.001	1493163	29	0.002	1493163	414	0.028
241	1493055	21	0.001	1492984	41	0.003	1492984	577	0.039
249	1492998	20	0.001	1492784	33	0.002	1492784	708	0.047
257	1493153	10	0.001	1493293	18	0.001	1493293	285	0.019
265	1493089	21	0.001	1493148	19	0.001	1493148	346	0.023
<b>Average</b>			<b>0.001</b>			<b>0.0012</b>			<b>0.0334</b>
<b>Total</b>			<b>0.022</b>			<b>0.027</b>			<b>0.734</b>

**Table A2.5: Percentage of gap pixels in NDVI images during 2009-2011.**

DOY	Year								
	2009			2010			2011		
	Good Pixel	Cloud Pixel	Percent	Good Pixel	Cloud Pixel	Percent	Good Pixel	Cloud Pixel	Percent
89	1256678			1256678			1256678	31	0.0025
97	1391569			1391569			1391569	45	0.0032
105	1441329			1441329			1441329	9	0.0006
113	1447462			1447462			1447462	2	0.0001
121	1486808			1486808			1486808	3	0.0002
129	1491320	1	0.0001	1491320	2	0.0001	1491320		
137	1492045			1492045			1492045	9	0.0006
145	1491912			1491912			1491912	30	0.0020
153	1491932			1491932	1	0.0001	1491932	279	0.0187
161	1492517	1	0.0001	1492517			1492517	26	0.0017
169	1492674			1492674	1	0.0001	1492674	67	0.0045
177	1492572	3	0.0002	1492572	3	0.0002	1492572	243	0.0163
185	1492931	3	0.0002	1492931	3	0.0002	1492931	7	0.0005
193	1492721			1492721	4	0.0003	1492721	138	0.0092
201	1493003	2	0.0001	1493003	2	0.0001	1493003	47	0.0031
209	1492823			1492823	7	0.0005	1492823	79	0.0053
217	1492878			1492878			1492878	28	0.0019
225	1492849			1492849	8	0.0005	1492849	71	0.0048
233	1492898			1492898	1	0.0001	1492898	7	0.0005
241	1492556			1492556	7	0.0006	1492556	24	0.0016
249	1492134			1492134	9	0.0006	1492134	2	0.0001
257	1492361			1492361	4	0.0003	1492361	1	0.0001
265	1491982			1491982	7	0.0005	1491982	17	0.0011
<b>Average</b>			<b>0.00003</b>			<b>0.00018</b>			<b>0.0034</b>
<b>Total</b>			<b>0.00067</b>			<b>0.004</b>			<b>0.076</b>

**Table A2.6: Percentage of gap pixels after in-filled with  $m \times m$  (in the range of  $3 \times 3$  to  $15 \times 15$ ) window sizes in  $T_S$  images during 2009-2011.**

DOY	Year								
	2009			2010			2011		
	Good Pixel	Cloud Pixel	Percent	Good Pixel	Cloud Pixel	Percent	Good Pixel	Cloud Pixel	Percent
89	367382	5966		373097	251		372898	450	
97	373346	82	0.022	373346	2	0.001	373344	4	0.001
105	373348	1	0.000	373348			372794	554	0.148
113	360181	1	0.000	360181	13167	3.527	373315	33	0.009
121	360015			360015	13333	3.571	373348		
129	373348			373348			373348		
137	366271	9	0.002	366271	7077	1.896	373348		
145	372448	0	0.000	372448	900	0.241	373324	24	0.006
153	373129	45	0.012	373129	219	0.059	373332	16	0.004
161	373348	0	0.000	373348			373031	317	0.085
169	373348	0	0.000	373348			373176	172	0.046
177	373348	35	0.009	373348			373328	20	0.005
185	373344	384	0.103	373344	4	0.001	373324	24	0.006
193	373346	1	0.000	373346	2	0.001	373173	175	0.047
201	373348			373348			373337	11	0.003
209	373348	8	0.002	373348			373317	31	0.008
217	373347	4	0.001	373347	1	0.000	373348		
225	373347	5	0.001	373347	1	0.000	373348		
233	373342			373342	6	0.002	373348		
241	373344			373344	4	0.001	373348		
249	372733			372733	615	0.165	373348		
257	373267	1	0.000	373267	81	0.022	373348		
265	373348			373348			373348		
<b>Average</b>			<b>0.007</b>			<b>0.431</b>			<b>0.017</b>
<b>Total</b>			<b>0.154</b>			<b>9.485</b>			<b>0.370</b>
<b>Gap-filled pixels (%)</b>			<b>98.93</b>			<b>84.70</b>			<b>96.76</b>

**Table A2.7: Coefficient of determination ( $r^2$ ), root mean square error (RMSE), slope, and intercept values between observed and predicted  $T_S$  using various window sizes during 2009.**

DOY	Parameter	Window sizes							Study area
		3×3	5×5	7×7	9×9	11×11	13×13	15×15	
97	$r^2$	0.90	0.85	0.81	0.79	0.77	0.75	0.74	0.35
	RMSE	0.80	1.01	1.13	1.21	1.27	1.31	1.34	2.15
	Slope	0.94	0.90	0.88	0.87	0.86	0.85	0.84	0.50
	Intercept	17.66	26.38	32.22	36.55	39.83	42.49	44.68	138.05
105	$r^2$	0.93	0.89	0.86	0.84	0.82	0.80	0.79	0.29
	RMSE	0.81	1.04	1.18	1.28	1.35	1.40	1.44	2.76
	Slope	0.95	0.93	0.91	0.89	0.88	0.87	0.87	0.44
	Intercept	12.72	20.62	25.64	29.57	32.78	35.32	37.73	155.87
113	$r^2$	0.92	0.88	0.85	0.83	0.81	0.80	0.79	0.53
	RMSE	0.99	1.23	1.37	1.46	1.52	1.57	1.60	2.45
	Slope	0.93	0.90	0.88	0.87	0.86	0.85	0.84	0.65
	Intercept	19.45	27.96	33.41	36.97	39.73	41.86	43.45	98.42
121	$r^2$	0.94	0.90	0.88	0.86	0.85	0.84	0.83	0.60
	RMSE	1.01	1.27	1.41	1.50	1.57	1.61	1.65	2.53
	Slope	0.97	0.95	0.93	0.92	0.91	0.91	0.90	0.69
	Intercept	9.61	15.22	19.24	22.23	24.62	26.62	28.41	90.74
129	$r^2$	0.89	0.84	0.80	0.77	0.75	0.73	0.72	0.40
	RMSE	1.32	1.63	1.81	1.93	2.01	2.08	2.13	3.38
	Slope	0.89	0.85	0.82	0.80	0.78	0.77	0.76	0.61
	Intercept	30.34	43.46	51.91	57.65	61.93	65.26	68.01	111.73
137	$r^2$	0.84	0.77	0.72	0.69	0.67	0.66	0.64	0.31
	RMSE	1.46	1.79	1.98	2.10	2.19	2.25	2.30	3.56
	Slope	0.93	0.90	0.88	0.87	0.86	0.86	0.85	0.63
	Intercept	19.40	28.03	33.17	36.76	39.43	41.61	43.33	107.18
145	$r^2$	0.86	0.80	0.76	0.73	0.72	0.70	0.69	0.37
	RMSE	1.11	1.37	1.51	1.60	1.67	1.72	1.75	2.92
	Slope	0.94	0.92	0.90	0.89	0.89	0.88	0.88	0.74
	Intercept	17.50	24.20	28.03	30.46	32.31	33.74	34.87	75.39
153	$r^2$	0.91	0.85	0.82	0.80	0.78	0.77	0.76	0.24
	RMSE	1.12	1.39	1.55	1.65	1.71	1.76	1.80	3.37
	Slope	0.92	0.89	0.86	0.85	0.84	0.83	0.82	0.39

DOY	Parameter	Window sizes							Study area
		3×3	5×5	7×7	9×9	11×11	13×13	15×15	
161	Intercept	22.47	33.37	40.18	44.60	47.72	50.20	52.13	176.18
	r <sup>2</sup>	0.85	0.78	0.73	0.70	0.68	0.66	0.65	0.13
	RMSE	1.09	1.36	1.51	1.61	1.68	1.73	1.77	3.66
	Slope	0.93	0.90	0.88	0.87	0.86	0.85	0.84	0.48
169	Intercept	20.24	29.11	34.62	38.97	42.27	44.68	46.81	154.68
	r <sup>2</sup>	0.89	0.83	0.79	0.77	0.75	0.73	0.72	0.35
	RMSE	0.95	1.18	1.31	1.40	1.46	1.51	1.54	2.53
	Slope	0.93	0.90	0.88	0.87	0.86	0.85	0.85	0.58
177	Intercept	21.09	29.56	35.09	38.30	40.74	42.80	44.27	124.04
	r <sup>2</sup>	0.86	0.79	0.74	0.71	0.69	0.67	0.66	0.36
	RMSE	1.20	1.50	1.67	1.78	1.85	1.91	1.95	2.74
	Slope	0.90	0.85	0.82	0.80	0.78	0.77	0.76	0.51
185	Intercept	30.03	44.24	53.34	59.26	63.55	66.89	69.43	141.58
	r <sup>2</sup>	0.77	0.66	0.59	0.54	0.51	0.49	0.47	0.20
	RMSE	1.23	1.55	1.73	1.85	1.94	2.00	2.04	3.10
	Slope	0.88	0.83	0.79	0.77	0.75	0.74	0.72	0.58
193	Intercept	35.01	50.51	60.24	67.32	72.49	76.27	79.71	122.27
	r <sup>2</sup>	0.81	0.72	0.66	0.62	0.60	0.58	0.56	0.24
	RMSE	0.98	1.23	1.38	1.47	1.53	1.57	1.60	2.37
	Slope	0.91	0.87	0.85	0.83	0.82	0.81	0.80	0.56
201	Intercept	26.09	37.46	44.79	49.21	52.42	55.37	57.50	129.63
	r <sup>2</sup>	0.86	0.79	0.75	0.72	0.70	0.68	0.67	0.32
	RMSE	0.76	0.94	1.05	1.12	1.16	1.20	1.22	1.94
	Slope	0.94	0.91	0.89	0.88	0.87	0.86	0.86	0.63
209	Intercept	18.87	27.37	32.68	36.27	38.79	40.75	42.41	110.81
	r <sup>2</sup>	0.90	0.85	0.82	0.80	0.78	0.77	0.76	0.34
	RMSE	0.82	1.00	1.11	1.17	1.22	1.25	1.28	2.16
	Slope	0.91	0.87	0.85	0.84	0.83	0.82	0.81	0.45
217	Intercept	26.13	36.92	43.46	48.01	51.42	54.12	56.40	162.79
	r <sup>2</sup>	0.81	0.73	0.69	0.66	0.63	0.62	0.60	0.21
	RMSE	0.85	1.04	1.14	1.20	1.25	1.29	1.31	2.40
	Slope	0.92	0.89	0.87	0.86	0.85	0.84	0.83	0.63
	Intercept	23.03	32.60	38.40	42.36	45.31	47.49	49.39	109.83

DOY	Parameter	Window sizes							Study area
		3×3	5×5	7×7	9×9	11×11	13×13	15×15	
225	$r^2$	0.85	0.78	0.74	0.70	0.68	0.66	0.65	0.34
	RMSE	0.79	0.97	1.08	1.14	1.19	1.22	1.25	1.81
	Slope	0.89	0.85	0.82	0.80	0.79	0.78	0.77	0.54
	Intercept	31.71	44.21	51.68	56.93	60.75	63.74	66.26	135.02
233	$r^2$	0.87	0.81	0.77	0.75	0.73	0.71	0.70	0.23
	RMSE	0.73	0.90	1.00	1.07	1.11	1.15	1.18	2.05
	Slope	0.95	0.93	0.92	0.91	0.90	0.90	0.89	0.50
	Intercept	13.49	19.35	23.19	25.87	27.94	29.47	30.71	145.93
241	$r^2$	0.91	0.86	0.83	0.81	0.80	0.78	0.77	0.43
	RMSE	0.51	0.63	0.70	0.75	0.79	0.82	0.84	1.54
	Slope	0.96	0.94	0.92	0.91	0.91	0.90	0.89	0.77
	Intercept	12.39	18.30	22.22	25.37	27.98	30.10	31.96	66.51
249	$r^2$	0.87	0.81	0.77	0.74	0.71	0.69	0.68	0.24
	RMSE	0.66	0.82	0.91	0.97	1.01	1.04	1.07	1.80
	Slope	0.88	0.83	0.80	0.78	0.77	0.75	0.74	0.44
	Intercept	34.95	49.22	58.13	64.13	68.72	72.23	75.20	164.37
257	$r^2$	0.84	0.78	0.73	0.70	0.68	0.66	0.65	0.18
	RMSE	0.84	1.01	1.11	1.18	1.23	1.27	1.30	2.14
	Slope	0.89	0.86	0.83	0.82	0.80	0.79	0.78	0.38
	Intercept	30.72	41.60	48.40	53.45	57.35	60.52	63.18	180.24
265	$r^2$	0.90	0.85	0.83	0.81	0.79	0.78	0.77	0.12
	RMSE	0.88	1.04	1.14	1.21	1.26	1.30	1.33	2.78
	Slope	0.94	0.91	0.90	0.89	0.88	0.87	0.87	0.27
	Intercept	18.40	24.95	29.19	32.34	34.68	36.59	38.23	211.57
Average	$r^2$	0.87	0.81	0.77	0.74	0.72	0.71	0.69	0.31
	RMSE	0.95	1.18	1.31	1.36	1.39	1.43	1.43	2.55
	Slope	0.92	0.89	0.87	0.85	0.84	0.83	0.83	0.54
	Intercept	22.33	32.03	38.15	42.39	45.58	48.10	50.19	132.40

Note: Gap pixels were in-filled only for the non-shaded window sizes (i.e.,  $RMSE \leq 2 K$ ).

**Table A2.8: Coefficient of determination ( $r^2$ ), root mean square error (RMSE), slope, and intercept values between observed and predicted  $T_S$  using various window sizes during 2010.**

DOY	Parameter	Window sizes							Study area
		3×3	5×5	7×7	9×9	11×11	13×13	15×15	
97	$r^2$	0.94	0.92	0.90	0.88	0.87	0.86	0.85	0.33
	RMSE	0.99	1.22	1.36	1.45	1.52	1.57	1.62	3.50
	Slope	0.95	0.92	0.91	0.90	0.89	0.88	0.87	0.40
	Intercept	14.60	21.35	25.78	29.09	31.86	34.17	36.34	166.96
105	$r^2$	0.93	0.89	0.87	0.85	0.84	0.83	0.81	0.32
	RMSE	0.92	1.14	1.27	1.36	1.43	1.49	1.53	3.61
	Slope	0.98	0.97	0.96	0.95	0.94	0.93	0.93	0.70
	Intercept	5.82	9.79	12.98	15.37	17.24	18.98	20.33	87.10
113	$r^2$	0.92	0.87	0.83	0.80	0.78	0.76	0.75	0.23
	RMSE	0.91	1.15	1.31	1.41	1.49	1.54	1.58	3.35
	Slope	0.92	0.88	0.86	0.84	0.83	0.81	0.80	0.52
	Intercept	21.66	33.02	40.46	45.72	49.66	52.81	55.50	136.10
121	$r^2$	0.88	0.81	0.76	0.72	0.70	0.68	0.66	0.26
	RMSE	1.36	1.71	1.92	2.06	2.15	2.22	2.28	3.50
	Slope	0.90	0.85	0.81	0.79	0.77	0.76	0.75	0.40
	Intercept	27.78	42.44	52.28	59.09	64.02	67.91	70.91	168.92
129	$r^2$	0.80	0.70	0.64	0.60	0.57	0.55	0.53	0.29
	RMSE	1.44	1.82	2.05	2.20	2.30	2.37	2.43	3.45
	Slope	0.90	0.86	0.83	0.81	0.80	0.79	0.78	0.66
	Intercept	27.99	40.77	48.90	54.60	58.60	61.89	64.45	97.47
137	$r^2$	0.90	0.85	0.81	0.78	0.75	0.74	0.72	0.23
	RMSE	1.56	1.97	2.23	2.40	2.52	2.61	2.68	4.52
	Slope	0.92	0.88	0.84	0.82	0.81	0.79	0.78	0.31
	Intercept	23.55	36.27	45.56	51.84	56.76	60.96	64.49	200.57
145	$r^2$	0.84	0.75	0.70	0.66	0.63	0.61	0.60	0.01
	RMSE	1.54	1.94	2.19	2.36	2.48	2.57	2.65	5.94
	Slope	0.94	0.91	0.90	0.88	0.87	0.87	0.86	0.11
	Intercept	17.83	25.89	30.38	33.93	36.44	38.30	39.87	259.89
153	$r^2$	0.90	0.84	0.80	0.78	0.76	0.75	0.74	0.45
	RMSE	1.22	1.52	1.69	1.80	1.88	1.93	1.98	2.97
	Slope	0.93	0.90	0.88	0.86	0.86	0.85	0.84	0.65

DOY	Parameter	Window sizes							Study area
		3×3	5×5	7×7	9×9	11×11	13×13	15×15	
161	Intercept	21.11	30.27	35.97	39.55	42.17	44.28	45.85	103.07
	r <sup>2</sup>	0.84	0.76	0.71	0.68	0.66	0.64	0.63	0.31
	RMSE	1.17	1.45	1.61	1.71	1.78	1.82	1.86	3.25
	Slope	0.92	0.89	0.87	0.85	0.84	0.83	0.82	0.75
169	Intercept	22.73	33.07	39.50	43.88	47.18	49.74	51.89	74.42
	r <sup>2</sup>	0.85	0.78	0.73	0.70	0.67	0.66	0.64	0.30
	RMSE	0.96	1.18	1.31	1.40	1.46	1.50	1.54	2.54
	Slope	0.91	0.88	0.85	0.83	0.82	0.81	0.80	0.64
177	Intercept	25.72	36.80	43.99	49.35	53.45	56.69	59.51	106.81
	r <sup>2</sup>	0.83	0.74	0.68	0.64	0.61	0.58	0.56	0.20
	RMSE	1.20	1.49	1.67	1.78	1.86	1.92	1.97	2.86
	Slope	0.86	0.79	0.75	0.72	0.70	0.69	0.67	0.37
185	Intercept	41.79	60.63	72.79	80.90	86.79	91.42	95.16	184.04
	r <sup>2</sup>	0.76	0.65	0.58	0.54	0.51	0.48	0.46	0.10
	RMSE	1.25	1.56	1.75	1.86	1.94	2.01	2.06	3.14
	Slope	0.89	0.84	0.81	0.79	0.77	0.76	0.75	0.38
193	Intercept	31.88	46.32	55.57	61.93	66.59	70.20	73.08	180.43
	r <sup>2</sup>	0.85	0.77	0.73	0.69	0.67	0.65	0.64	0.09
	RMSE	1.05	1.31	1.46	1.55	1.61	1.66	1.70	3.04
	Slope	0.91	0.87	0.84	0.83	0.81	0.80	0.80	0.28
201	Intercept	27.09	38.95	46.31	51.15	54.70	57.57	59.85	212.68
	r <sup>2</sup>	0.87	0.81	0.77	0.75	0.73	0.71	0.70	0.46
	RMSE	0.94	1.16	1.28	1.36	1.42	1.46	1.50	2.11
	Slope	0.94	0.91	0.89	0.88	0.87	0.86	0.86	0.71
209	Intercept	18.66	26.50	31.27	34.84	37.66	39.82	41.66	86.18
	r <sup>2</sup>	0.86	0.79	0.74	0.71	0.68	0.66	0.65	0.40
	RMSE	0.90	1.11	1.23	1.31	1.36	1.41	1.44	2.13
	Slope	0.89	0.85	0.82	0.80	0.78	0.77	0.76	0.69
217	Intercept	31.49	45.02	53.62	59.75	64.36	67.99	70.98	92.12
	r <sup>2</sup>	0.86	0.79	0.75	0.72	0.70	0.68	0.66	0.34
	RMSE	0.93	1.14	1.26	1.34	1.40	1.45	1.48	2.17
	Slope	0.92	0.89	0.87	0.86	0.85	0.84	0.83	0.57
	Intercept	22.41	31.58	37.27	41.44	44.70	47.31	49.58	125.99

DOY	Parameter	Window sizes							Study area
		3×3	5×5	7×7	9×9	11×11	13×13	15×15	
225	$r^2$	0.86	0.79	0.74	0.71	0.69	0.67	0.66	0.05
	RMSE	0.90	1.12	1.24	1.32	1.38	1.42	1.46	2.99
	Slope	0.91	0.87	0.84	0.83	0.82	0.81	0.80	0.22
	Intercept	26.90	38.28	45.17	49.73	52.93	55.42	57.50	226.55
233	$r^2$	0.84	0.76	0.71	0.67	0.64	0.62	0.61	0.10
	RMSE	0.93	1.15	1.28	1.37	1.43	1.47	1.51	2.71
	Slope	0.90	0.86	0.83	0.81	0.79	0.78	0.77	0.33
	Intercept	28.48	40.93	49.37	55.28	59.81	63.53	66.34	192.99
241	$r^2$	0.83	0.75	0.69	0.65	0.62	0.60	0.58	0.24
	RMSE	1.02	1.26	1.40	1.49	1.56	1.62	1.66	2.41
	Slope	0.88	0.82	0.79	0.76	0.74	0.73	0.71	0.45
	Intercept	35.32	51.34	61.33	68.67	74.36	78.90	82.63	156.54
249	$r^2$	0.85	0.76	0.70	0.65	0.62	0.60	0.58	0.08
	RMSE	1.18	1.49	1.68	1.80	1.89	1.95	2.00	3.30
	Slope	0.89	0.84	0.80	0.77	0.75	0.73	0.72	0.23
	Intercept	29.92	46.53	57.87	65.69	71.38	75.84	79.52	218.33
257	$r^2$	0.77	0.66	0.59	0.54	0.51	0.49	0.47	0.07
	RMSE	1.11	1.40	1.57	1.69	1.77	1.83	1.87	3.24
	Slope	0.88	0.83	0.80	0.78	0.77	0.76	0.75	0.34
	Intercept	33.17	47.24	55.05	60.70	64.89	68.20	71.03	185.98
265	$r^2$	0.86	0.80	0.76	0.73	0.71	0.69	0.68	0.08
	RMSE	0.82	1.02	1.13	1.20	1.25	1.29	1.32	2.60
	Slope	0.96	0.94	0.93	0.92	0.91	0.90	0.89	0.30
	Intercept	10.78	16.38	20.91	24.03	26.48	28.56	30.19	199.04
Average	$r^2$	0.86	0.78	0.73	0.70	0.68	0.66	0.64	0.22
	RMSE	1.10	1.38	1.47	1.51	1.58	1.61	1.63	3.15
	Slope	0.91	0.87	0.85	0.83	0.82	0.81	0.80	0.46
	Intercept	24.85	36.33	43.74	48.93	52.82	55.93	58.49	157.37

Note: Gap pixels were in-filled only for the non-shaded window sizes (i.e.,  $RMSE \leq 2 K$ ).

**Table A2.9: Coefficient of determination ( $r^2$ ), root mean square error (RMSE), slope, and intercept values between observed and predicted  $T_S$  using various window sizes during 2011.**

DOY	Parameter	Window sizes							Study area
		3×3	5×5	7×7	9×9	11×11	13×13	15×15	
97	$r^2$	0.87	0.81	0.77	0.74	0.72	0.70	0.69	0.20
	RMSE	0.82	1.01	1.11	1.18	1.23	1.26	1.30	2.12
	Slope	0.89	0.86	0.83	0.81	0.80	0.79	0.78	0.31
	Intercept	28.49	39.90	46.58	51.42	55.02	57.82	60.28	190.01
105	$r^2$	0.88	0.82	0.78	0.75	0.73	0.71	0.70	0.28
	RMSE	1.11	1.37	1.52	1.62	1.69	1.74	1.78	2.79
	Slope	0.90	0.86	0.83	0.81	0.79	0.78	0.77	0.38
	Intercept	26.45	38.73	46.42	52.02	56.21	59.42	62.44	170.90
113	$r^2$	0.90	0.84	0.81	0.78	0.76	0.75	0.74	0.49
	RMSE	1.10	1.38	1.54	1.64	1.72	1.77	1.81	2.57
	Slope	0.95	0.93	0.91	0.89	0.88	0.88	0.87	0.66
	Intercept	13.51	20.98	26.15	29.86	32.73	35.06	36.97	96.76
121	$r^2$	0.91	0.85	0.81	0.79	0.77	0.75	0.74	0.47
	RMSE	1.01	1.28	1.44	1.54	1.61	1.67	1.72	2.66
	Slope	0.93	0.89	0.87	0.85	0.84	0.83	0.82	0.70
	Intercept	19.81	30.22	37.17	42.22	46.05	49.04	51.61	84.88
129	$r^2$	0.87	0.80	0.76	0.73	0.70	0.69	0.67	0.42
	RMSE	1.01	1.27	1.43	1.52	1.59	1.65	1.69	2.58
	Slope	0.93	0.89	0.87	0.86	0.84	0.84	0.83	0.76
	Intercept	21.30	31.55	38.04	42.31	45.52	47.98	49.82	71.36
137	$r^2$	0.90	0.85	0.81	0.78	0.76	0.75	0.73	0.42
	RMSE	0.87	1.09	1.22	1.31	1.37	1.42	1.47	2.33
	Slope	0.94	0.92	0.90	0.89	0.88	0.87	0.86	0.66
	Intercept	16.17	23.55	28.75	32.81	36.18	39.04	41.44	98.83
145	$r^2$	0.94	0.90	0.88	0.86	0.85	0.84	0.83	0.40
	RMSE	0.78	0.97	1.08	1.15	1.21	1.25	1.29	2.49
	Slope	0.96	0.94	0.93	0.92	0.91	0.91	0.90	0.56
	Intercept	10.98	16.67	20.37	23.19	25.41	27.14	28.77	127.74
153	$r^2$	0.90	0.85	0.82	0.80	0.78	0.77	0.76	0.45
	RMSE	0.98	1.21	1.33	1.42	1.47	1.52	1.55	2.52
	Slope	0.91	0.87	0.85	0.84	0.82	0.81	0.81	0.65

DOY	Parameter	Window sizes							Study area
		3×3	5×5	7×7	9×9	11×11	13×13	15×15	
161	Intercept	26.17	36.96	43.53	48.02	51.31	53.94	56.07	100.76
	r <sup>2</sup>	0.87	0.81	0.77	0.73	0.71	0.69	0.68	0.32
	RMSE	1.45	1.78	1.98	2.10	2.20	2.26	2.32	3.46
	Slope	0.89	0.84	0.81	0.79	0.77	0.76	0.75	0.43
169	Intercept	32.18	45.91	54.91	61.43	66.20	69.99	73.08	166.18
	r <sup>2</sup>	0.82	0.73	0.67	0.64	0.61	0.59	0.57	0.29
	RMSE	1.50	1.89	2.12	2.27	2.37	2.44	2.50	3.64
	Slope	0.91	0.88	0.85	0.84	0.82	0.82	0.81	0.62
177	Intercept	25.14	36.37	43.43	48.22	51.54	54.04	56.10	110.57
	r <sup>2</sup>	0.88	0.83	0.79	0.76	0.74	0.73	0.71	0.49
	RMSE	1.12	1.41	1.58	1.69	1.77	1.82	1.87	2.63
	Slope	0.95	0.93	0.92	0.91	0.90	0.90	0.89	0.74
185	Intercept	14.17	20.42	24.21	26.87	28.89	30.49	31.79	74.38
	r <sup>2</sup>	0.89	0.83	0.79	0.77	0.75	0.73	0.72	0.42
	RMSE	1.00	1.24	1.38	1.47	1.53	1.58	1.62	2.64
	Slope	0.92	0.89	0.86	0.85	0.84	0.83	0.82	0.70
193	Intercept	22.70	33.20	39.66	44.21	47.56	50.08	52.05	87.09
	r <sup>2</sup>	0.90	0.85	0.82	0.79	0.78	0.76	0.75	0.39
	RMSE	1.07	1.33	1.49	1.59	1.66	1.72	1.76	2.80
	Slope	0.94	0.91	0.89	0.88	0.87	0.86	0.85	0.54
201	Intercept	18.53	26.88	32.07	35.86	38.66	40.85	42.75	134.05
	r <sup>2</sup>	0.89	0.83	0.79	0.76	0.74	0.72	0.71	0.44
	RMSE	1.04	1.30	1.46	1.56	1.63	1.68	1.72	2.68
	Slope	0.94	0.91	0.89	0.87	0.86	0.86	0.85	0.75
209	Intercept	18.26	26.90	32.90	36.67	39.56	42.11	43.99	71.74
	r <sup>2</sup>	0.94	0.90	0.88	0.86	0.85	0.84	0.84	0.61
	RMSE	0.58	0.72	0.80	0.86	0.90	0.93	0.95	1.90
	Slope	0.97	0.96	0.96	0.95	0.95	0.95	0.95	1.06
217	Intercept	8.14	11.25	12.45	13.35	13.95	14.14	14.42	-17.90
	r <sup>2</sup>	0.90	0.85	0.82	0.80	0.78	0.77	0.76	0.33
	RMSE	0.80	0.99	1.11	1.18	1.23	1.27	1.31	2.23
	Slope	0.95	0.93	0.92	0.90	0.90	0.89	0.88	0.50
217	Intercept	13.88	20.26	24.70	28.07	30.72	32.88	34.72	146.37

DOY	Parameter	Window sizes							Study area
		3×3	5×5	7×7	9×9	11×11	13×13	15×15	
225	r <sup>2</sup>	0.87	0.81	0.77	0.74	0.71	0.70	0.68	0.06
	RMSE	0.91	1.12	1.24	1.32	1.38	1.42	1.46	3.08
	Slope	0.90	0.85	0.83	0.81	0.80	0.79	0.78	0.24
	Intercept	30.25	42.76	50.50	55.54	59.17	61.96	64.27	220.02
233	r <sup>2</sup>	0.84	0.77	0.72	0.69	0.66	0.65	0.63	0.20
	RMSE	0.91	1.13	1.25	1.33	1.39	1.44	1.47	2.51
	Slope	0.93	0.90	0.89	0.87	0.86	0.85	0.84	0.52
	Intercept	19.04	27.80	33.40	37.81	41.32	43.97	46.26	141.18
241	r <sup>2</sup>	0.89	0.84	0.81	0.78	0.76	0.75	0.74	0.46
	RMSE	0.81	0.99	1.10	1.18	1.23	1.27	1.30	1.92
	Slope	0.92	0.89	0.87	0.85	0.84	0.83	0.82	0.61
	Intercept	23.12	32.50	38.39	42.73	45.99	48.54	50.79	111.79
249	r <sup>2</sup>	0.94	0.91	0.89	0.87	0.86	0.85	0.85	0.37
	RMSE	0.81	0.98	1.09	1.16	1.21	1.25	1.29	2.60
	Slope	0.97	0.96	0.95	0.95	0.94	0.94	0.93	0.47
	Intercept	8.41	11.84	14.24	15.98	17.34	18.51	19.51	154.68
257	r <sup>2</sup>	0.83	0.75	0.70	0.66	0.64	0.61	0.59	0.10
	RMSE	0.69	0.85	0.94	1.01	1.06	1.10	1.13	3.09
	Slope	0.92	0.88	0.85	0.83	0.82	0.81	0.80	0.62
	Intercept	23.85	34.96	42.51	47.67	51.74	55.12	57.75	109.65
265	r <sup>2</sup>	0.94	0.91	0.88	0.87	0.85	0.84	0.84	0.17
	RMSE	0.67	0.83	0.93	0.99	1.04	1.08	1.11	2.51
	Slope	0.96	0.94	0.93	0.92	0.91	0.90	0.90	0.25
	Intercept	12.44	17.92	21.39	24.26	26.51	28.22	29.88	215.86
Average	r <sup>2</sup>	0.89	0.83	0.80	0.77	0.75	0.74	0.72	0.35
	RMSE	0.96	1.19	1.29	1.34	1.40	1.44	1.48	2.62
	Slope	0.93	0.90	0.88	0.87	0.86	0.85	0.84	0.58
	Intercept	19.68	28.52	34.17	38.21	41.25	43.65	45.67	121.22

Note: Gap pixels were in-filled only for the non-shaded window sizes (i.e., RMSE ≤ 2 K).

**Table A2.10: Coefficient of determination ( $r^2$ ), root mean square error (RMSE), slope, and intercept values between observed and predicted NMDI and NDVI using 3×3 window size.**

DOY	Parameter	Year					
		2009		2010		2011	
		NMDI	NDVI	NMDI	NDVI	NMDI	NDVI
97	$r^2$	0.855	0.819	0.960	0.839	0.674	0.697
	RMSE	0.033	0.031	0.040	0.035	0.033	0.033
	Slope	0.922	0.895	0.982	0.911	0.820	0.906
	Intercept	0.066	0.012	0.009	0.040	0.148	0.014
105	$r^2$	0.953	0.929	0.747	0.916	0.858	0.923
	RMSE	0.039	0.040	0.037	0.026	0.030	0.025
	Slope	0.961	0.911	0.899	0.951	0.940	0.967
	Intercept	0.029	0.019	0.038	0.022	0.051	0.003
113	$r^2$	0.973	0.971	0.781	0.934	0.966	0.972
	RMSE	0.039	0.031	0.033	0.025	0.035	0.031
	Slope	0.998	0.995	0.862	0.968	0.966	0.968
	Intercept	0.001	0.003	0.054	0.017	0.023	0.010
121	$r^2$	0.845	0.929	0.728	0.920	0.894	0.939
	RMSE	0.033	0.026	0.036	0.025	0.037	0.030
	Slope	0.940	0.961	0.874	0.957	0.964	0.962
	Intercept	0.022	0.019	0.049	0.022	0.013	0.019
129	$r^2$	0.807	0.925	0.741	0.920	0.718	0.904
	RMSE	0.030	0.025	0.028	0.024	0.029	0.028
	Slope	0.908	0.960	0.919	0.962	0.875	0.948
	Intercept	0.035	0.020	0.030	0.021	0.044	0.027
137	$r^2$	0.798	0.934	0.833	0.907	0.807	0.910
	RMSE	0.028	0.023	0.020	0.024	0.024	0.026
	Slope	0.921	0.970	0.934	0.963	0.920	0.953
	Intercept	0.028	0.015	0.026	0.023	0.032	0.029
145	$r^2$	0.821	0.928	0.853	0.937	0.858	0.938
	RMSE	0.024	0.025	0.020	0.022	0.021	0.025
	Slope	0.931	0.969	0.914	0.954	0.935	0.962
	Intercept	0.027	0.017	0.034	0.028	0.027	0.024
153	$r^2$	0.839	0.917	0.891	0.936	0.972	0.985
	RMSE	0.021	0.027	0.019	0.025	0.011	0.015
	Slope	0.925	0.951	0.957	0.977	0.988	0.995

DOY	Parameter	Year					
		2009		2010		2011	
		NMDI	NDVI	NMDI	NDVI	NMDI	NDVI
161	Intercept	0.031	0.029	0.019	0.017	0.005	0.004
	r <sup>2</sup>	0.881	0.938	0.902	0.937	0.916	0.944
	RMSE	0.020	0.026	0.017	0.025	0.017	0.026
	Slope	0.945	0.968	0.952	0.971	0.965	0.980
169	Intercept	0.024	0.023	0.021	0.021	0.016	0.015
	r <sup>2</sup>	0.921	0.952	0.912	0.949	0.911	0.933
	RMSE	0.017	0.023	0.016	0.022	0.016	0.026
	Slope	0.965	0.981	0.958	0.979	0.964	0.982
177	Intercept	0.016	0.014	0.019	0.015	0.017	0.014
	r <sup>2</sup>	0.903	0.935	0.874	0.899	0.926	0.952
	RMSE	0.017	0.025	0.019	0.028	0.016	0.022
	Slope	0.967	0.974	0.935	0.952	0.963	0.981
185	Intercept	0.016	0.019	0.031	0.036	0.018	0.014
	r <sup>2</sup>	0.929	0.940	0.872	0.918	0.911	0.949
	RMSE	0.016	0.025	0.018	0.027	0.015	0.020
	Slope	0.959	0.976	0.935	0.967	0.959	0.979
193	Intercept	0.020	0.018	0.031	0.026	0.019	0.016
	r <sup>2</sup>	0.917	0.946	0.888	0.918	0.902	0.942
	RMSE	0.015	0.020	0.015	0.021	0.015	0.021
	Slope	0.961	0.984	0.951	0.969	0.953	0.973
201	Intercept	0.018	0.014	0.024	0.025	0.022	0.021
	r <sup>2</sup>	0.879	0.945	0.892	0.913	0.900	0.937
	RMSE	0.017	0.018	0.015	0.020	0.015	0.021
	Slope	0.925	0.969	0.940	0.955	0.955	0.980
209	Intercept	0.036	0.024	0.028	0.035	0.022	0.016
	r <sup>2</sup>	0.872	0.935	0.870	0.922	0.878	0.934
	RMSE	0.016	0.017	0.015	0.018	0.014	0.020
	Slope	0.951	0.972	0.937	0.971	0.931	0.966
217	Intercept	0.023	0.022	0.030	0.023	0.033	0.026
	r <sup>2</sup>	0.902	0.945	0.880	0.921	0.896	0.941
	RMSE	0.014	0.016	0.016	0.020	0.014	0.018
	Slope	0.950	0.976	0.938	0.967	0.947	0.974
217	Intercept	0.024	0.019	0.029	0.026	0.025	0.020

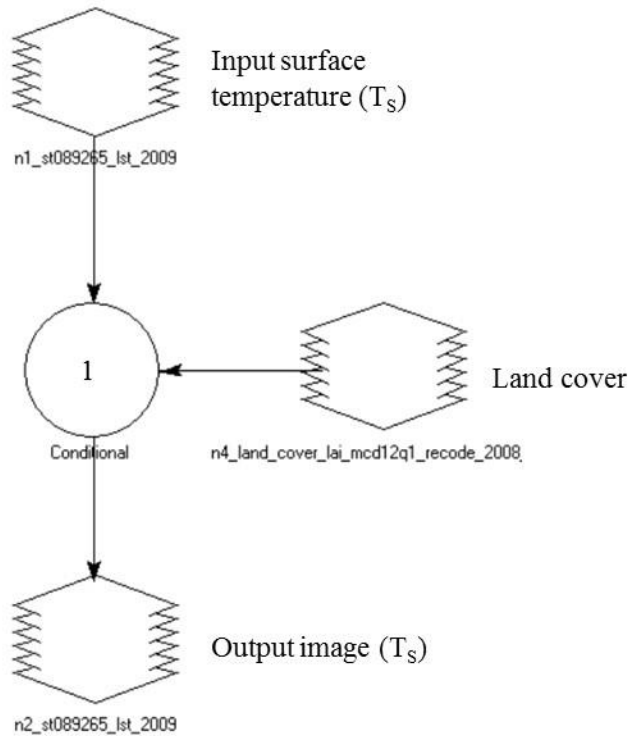
DOY	Parameter	Year					
		2009		2010		2011	
		NMDI	NDVI	NMDI	NDVI	NMDI	NDVI
225	r <sup>2</sup>	0.900	0.940	0.905	0.943	0.862	0.912
	RMSE	0.015	0.017	0.017	0.023	0.014	0.020
	Slope	0.946	0.967	0.955	0.976	0.934	0.961
	Intercept	0.026	0.025	0.020	0.017	0.032	0.030
233	r <sup>2</sup>	0.902	0.946	0.895	0.943	0.871	0.903
	RMSE	0.015	0.017	0.016	0.021	0.015	0.020
	Slope	0.947	0.973	0.939	0.979	0.920	0.953
	Intercept	0.025	0.020	0.027	0.016	0.037	0.036
241	r <sup>2</sup>	0.910	0.950	0.876	0.930	0.894	0.945
	RMSE	0.015	0.015	0.017	0.020	0.017	0.019
	Slope	0.950	0.973	0.932	0.964	0.940	0.972
	Intercept	0.022	0.020	0.030	0.026	0.027	0.020
249	r <sup>2</sup>	0.903	0.954	0.876	0.909	0.878	0.952
	RMSE	0.017	0.016	0.020	0.022	0.020	0.018
	Slope	0.937	0.970	0.933	0.963	0.915	0.978
	Intercept	0.027	0.021	0.028	0.024	0.036	0.016
257	r <sup>2</sup>	0.899	0.949	0.851	0.947	0.857	0.960
	RMSE	0.019	0.017	0.023	0.021	0.023	0.017
	Slope	0.945	0.978	0.887	0.973	0.929	0.982
	Intercept	0.024	0.016	0.047	0.017	0.031	0.012
265	r <sup>2</sup>	0.949	0.902	0.930	0.839	0.848	0.921
	RMSE	0.019	0.020	0.022	0.026	0.025	0.024
	Slope	0.975	0.942	0.946	0.910	0.908	0.936
	Intercept	0.017	0.024	0.031	0.037	0.037	0.037
Average	r <sup>2</sup>	0.935	0.887	0.922	0.857	0.927	0.873
	RMSE	0.019	0.021	0.019	0.023	0.019	0.022
	Slope	0.966	0.945	0.963	0.929	0.966	0.936
	Intercept	0.018	0.026	0.024	0.030	0.019	0.032

Note: Gap pixels were in-filled only for the non-shaded boxes (i.e., RMSE  $\leq$  0.03).

## **Appendix A3: Model development for the FFDFS systems**

### A3.1 Input variables of FFDFS system

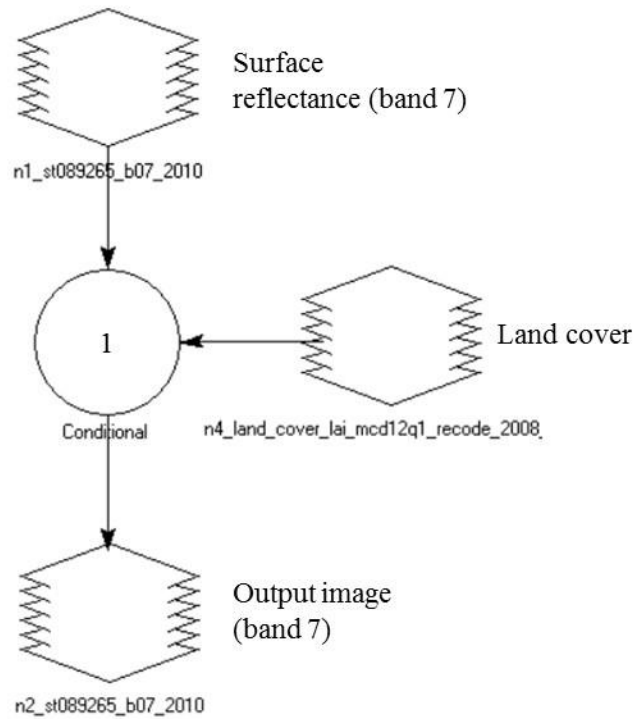
Surface temperature ( $T_s$ )



---

```
'CONDITIONAL {  
(land_cover_lai_mcd12q1_recode_2008 >=6 and  
land_cover_lai_mcd12q1_recode_2008 <=9)  
(st089265_lst_2009 * 2)}
```

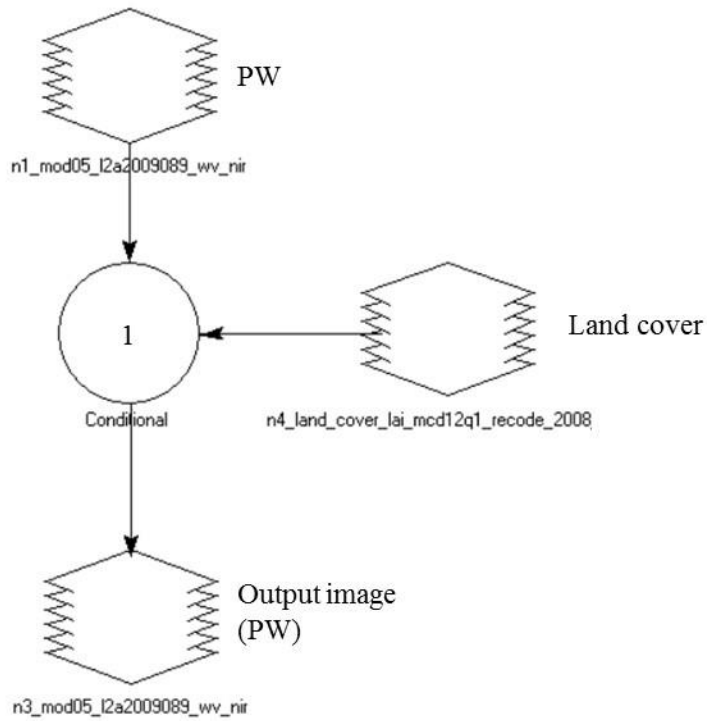
Surface reflectance (spectral bands: 1,2,6,7)



---

```
1CONDITIONAL {  
(land_cover_lai_mcd12q1_recode_2008 >=6 and  
land_cover_lai_mcd12q1_recode_2008 <=9)  
st089265_b07_2010}
```

Precipitable water (PW)

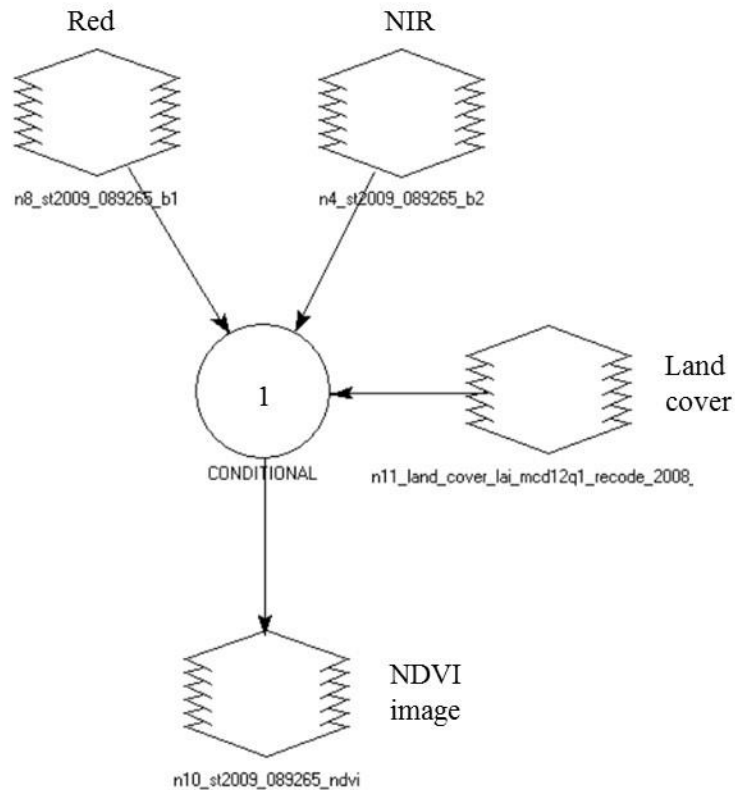


---

<sup>1</sup>CONDITIONAL {  
((land\_cover\_lai\_mcd12q1\_recode\_2008 >=6) and  
(land\_cover\_lai\_mcd12q1\_recode\_2008 <=9))  
mod05\_l2a2009089\_wv\_nir}

### A3.2 Computation of the indices

#### Normalized difference vegetation index (NDVI)



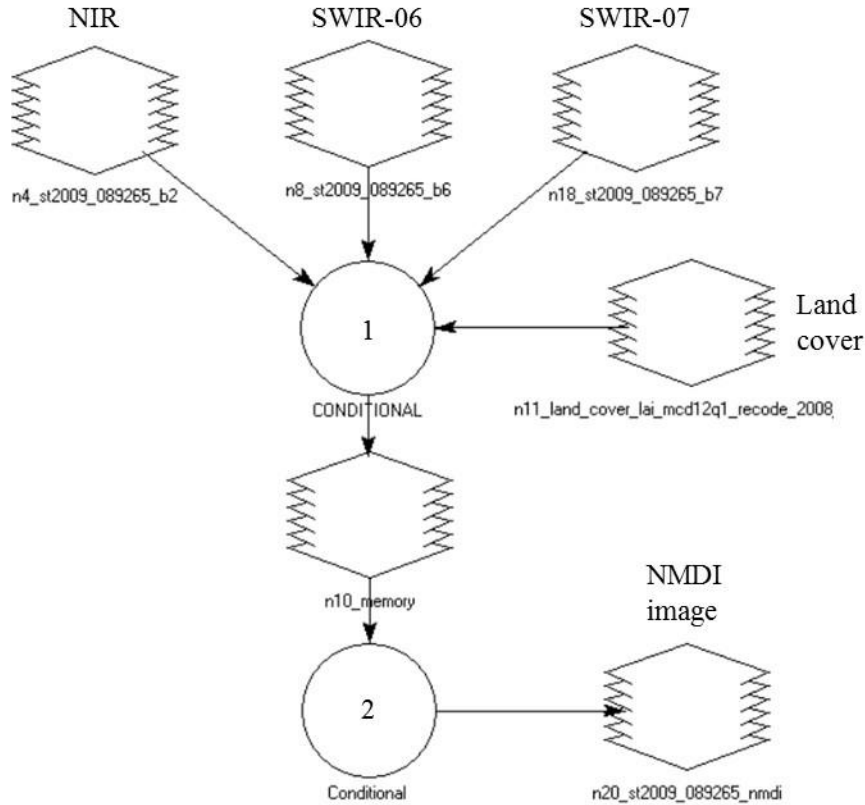

---

```

1CONDITIONAL {
(st2009_089265_b2 == 0 OR $n8_st2009_089265_b1 == 0) -1,
(st2009_089265_b2 - $n8_st2009_089265_b1 == 0) -2,
(st2009_089265_b2 < $n8_st2009_089265_b1 ) -3,
(st2009_089265_b2 >0 and $n8_st2009_089265_b1>0)
(((st2009_089265_b2 - $n8_st2009_089265_b1)/(st2009_089265_b2
+ $n8_st2009_089265_b1))*10000}

```

Normalized difference vegetation index (NMDI)




---

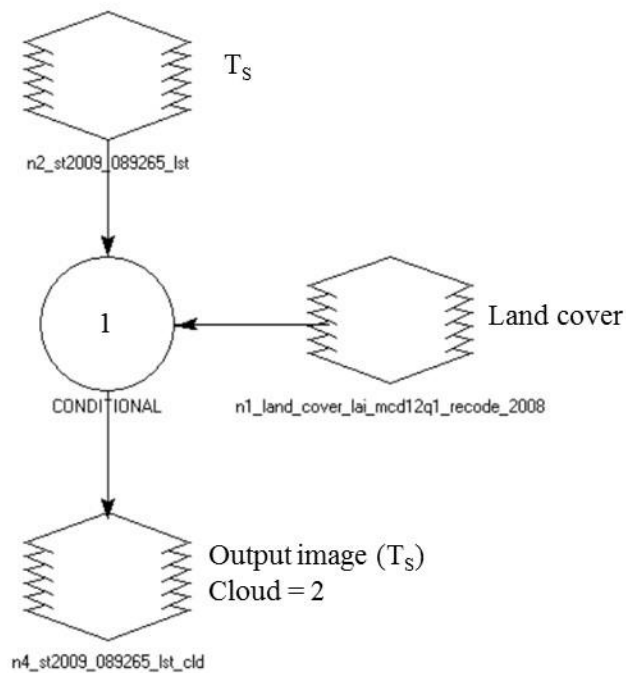
<sup>1</sup>CONDITIONAL{(st2009\_089265\_b2 == 0 OR \$n8\_st2009\_089265\_b6 == 0 OR \$n18\_st2009\_089265\_b7 ==0) -1,  
(st2009\_089265\_b2 - (\$n8\_st2009\_089265\_b6 - \$n18\_st2009\_089265\_b7) == 0) -2,  
(st2009\_089265\_b2 < (\$n8\_st2009\_089265\_b6 - \$n18\_st2009\_089265\_b7) ) -3,  
(st2009\_089265\_b2 >0 and \$n8\_st2009\_089265\_b6>0 and \$n18\_st2009\_089265\_b7 >0) ((st2009\_089265\_b2 - (\$n8\_st2009\_089265\_b6 - \$n18\_st2009\_089265\_b7))/(st2009\_089265\_b2 + (\$n8\_st2009\_089265\_b6 - \$n18\_st2009\_089265\_b7)))\*10000}

---

<sup>2</sup>CONDITIONAL{(\$n10\_memory >= -3 and \$n10\_memory <= 10000) \$n10\_memory,  
(\$n10\_memory > 10000) 10000}

### A3.3 Computation of cloud pixels

Cloud pixels ( $T_s$ )

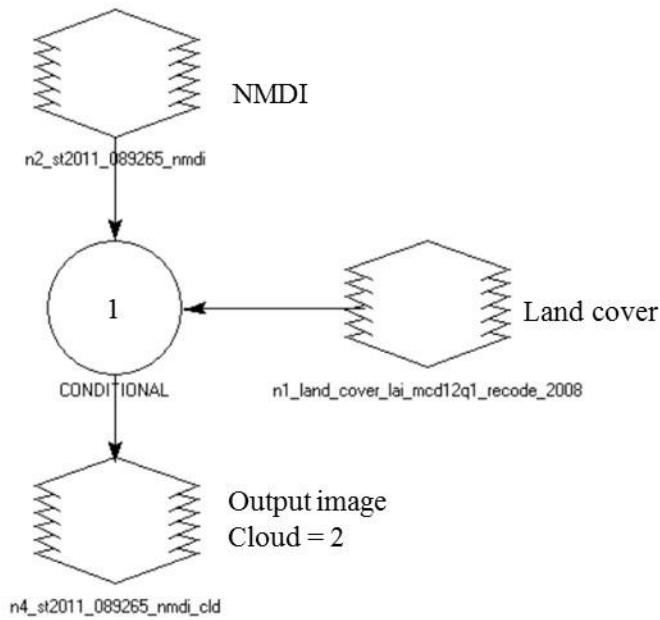



---

```

1CONDITIONAL {
(land_cover_lai_mcd12q1_recode_2008 >5 and
land_cover_lai_mcd12q1_recode_2008 <10) and
(st2009_089265_lst > 0 )) 1,
((land_cover_lai_mcd12q1_recode_2008 >5 and
land_cover_lai_mcd12q1_recode_2008 <10) and
(st2009_089265_lst == 0)) 2}
  
```

Cloud pixels (NMDI or NDVI)

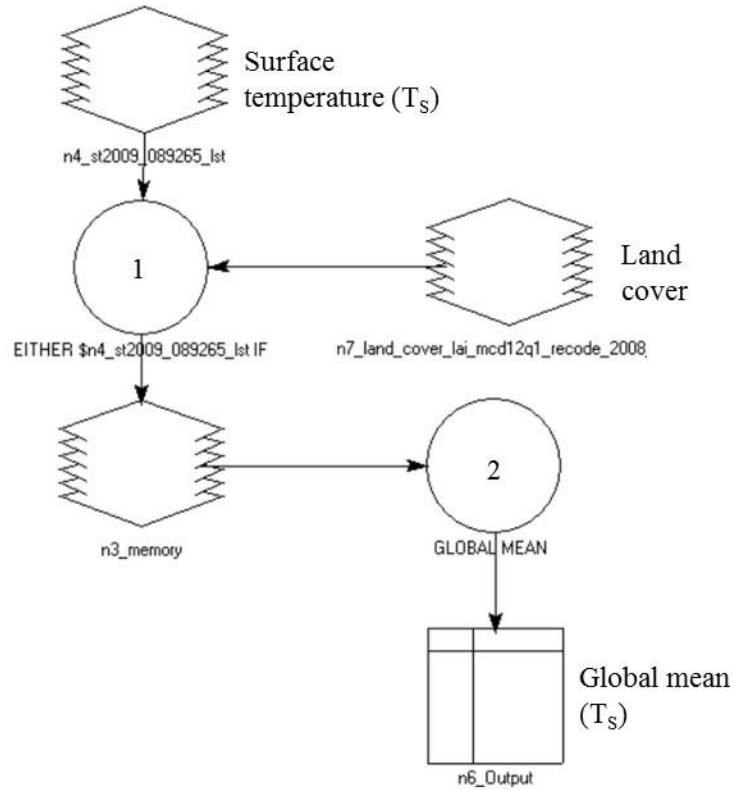


---

```
1CONDITIONAL {  
(land_cover_lai_mcd12q1_recode_2008 > 5 and  
land_cover_lai_mcd12q1_recode_2008 < 10) and  
(st2011_089265_nmdi > 0)) 1,  
((land_cover_lai_mcd12q1_recode_2008 > 5 and  
land_cover_lai_mcd12q1_recode_2008 < 10) and  
(st2011_089265_nmdi == -1)) 2}
```

### A3.4 Study area mean values

Study area mean ( $T_s$ )



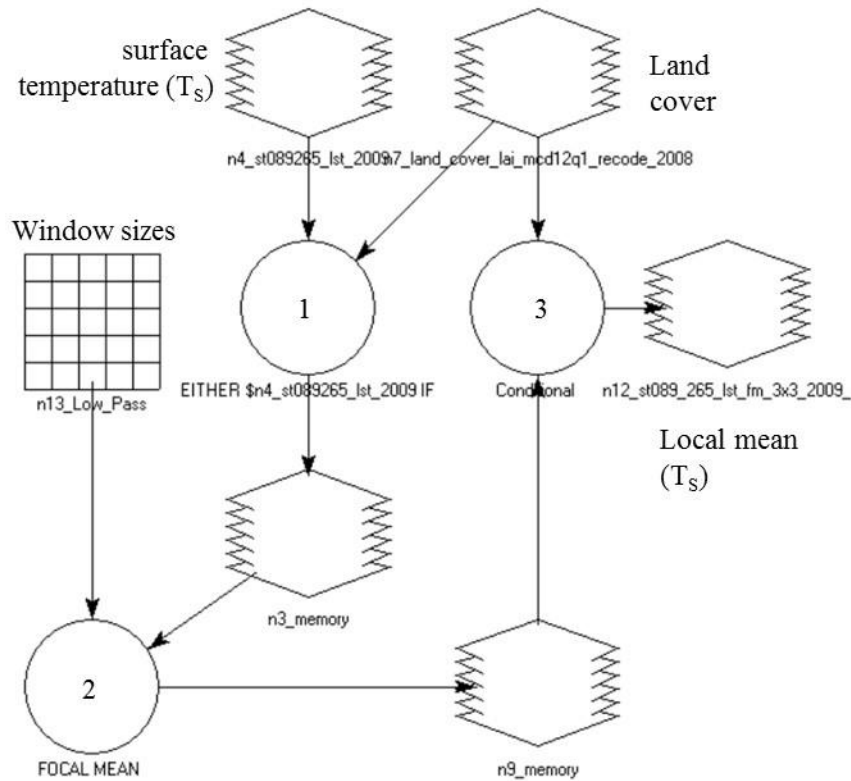

---

<sup>1</sup>EITHER st2009\_089265\_lst IF((st2009\_089265\_lst > 0) and  
(\$n7\_land\_cover\_lai\_mcd12q1\_recode\_2008 >= 6) and  
(\$n7\_land\_cover\_lai\_mcd12q1\_recode\_2008 <= 9)) OR 0 OTHERWISE

---

<sup>2</sup>GLOBAL MEAN (memory, IGNORE 0)

Local mean ( $T_s$ )




---

<sup>1</sup>EITHER st089265\_lst\_2009 IF((st089265\_lst\_2009 > 0) and (\$n7\_land\_cover\_lai\_mcd12q1\_recode\_2008 >=6) and (\$n7\_land\_cover\_lai\_mcd12q1\_recode\_2008 <=9)) OR 0 OTHERWISE

---

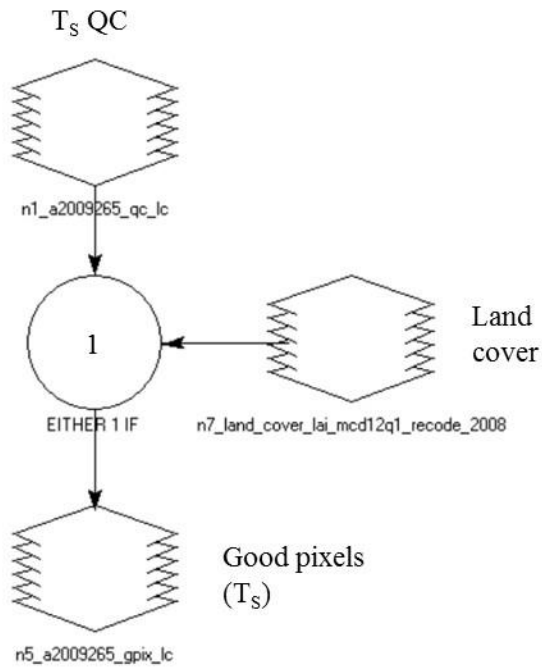
<sup>2</sup>FOCAL MEAN ( memory , \$n13\_Custom\_Integer , IGNORE\_VALUE 0 )

---

<sup>3</sup>CONDITIONAL {(\$n7\_land\_cover\_lai\_mcd12q1\_recode\_2008 >=6 and \$n7\_land\_cover\_lai\_mcd12q1\_recode\_2008 <=9) \$n9\_memory}

### A3.5 Good quality pixels

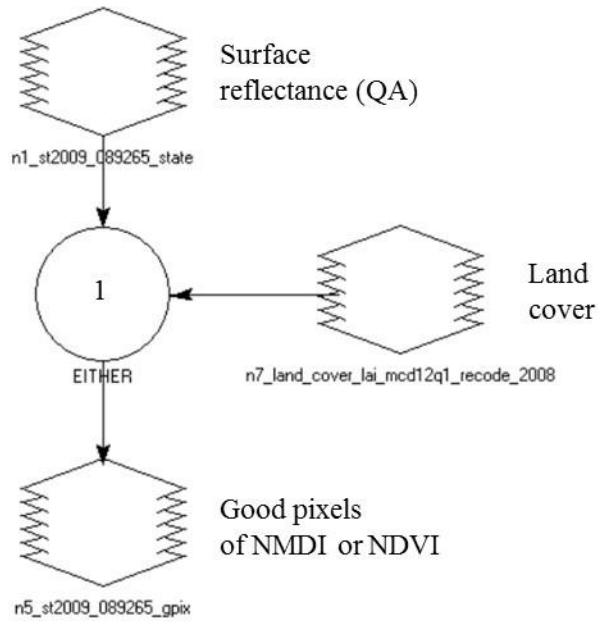
#### Good quality pixels ( $T_S$ )



---

<sup>1</sup>EITHER 1 IF ( (a2009265\_qc\_lc == 0 OR a2009265\_qc\_lc == 65) and  
(\$n7\_land\_cover\_lai\_mcd12q1\_recode\_2008 >= 6 and  
\$n7\_land\_cover\_lai\_mcd12q1\_recode\_2008 <=9)) OR 0 OTHERWISE

Good quality pixels NMDI or NDVI

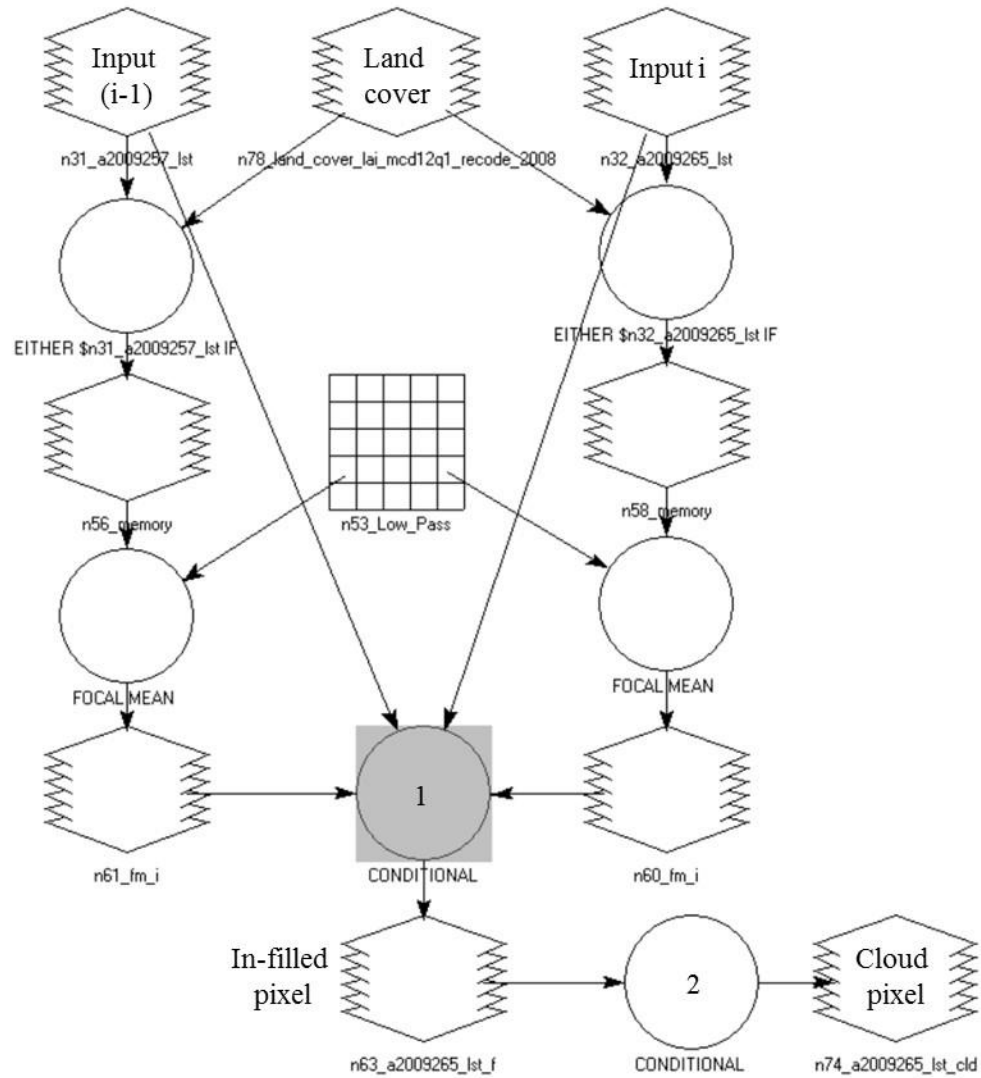


---

```
EITHER 1 IF ((st2009_089265_state == 72 or
st2009_089265_state == 80 or st2009_089265_state ==
36936 or st2009_089265_state == 36944 or
st2009_089265_state == 88) and
($n7_land_cover_lai_mcd12q1_recode_2008 >= 6 and
$n7_land_cover_lai_mcd12q1_recode_2008 <=9)) OR 0
OTHERWISE
```

### A3.6 Data gap-infill

Data gap in-fill ( $T_s$ )



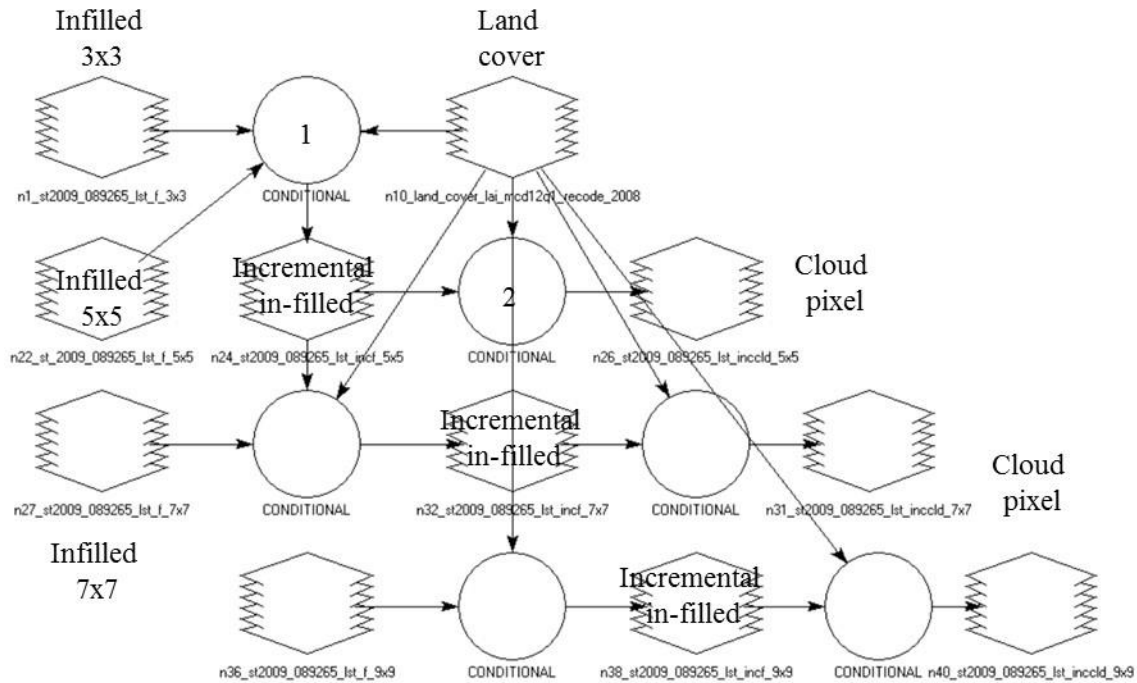

---

<sup>1</sup>CONDITIONAL {(\$n32\_a2009265\_lst > 0) \$n32\_a2009265\_lst,  
 ((\$n61\_fm\_i > 0 and \$n60\_fm\_i > 0) and (\$n32\_a2009265\_lst == 0) and  
 (\$n31\_a2009257\_lst > 0)) (\$n31\_a2009257\_lst + (\$n61\_fm\_i - \$n60\_fm\_i))}

---

<sup>2</sup>CONDITIONAL {(\$n34\_land\_cover\_lai\_mcd12q1\_recode\_2008 == 0) 0,  
 (\$n63\_a2009265\_lst\_f > 0) 1, (\$n63\_a2009265\_lst\_f == 0) 2}

Incremental in-fill ( $T_S$ )

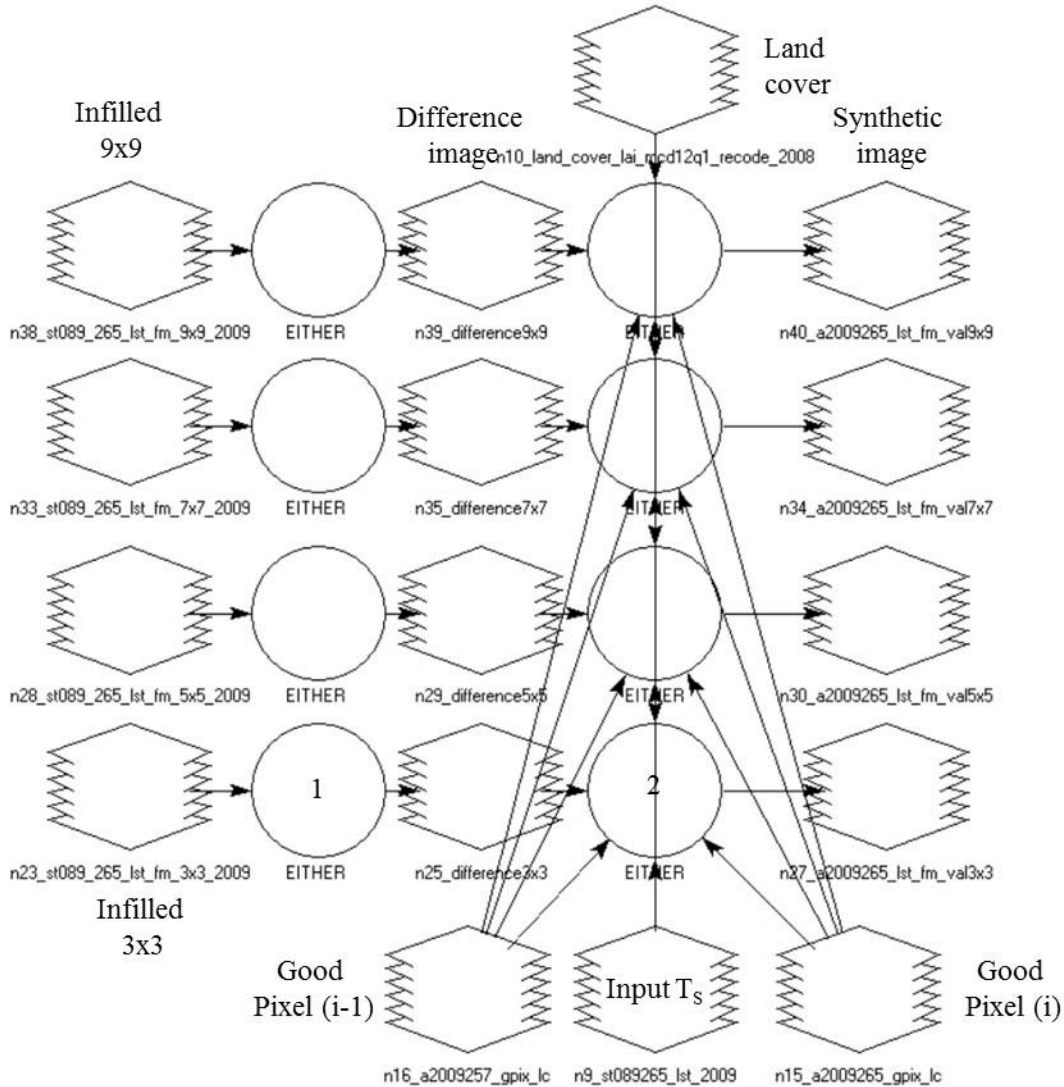


<sup>1</sup>CONDITIONAL {(\$n10\_land\_cover\_lai\_mcd12q1\_recode\_2008 == 0) 0,  
 ((st2009\_089265\_lst\_f\_3x3 == 0) and (\$n22\_st\_2009\_089265\_lst\_f\_5x5 == 0)) 0,  
 (st2009\_089265\_lst\_f\_3x3 > 0) st2009\_089265\_lst\_f\_3x3,  
 ((st2009\_089265\_lst\_f\_3x3 == 0) and (\$n22\_st\_2009\_089265\_lst\_f\_5x5 > 0) and  
 (\$n10\_land\_cover\_lai\_mcd12q1\_recode\_2008 >= 6 and  
 \$n10\_land\_cover\_lai\_mcd12q1\_recode\_2008 <= 9))  
 (\$n22\_st\_2009\_089265\_lst\_f\_5x5)}

<sup>2</sup>CONDITIONAL {(\$n34\_land\_cover\_lai\_mcd12q1\_recode\_2008 == 0) 0,  
 (\$n63\_a2009265\_lst\_f > 0) 1, (\$n63\_a2009265\_lst\_f == 0) 2}

### A3.7 Validation of data gap-infill

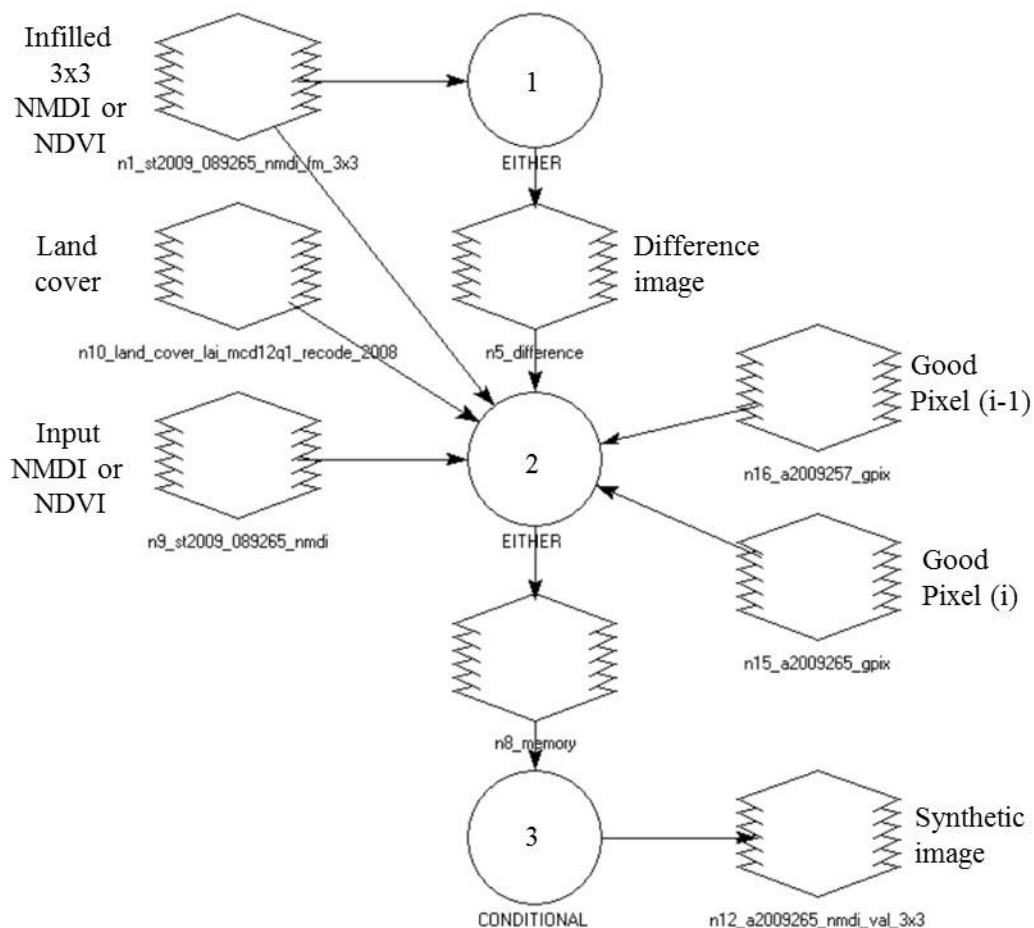
Validation using synthetic image ( $T_s$ )



<sup>1</sup>EITHER ( $\$n23\_st089\_265\_lst\_fm\_3x3\_2009(23) - \$n23\_st089\_265\_lst\_fm\_3x3\_2009(22)$ ) IF ( $\$n23\_st089\_265\_lst\_fm\_3x3\_2009(23) > 0$  and  $\$n23\_st089\_265\_lst\_fm\_3x3\_2009(22) > 0$ ) OR 0 OTHERWISE

<sup>2</sup>EITHER ( $\$n25\_difference3x3 + \$n9\_st089265\_lst\_2009(22)$ ) IF ( $\$n9\_st089265\_lst\_2009(22) > 0$  and ( $\$n15\_a2009265\_gpix\_lc == 1$  and  $\$n16\_a2009257\_gpix\_lc == 1$ ) and ( $\$n10\_land\_cover\_lai\_mcd12q1\_recode\_2008 >= 6$ ) and ( $\$n10\_land\_cover\_lai\_mcd12q1\_recode\_2008 <= 9$ )) OR 0 OTHERWISE

Validation using synthetic image (NMDI or NDVI)



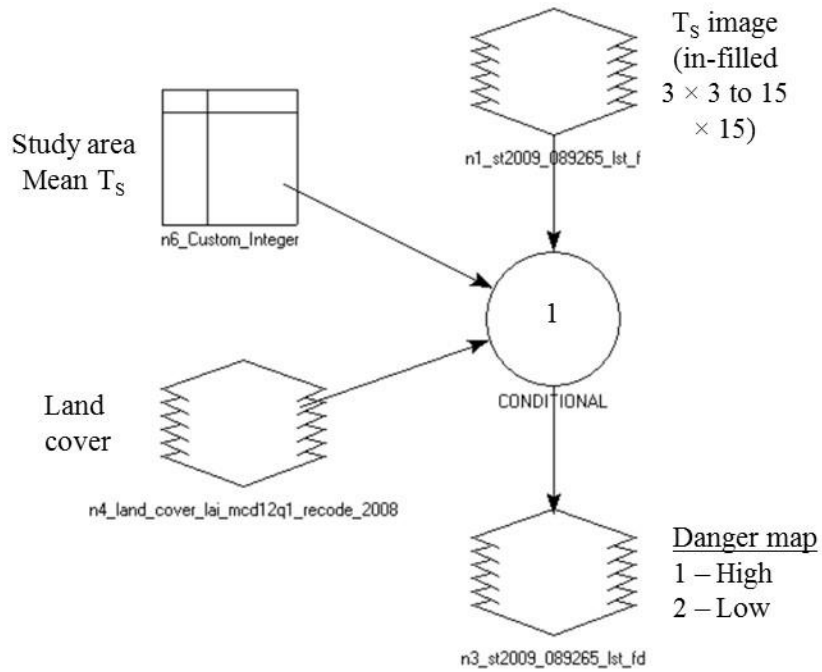
<sup>1</sup>EITHER (st2009\_089265\_nmdi\_fm\_3x3(23) - st2009\_089265\_nmdi\_fm\_3x3(22)) IF (st2009\_089265\_nmdi\_fm\_3x3(23) >0 and st2009\_089265\_nmdi\_fm\_3x3(22) >0 ) OR 0 OTHERWISE

<sup>2</sup>EITHER (\$n5\_difference + \$n9\_st2009\_089265\_nmdi(22)) IF (\$n9\_st2009\_089265\_nmdi(22) >0 and (\$n15\_a2009265\_gpix ==1 and \$n16\_a2009257\_gpix ==1) and (\$n10\_land\_cover\_lai\_mcd12q1\_recode\_2008 >=6) and (\$n10\_land\_cover\_lai\_mcd12q1\_recode\_2008 <=9)) OR 0 OTHERWISE

<sup>3</sup>CONDITIONAL {(\$n8\_memory >= 10000) 10000, (\$n8\_memory < 10000) \$n8\_memory}

### A3.8 Fire danger maps

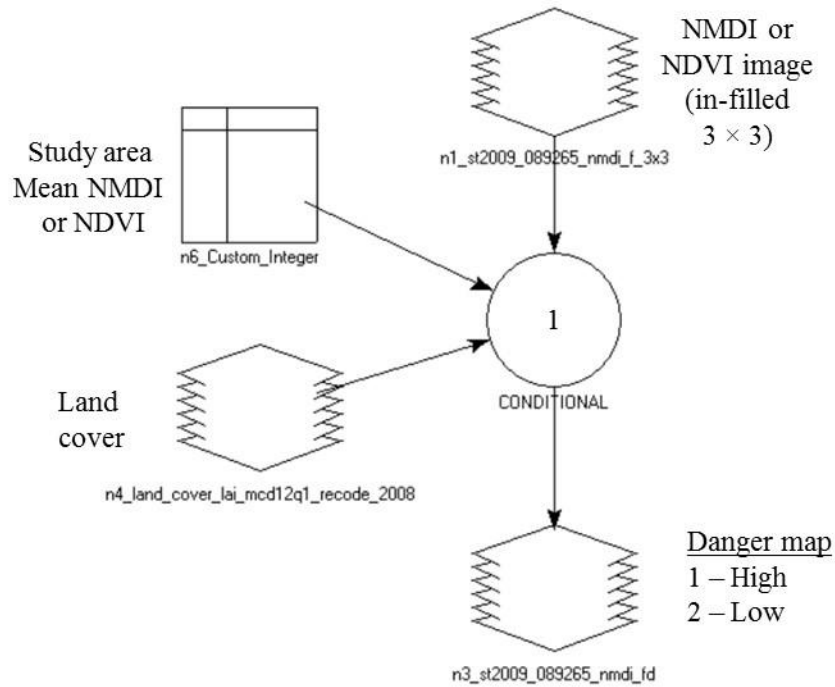
Fire danger map ( $T_S$ : either high or low)




---

<sup>1</sup>CONDITIONAL {(st2009\_089265\_lst\_f <= 0) 0,  
 ((st2009\_089265\_lst\_f >= \$n6\_Custom\_Integer) and  
 (land\_cover\_lai\_mcd12q1\_recode\_2008 >=6 and  
 land\_cover\_lai\_mcd12q1\_recode\_2008 <=9)) 1,  
 ((st2009\_089265\_lst\_f < \$n6\_Custom\_Integer) and  
 (land\_cover\_lai\_mcd12q1\_recode\_2008 >=6 and  
 land\_cover\_lai\_mcd12q1\_recode\_2008 <=9 )) 2}

Fire danger (NMDI or NDVI, either high or low)



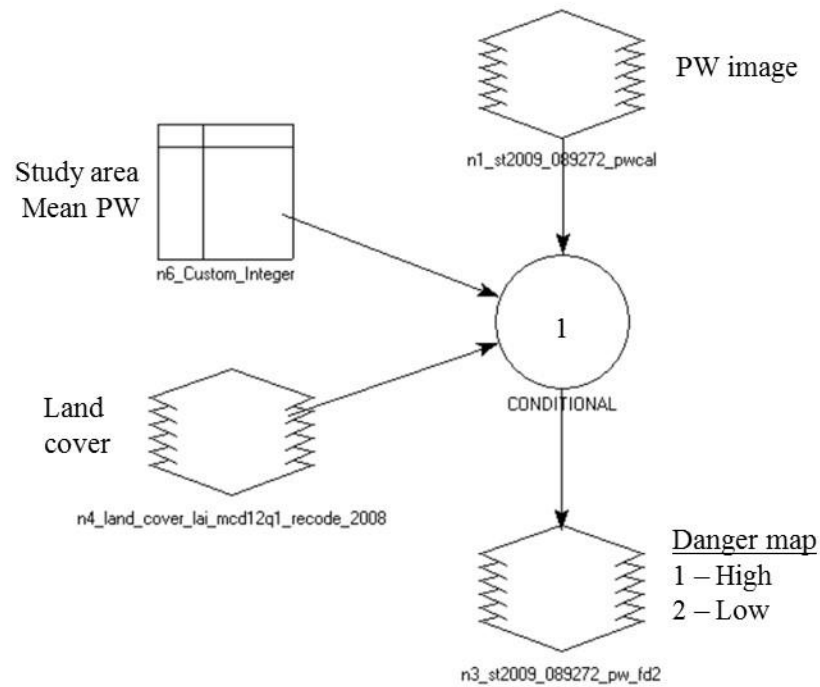

---

```

1CONDITIONAL {
(st2009_089265_nmdi_f_3x3 <= 0) 0,
((st2009_089265_nmdi_f_3x3 <= $n6_Custom_Integer) and
(land_cover_lai_mcd12q1_recode_2008 >=6 and
land_cover_lai_mcd12q1_recode_2008 <=9)) 1,
((st2009_089265_nmdi_f_3x3 > $n6_Custom_Integer) and
(land_cover_lai_mcd12q1_recode_2008 >=6 and
land_cover_lai_mcd12q1_recode_2008 <=9 )) 2}

```

Fire danger (PW, either high or low)




---

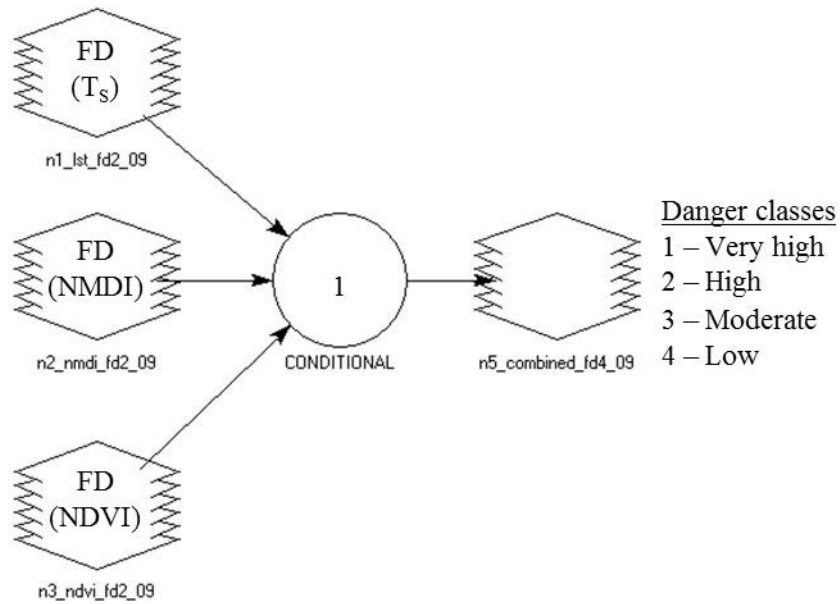
```

1CONDITIONAL {
(st2009_089272_pwcal < 0) 0,
((st2009_089272_pwcal >=0 and st2009_089272_pwcal <=
$n6_Custom_Integer) and (land_cover_lai_mcd12q1_recode_2008
>=6 and land_cover_lai_mcd12q1_recode_2008 <=9)) 1,
((st2009_089272_pwcal > $n6_Custom_Integer) and
(land_cover_lai_mcd12q1_recode_2008 >=6 and
land_cover_lai_mcd12q1_recode_2008 <=9 )) 2}

```

### A3.9 Combined fire danger maps

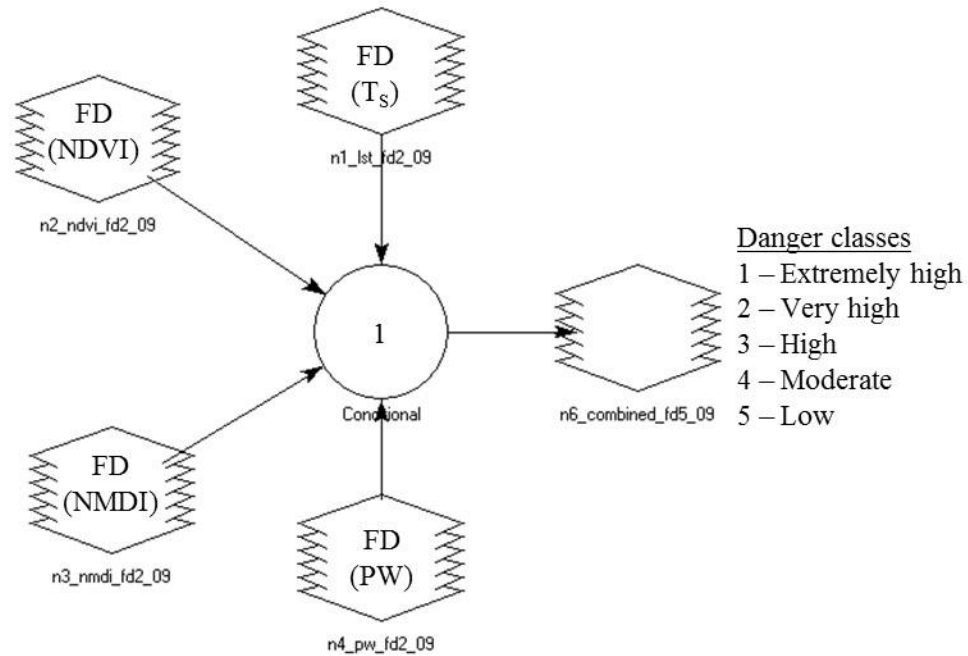
Combined fire danger ( $T_s$ , NMDI, and NDVI), 8-day forecasting




---

<sup>1</sup>CONDITIONAL {  
 (lst\_fd2\_09 == 1 and nmdi\_fd2\_09 == 1 and ndvi\_fd2\_09 == 1) 1,  
 (lst\_fd2\_09 == 1 and nmdi\_fd2\_09 == 1 and ndvi\_fd2\_09 == 2) 2,  
 (lst\_fd2\_09 == 1 and nmdi\_fd2\_09 == 2 and ndvi\_fd2\_09 == 1) 2,  
 (lst\_fd2\_09 == 2 and nmdi\_fd2\_09 == 1 and ndvi\_fd2\_09 == 1) 2,  
 (lst\_fd2\_09 == 1 and nmdi\_fd2\_09 == 2 and ndvi\_fd2\_09 == 2) 3,  
 (lst\_fd2\_09 == 2 and nmdi\_fd2\_09 == 1 and ndvi\_fd2\_09 == 2) 3,  
 (lst\_fd2\_09 == 2 and nmdi\_fd2\_09 == 2 and ndvi\_fd2\_09 == 1) 3,  
 (lst\_fd2\_09 == 2 and nmdi\_fd2\_09 == 2 and ndvi\_fd2\_09 == 2) 4}

Combined fire danger ( $T_s$ , NMDI, NDVI, and PW), daily scale forecasting




---

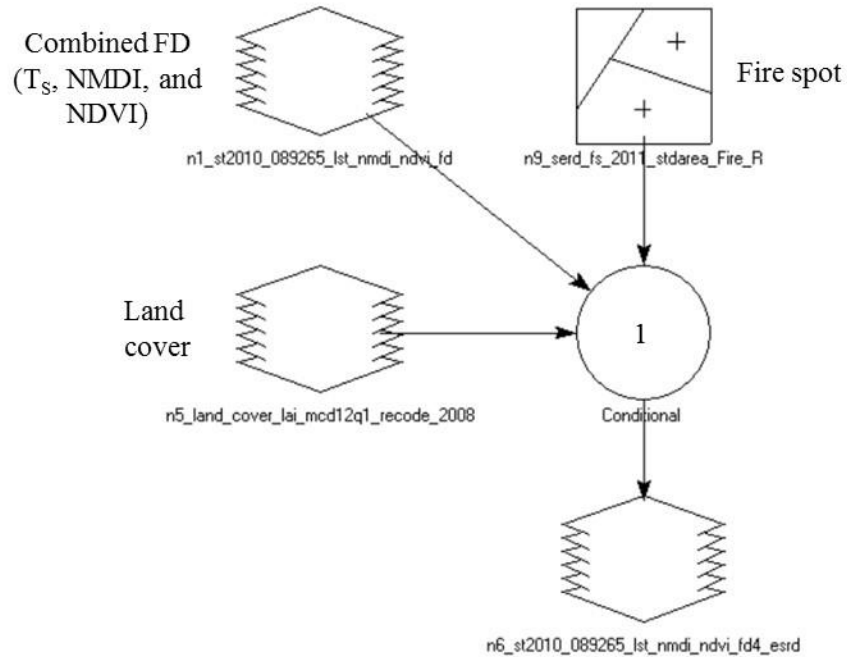
```

1CONDITIONAL {
(lst_fd2_09 == 1 and ndvi_fd2_09 == 1 and nmdi_fd2_09 == 1 and pw_fd2_09 ==1) 1,
(lst_fd2_09 == 1 and ndvi_fd2_09 == 1 and nmdi_fd2_09 == 1 and pw_fd2_09 ==2) 2,
(lst_fd2_09 == 1 and ndvi_fd2_09 == 1 and nmdi_fd2_09 == 2 and pw_fd2_09 ==1) 2,
(lst_fd2_09 == 1 and ndvi_fd2_09 == 2 and nmdi_fd2_09 == 1 and pw_fd2_09 ==1) 2,
(lst_fd2_09 == 2 and ndvi_fd2_09 == 1 and nmdi_fd2_09 == 1 and pw_fd2_09 ==1) 2,
(lst_fd2_09 == 1 and ndvi_fd2_09 == 1 and nmdi_fd2_09 == 2 and pw_fd2_09 ==2) 3,
(lst_fd2_09 == 1 and ndvi_fd2_09 == 2 and nmdi_fd2_09 == 1 and pw_fd2_09 ==2) 3,
(lst_fd2_09 == 1 and ndvi_fd2_09 == 2 and nmdi_fd2_09 == 2 and pw_fd2_09 ==1) 3,
(lst_fd2_09 == 2 and ndvi_fd2_09 == 1 and nmdi_fd2_09 == 1 and pw_fd2_09 ==2) 3,
(lst_fd2_09 == 2 and ndvi_fd2_09 == 1 and nmdi_fd2_09 == 2 and pw_fd2_09 ==1) 3,
(lst_fd2_09 == 2 and ndvi_fd2_09 == 2 and nmdi_fd2_09 == 1 and pw_fd2_09 ==1) 3,
(lst_fd2_09 == 2 and ndvi_fd2_09 == 2 and nmdi_fd2_09 == 2 and pw_fd2_09 ==1) 4,
(lst_fd2_09 == 2 and ndvi_fd2_09 == 2 and nmdi_fd2_09 == 1 and pw_fd2_09 ==2) 4,
(lst_fd2_09 == 2 and ndvi_fd2_09 == 1 and nmdi_fd2_09 == 2 and pw_fd2_09 ==2) 4,
(lst_fd2_09 == 1 and ndvi_fd2_09 == 2 and nmdi_fd2_09 == 2 and pw_fd2_09 ==2) 4,
(lst_fd2_09 == 2 and ndvi_fd2_09 == 2 and nmdi_fd2_09 == 2 and pw_fd2_09 ==2) 5}

```

### A3.10 Comparison of fire danger map and fire spot

#### Combined fire danger ( $T_s$ , NMDI, and NDVI) and Fire Spot



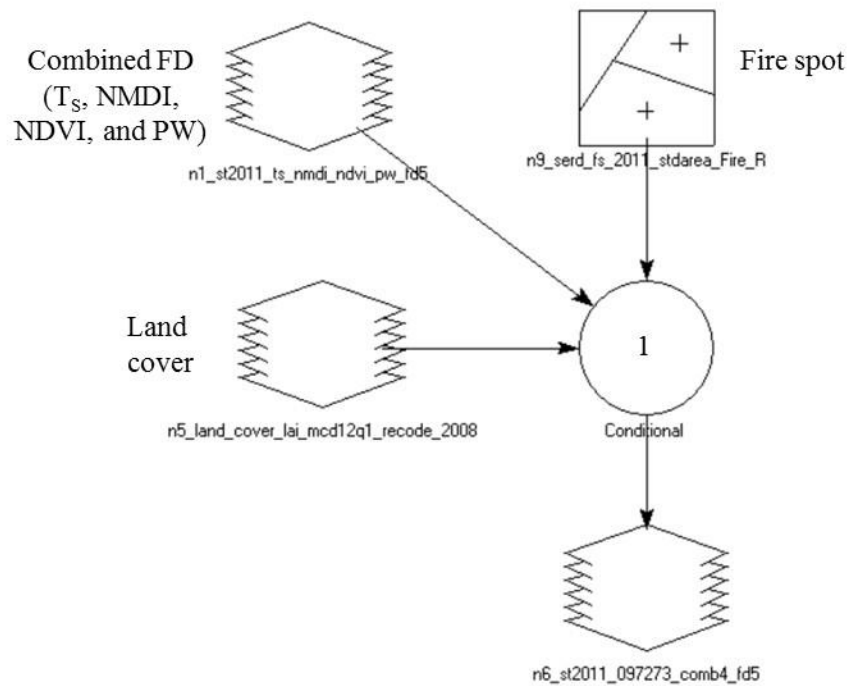

---

```

1CONDITIONAL {
((($n5_land_cover_lai_mcd12q1_recode_2008 >=6 and
$n5_land_cover_lai_mcd12q1_recode_2008 <=9) and
($n9_ser_d_fs_2011_stdarea_Fire_R >=1))
($n9_ser_d_fs_2011_stdarea_Fire_R * 10 +
st2010_089265_lst_nmdi_ndvi_fd)}

```

Combined fire danger ( $T_s$ , NMDI, NDVI, and PW) and Fire Spot




---

```

1CONDITIONAL {
(( $\$n5\_land\_cover\_lai\_mcd12q1\_recode\_2008 \geq 6$  and
 $\$n5\_land\_cover\_lai\_mcd12q1\_recode\_2008 \leq 9$ ) and
( $\$n9\_ser\_d\_fs\_2011\_stdarea\_Fire\_R \geq 1$ ))
( $\$n9\_ser\_d\_fs\_2011\_stdarea\_Fire\_R * 10 +$ 
 $st2011\_ts\_nmdi\_ndvi\_pw\_fd5$ )}

```